Elsevier Editorial System(tm) for Energy Conversion and Management

Manuscript Draft

Manuscript Number: ECM-D-16-02929R1

Title: Thermo-economic analysis and optimization of a combined cooling and power (CCP) system for engine waste heat recovery

Article Type: Original research paper

Section/Category: 1. Energy Conservation and Efficient Utilization

Keywords: Internal combustion engine; Waste heat recovery; Brayton cycle; Organic Rankine cycle; Ejector refrigeration cycle; Optimization.

Corresponding Author: Prof. Jiangfeng Wang, Ph.D.

Corresponding Author's Institution: Xi'an Jiaotong University

First Author: Jiaxi Xia

Order of Authors: Jiaxi Xia; Jiangfeng Wang, Ph.D.; Juwei Lou; Pan Zhao; Yiping Dai

Abstract: A combined cooling and power (CCP) system is developed, which comprises a CO2 Brayton cycle (BC), an organic Rankine cycle (ORC) and an ejector refrigeration cycle for the cascade utilization of waste heat from an internal combustion engine. By establishing mathematical model to simulate the overall system, thermodynamic analysis and exergoeconomic analysis are conducted to examine the effects of five key parameters including the compressor pressure ratio, the compressor inlet temperature, the BC turbine inlet temperature, the ORC turbine inlet pressure and the ejector primary flow pressure on system performance. What's more, a single-objective optimization by means of genetic algorithm (GA) is carried out to search the optimal system performance from viewpoint of exergoeconomic. Results show that the increases of the BC turbine inlet temperature, the ORC turbine inlet pressure and the ejector primary flow pressure are benefit to both thermodynamic and exergoeconimic performances of the CCP system. However, the rises in compressor pressure ratio and compressor inlet temperature will lead to worse system performances. By the single-objective optimization, the lowest average cost per unit of exergy product for the overall system is obtained.

Dear Editor:

Thank you very much for your attention and the reviewers' evaluation and comments on our manuscript entitled "Thermo-economic analysis and optimization of a combined cooling and power (CCP) system for engine waste heat recovery". Based on these comments and suggestions, we have made careful modifications on the original manuscript. All the issues raised in the comments are addressed and the changes made to the text are highlighted.

We hope that these revisions are satisfactory and that the revised manuscript will be acceptable to be published on Energy Conversion and Management.

Thank you again for your work concerning our paper.

Best regards

Sincerely,

Jiangfeng Wang (on behalf of the authors' team)

Institute of Turbomachinery

State Key Laboratory of Multiphase Flow in Power Engineering

School of Energy & Power Engineering

Xi'an Jiaotong University

Xi'an 710049, China

## Highlights

- A combined cooling and power system was proposed for engine waste heat recovery.
- Effects of key parameters on thermodynamic performance of the system were studied.
- Exergoeconomic parameter analysis was performed for the system.
- A single-objective optimization by means of genetic algorithm was carried out.

# Thermo-economic analysis and optimization of a combined cooling and power (CCP) system for engine waste heat recovery

Jiaxi Xia, Jiangfeng Wang*, Juwei Lou, Pan Zhao, Yiping Dai

Institute of Turbomachinery, State Key Laboratory of Multiphase Flow in Power Engineering, School of Energy and Power Engineering,

Xi'an Jiaotong University, Xi'an, China, 710049, China

## Abstract

A combined cooling and power (CCP) system is developed, which comprises a $CO_2$ Brayton cycle (BC), an organic Rankine cycle (ORC) and an ejector refrigeration cycle for the cascade utilization of waste heat from an internal combustion engine. By establishing mathematical model to simulate the overall system, thermodynamic analysis and exergoeconomic analysis are conducted to examine the effects of five key parameters including the compressor pressure ratio, the compressor inlet temperature, the BC turbine inlet temperature, the ORC turbine inlet pressure and the ejector primary flow pressure on system performance. What's more, a single-objective optimization by means of genetic algorithm (GA) is carried out to search the optimal system performance from viewpoint of exergoeconomic. Results show that the increases of the BC turbine inlet temperature, the ORC turbine inlet pressure and the ejector primary flow pressure are benefit to both thermodynamic and exergoeconimic performances of the CCP system. However, the rises in compressor pressure ratio and compressor inlet temperature will lead to worse system performances. By the single-objective optimization, the lowest average cost per unit of exergy product for

the overall system is obtained.

**Key words**: Internal combustion engine; Waste heat recovery; Brayton cycle; Organic Rankine cycle; Ejector refrigeration cycle; Optimization.

**Nomenclature**

| | |
|---|---|
| $A$ | area, $m^2$ |
| $Bo$ | boiling number |
| $C$ | cost rate, \$ $year^{-1}$ |
| $CRF$ | capital recovery factor |
| $CEPCI$ | chemical engineering plant cost index |
| $c$ | average cost per unit of exergy, \$ $(MWh)^{-1}$ |
| $c_p$ | specific heat, kJ kg $K^{-1}$ |
| $D$ | diameter, m |
| $E$ | exergy flow rate, kJ $s^{-1}$ |
| $f$ | friction factor |
| $G$ | mass velocity, kg $m^{-2}$ $s^{-1}$ |
| $h$ | enthalpy, kJ $kg^{-1}$ |
| $i_{eff}$ | interest rate |
| $L$ | length, m |
| $M$ | mass flow rate, kg $s^{-1}$ |
| $n$ | lifetime, year |
| $Nu$ | Nusselt number |

| | |
|---|---|
| $P$ | pressure, MPa |
| $Pr$ | Prandtl number |
| $P_t$ | center distance between tubes, m |
| $p_r$ | reduced pressure |
| $Q$ | heat transfer rate, kW |
| $Q_{vs}$ | volumetric steam flow, $m^3\ s^{-1}$ |
| $q_m$ | average imposed wall heat flux, $W\ m^{-2}$ |
| $r$ | enthalpy of vaporization, $kJ\ kg^{-1}$ |
| $s$ | entropy, $kJ\ kg^{-1}\ K^{-1}$ |
| $T$ | temperature, K |
| $U$ | overall heat transfer coefficient, $W\ m^{-2}\ K^{-1}$ |
| $V$ | volume, $m^3$ |
| $v$ | velocity, $m\ s^{-1}$ |
| $W$ | power, kW |
| $X$ | size or capacity parameter |
| $x$ | vapor quality |
| $Z$ | annually levelized cost value, $\$\ year^{-1}$ |
| | |
| *Greek symbol* | |
| $\alpha$ | convection heat transfer coefficient, $W\ m^{-2}\ K^{-1}$ |
| $\eta$ | efficiency, % |
| $\lambda$ | thickness, m |

| | |
|---|---|
| $\rho$ | density, kg $m^{-3}$ |
| $\mu$ | dynamic viscosity, $m^2$ $s^{-1}$ |
| $\pi$ | compressor pressure ratio |
| | |
| *subscript* | |
| 1-29 | state points |
| a-e | state points |
| 0 | ambient state |
| BC | Brayton cycle |
| BM | bare module |
| bt | BC turbine |
| cf | cold fluid |
| cnd | condensation |
| comp | compressor |
| cool | refrigeration capacity output |
| cond1 | condenser 1 |
| cond2 | condenser 2 |
| D | destruction |
| eq | equipment |
| es | equivalent diameter |
| evp | evaporation |
| exg | exergy |

| | |
|---|---|
| evap | evaporator |
| F | fuel |
| gh | gas heater |
| he | heat exchanger |
| hf | hot fluid |
| in | inside |
| ip | inlet pipe |
| L | loss |
| l | liquid |
| M | material |
| m | mean |
| ORC | Organic Rankine cycle |
| ot | ORC turbine |
| out | outside |
| P | product; pressure |
| pc | precooler |
| pump | pump |
| pump1 | pump 1 |
| pump2 | pump 2 |
| sp | single-phase |
| sep | separator |
| turb | turbine |

| | |
|---|---|
| v | vapor |
| w | tube wall |
| wbt | power produced by BC turbine |
| wot | power produced by ORC turbine |

## 1. Introduction

With the development of world economy and industry, the energy shortage and environmental problems caused by fossil fuel consumption have attracted more and more attention. Internal combustion engines（ICES）which act as the major source of motive power, consume a large proportion of petroleum resources in the world. It is reported that only about one-third of the fuel energy in the internal combustion engines is converted into mechanical work, the remaining energy is mainly wasted by rejecting heat to the environment through the exhaust and the coolant [1]. Therefore, it would be of great significance to recover the waste heat effectively from Internal combustion engines.

The technique of organic Rankine cycle (ORC) has been proven to be a potential method to convert the engine waste heat into power, since it presents some advantages of operation flexibility and desirable efficiency [2, 3]. Much work has been carried out on the ORC configurations for the engine waste heat recovery. Vaja et al. [4] examined three different ORC setups, namely a simple cycle only recovering engine exhaust gases, a simple cycle recovering both exhaust gases and engine cooling water with a preheater and a cycle with regeneration. Tahani et al. [5] introduced two

different kinds of ORC including the preheat and two-stage configurations for the waste heat recovery of engine exhaust gases and coolant. He et al. [6] developed a combined thermodynamic system which contains two cycles: an ORC for the recovery of waste heat from high temperature exhaust gases and the lubricant, a Kalina cycle for the recovery of waste heat from cooling water. Wang et al. [7] studied the thermal performance of a dual-loop ORC coupled with a gasoline engine. Kim et al. [8] proposed a highly efficient single-loop ORC for the waste heat recovery of exhaust gases and coolant from a gasoline vehicle. Since the choice of working fluids had a great influence on thermodynamic performance of an ORC [9], other researchers had put their focuses on working fluid selection [10-13], considering both pure working fluids and zeotropic mixtures for ORCs used in waste heat recovery of ICEs.

Regarding all these studies mentioned above, the heat exchanges between exhaust gases and organic working fluids were conducted directly, that may cause decompositions of organic working fluids, due to the high temperature of exhaust gases (about 450-600℃) and the low decomposition temperatures of organic working fluids (about 200-300℃). In order to avoid this issue, an intermediate loop with thermal oil is placed between the exhaust gases and the ORC [14, 15]. Although the stability and safety of the system could be improved through this method, the great amount of high-temperature exhaust gases heat is not exploited at all. Several studies has been performed on exploring novel dual-loop systems combined ORCs with other thermodynamic cycles for engine waste heat recovery. Mliller et al. [16] developed a

system that combined ORC with thermoelectric conversion. Through a thermoelectric generator (TEG), the high temperature exhaust heat was converted into power, and the working fluid of ORC was preheated. But the application of this combined system is constrained due to the low energy conversion capacity of TEG [17]. Zhang et al. [18] analyzed the characteristics of a dual loop ORC system which was combined with a vehicular light-duty diesel engine. Yang et al. [19] explored system performance of the dual loop ORC system used for diesel engine waste heat recovery under various operating conditions. Choi et al. [20] presented a dual-loop power generation system including an upper trilateral cycle with water and a bottoming ORC. The former utilized the waste heat from the high-temperature exhaust gases discharged by a marine engine, and the latter reused the turbine exhaust heat of the upper cycle and the low-temperature exhaust gases waste heat. Shu et al. [21] designed a novel dual-loop ORC system which consists of a high-temperature (HT) loop and a low-temperature (LT). The HT loop was a steam Rankine cycle used for the waste heat recovery of the high-temperature part of exhaust gases, while the LT loop was an organic Ranking cycle recovering the coolant heat, the turbine exhaust heat from HT loop and the waste heat from low-temperature part of exhaust gases. With regard to the same dual-loop ORC system, Song et al. [22] considered the exploiting of wet steam expansion by applying a screw expander to the HT loop, and investigated the effect of the HT loop parameters on LT loop. Zhou et al. [23] studied the dual-loop ORC with zeotropic mixtures as the working fluid in the low temperature loop.

For the sake of satisfying the diverse consumers' demands, the combined cooling

and power (CCP) concept is also introduced for the engine waste heat recovery by a number of researchers. Liang et al. [24] developed a power and cooling cogeneration system which included an ORC and an absorption refrigeration cycle to utilize the exhaust gases heat of a marine engine. Wang [25] integrated the transcritical $CO_2$ refrigeration cycle with the supercritical $CO_2$ cycle to recover the waste heat of an ICE, producing both cooling and power energy.

However, for the dual-loop ORCs, most of the recent studies only considered the steam Rankine cycle as the HT loop for the heat recovery of high-temperature exhaust gases, neglecting the Brayton cycle, which has been proven to be suitable for recovering waste heat from high-temperature heat source, due to its highly efficiency, small structure and simply layout [26-28]. Even though Zhang et al. [17] have done some work about this, the waste heat recovery of the engine coolant was not taken into account, and the detailed parameter analysis including both HT-loop and LT-loop were not given. Meanwhile, in order to avoid the issue of the mismatching mass flow rate which is caused by the setting in series of the preheater utilized engine coolant heat and the evaporator utilized the residual heat of HT loop, only a part of engine coolant heat could be recovered [4, 5, 21]. What's more, few studies conducted the performance from the viewpoint of exergoeconomic for the system used for engine waste heat recovery. Referring to the CCP systems, little information has been published concerning their applications to recover both exhaust gases heat and coolant heat from engines.

In this study, an organic Rankine cycle coupled with a $CO_2$ Brayton cycle is

considered. In order to utilize the energy source more efficiently, an ejector refrigeration cycle is added as well, since it can utilize low-grade heat sources and has advantages of lower costs, higher reliability and simpler operation [29]. Therefore, a combined cooling and power (CCP) system is designed to recover the waste heat of an engine. The $CO_2$ Brayton cycle is used to recover the waste heat of the high temperature exhaust gases, the organic Rankine cycle with a separator is utilized to make full use of the coolant heat and the residual heat of Brayton cycle, while the ejector refrigeration cycle is applied to reuse the waste heat of the low temperature exhaust gases. The effects of five key parameters on thermodynamic and exergoeconimic performances of the CCP system are examined. Furthermore, a single-objective optimization by means of genetic algorithm is carried out to obtain a better system performance.

## 2. System description

The CCP system designed for this study is shown in Fig. 1. It consists of a $CO_2$ Brayton cycle (BC), an organic Rankine cycle (ORC), and an ejector refrigeration cycle, which produces both power and refrigeration simultaneously. The high temperature exhaust gases are firstly delivered to the gas heater to drive the BC. Cooled $CO_2$ from the precooler is compressed to supercritical state by compressor, and then passes through the gas heater to absorb heat, becoming high temperature and high pressure vapor. The supercritical $CO_2$ enters to BC turbine where it expands to produce power, and the $CO_2$ exhaust is cooled by the vapor generator 1 and precooler in turn to complete the $CO_2$ Brayton cycle.

For the sake of recovering residual heat of $CO_2$ exhaust from the BC turbine, the bottoming loop (ORC) is coupled to the upper loop (BC) via vapor generator 1. Liquid organic working fluid from condenser 1 is pressured by pump 1 and delivered to the preheater, where it is heated by jacket water and becomes two-phase state. The two-phase working fluid is then delivered to separator and separated into saturated vapor and saturated liquid. After the separation process, saturated liquid goes through vapor generator 1 to absorb heat from $CO_2$ exhaust, producing superheated vapor. Then the superheated vapor is mixed with the saturated vapor from separator, and expands through the ORC turbine for power generation. At last, the exhaust from the ORC turbine is condensed to be liquid.

The ejector refrigeration cycle is used to recover the residual heat energy of exhaust gases after releasing heat through the gas heater. Liquid working fluid is divided into two parts after the condensation process in condenser 2. One part of working fluid enters pump 2 to be pumped to vapor generator 2, producing superheated vapor by absorbing heat from exhaust gas. The other part of working fluid passes through the throttle valve, being vaporized to vapor state in evaporator by absorbing heat from the cooling side, producing cooling capacity. After that, these two parts of working fluids are mixed in the ejector, and then enter condenser 2 to be condensed to liquid.

Isobutane is selected as the working fluid for Organic Rankine cycle and ejector refrigeration cycle, since it is suitable for high-temperature ORCs [30, 31] and has good performance in thermodynamic and environmental fields [32]. In addition, water at ambient temperature is chosen as the coolant in the precooler and condensers.

## 3. Mathematical models and performance criteria

In order to simplify the simulation of the system, several assumptions are employed as follows:

(1) The system reaches a steady state.

(2) The pressure losses in pipes are neglected and there is a 2% pressure drop in each heat exchanger.

(3) The heat losses in each component are not taken into account.

(4) The working fluid at the condenser outlet is saturated liquid. And the state of evaporator outlet is saturated vapor.

(5) The isentropic efficiencies of turbines and compressor are 80%, and those of pumps are set to be 70%.

(6) The exhaust temperature at the outlet of vapor generator 2 is confined to be over 110℃, in order to avoid the low-temperature corrosion [33].

### *3.1 Thermodynamic analysis*

#### *3.1.1 Energy analysis*

The mathematical model of energy analysis for each component is established based on the principles of mass and energy conservation, the equations are given by

$$\sum M_{\text{in}} = \sum M_{\text{out}} \tag{1}$$

$$\sum Q - \sum W = \sum M_{\text{out}} \cdot h_{\text{out}} - \sum M_{\text{in}} \cdot h_{\text{in}} \tag{2}$$

The detailed energy balance equations for the CCP system components are listed in Table 1.

The net power output of Brayton cycle is expressed as

$$W_{\mathrm{BC}} = W_{\mathrm{bt}} - W_{\mathrm{comp}} \tag{3}$$

The net power output of organic Rankine is calculated as

$$W_{\mathrm{ORC}} = W_{\mathrm{ot}} - W_{\mathrm{pump1}} \tag{4}$$

The net power output of system is given by

$$W_{\mathrm{net}} = W_{\mathrm{bt}} + W_{\mathrm{ot}} - W_{\mathrm{comp}} - W_{\mathrm{pump1}} - W_{\mathrm{pump2}} \tag{5}$$

The cooling capacity output is

$$Q_{\mathrm{cool}} = M_{28} \cdot (h_{28} - h_{29}) \tag{6}$$

*3.1.2 Exergy analysis*

Exergy is the maximum theoretical work obtainable from an overall system consisting of a system and the environment as the system comes into equilibrium with the environment (passes to the dead state). The exergy flow rate of a fluid at *k*th state point is expressed as

$$E_{\mathrm{k}} = M_{\mathrm{k}} \cdot [(h_{\mathrm{k}} - h_0) - T_0 \cdot (s_{\mathrm{k}} - s_0)] \tag{7}$$

where the subscript 0 denotes the state of ambient conditions.

The exergy rate balance equation for each component is written as

$$E_{\mathrm{F}} = E_{\mathrm{P}} + E_{\mathrm{D}} + E_{\mathrm{L}} \tag{8}$$

The detailed calculations of $E_{\mathrm{F}}$, $E_{\mathrm{P}}$, $E_{\mathrm{D}}$ and $E_{\mathrm{L}}$ for each component in the CCP system are listed in Table 2.

The exergy efficiency is used to evaluate the thermodynamic performance of the system, which is given by

$$\eta_{\mathrm{exg}} = \frac{W_{\mathrm{net}} + E_{\mathrm{cool}}}{(E_{\mathrm{a}} - E_{\mathrm{c}}) + (E_{\mathrm{d}} - E_{\mathrm{e}})} \tag{9}$$

where $E_{\mathrm{cool}}$ denotes the exergy rate of refrigeration process in the evaporator, which is equal to ($E_{29} - E_{28}$).

*3.2 Exergoeconomic analysis*

*3.2.1 Size of main equipments*

*1) Areas of heat exchangers*

In this study, all heat exchangers are set as shell-and-tube type. Single-phase heat transfer process occurs in the gas heater and the precooler, two-phase heat transfer process takes place in the evaporator, while both single-phase and two-phase heat transfer processes are conducted in the vapor generators and condensers. As the thermodynamic properties of the working fluid will undergo changes in heat convection heat transfer process, this process is discretized to many subsections for each heat exchanger. For one subsection, the properties of working fluid are assumed to be constant. The heat transfer equation for each subsection is given by

$$Q_{\mathrm{i}} = U_{\mathrm{i}} \cdot A_{\mathrm{i}} \cdot \Delta t_{\mathrm{i}} \tag{10}$$

where $\Delta t_{\mathrm{i}}$ is the log-mean temperature difference (LMTD)

$$\Delta t_{\mathrm{i}} = \frac{(T_{\mathrm{hf,i+1}} - T_{\mathrm{cf,i+1}}) - (T_{\mathrm{hf,i}} - T_{\mathrm{cf,i}})}{\ln \dfrac{T_{\mathrm{hf,i+1}} - T_{\mathrm{cf,i+1}}}{T_{\mathrm{hf,i}} - T_{\mathrm{cf,i}}}} \tag{11}$$

The total heat transfer coefficient for each subsection is calculated as

$$\frac{1}{U_{\mathrm{i}}} = \frac{1}{\alpha_{\mathrm{hf,i}}} + \frac{\delta}{\lambda} + \frac{1}{\alpha_{\mathrm{cf,i}}} \tag{12}$$

For single-phase flow, the convection heat transfer coefficient at the tube side is [34]

$$\alpha_{\mathrm{s,in}} = \frac{\lambda_{\mathrm{f}}}{D_{\mathrm{in}}}\left[\frac{\frac{f}{8}\cdot Re\cdot Pr}{12.7\cdot\left(\frac{f}{8}\right)^{0.5}\cdot\left(Pr^{\frac{2}{3}}-1\right)+1.07}\right] \tag{13}$$

In Eq. (13), *f*, *Re* and *Pr* denote the Darcy friction factor, the Reynolds number and the Prandtl number, respectively, which are defined as

$$f = (0.790\ln Re - 1.64)^{-2} \tag{14}$$

$$\mathrm{Re} = \frac{G_{\mathrm{in}} D_{\mathrm{in}}}{\mu} \tag{15}$$

$$\mathrm{Pr} = \frac{c_{\mathrm{p}}\mu}{\lambda} \tag{16}$$

where $G_{\mathrm{in}}$ is the mass velocity of the flow inside the tube, being given by

$$G_{\mathrm{in}} = \frac{4M}{N\cdot\pi\cdot D_{\mathrm{in}}{}^{2}} \tag{17}$$

The convection heat transfer coefficient for single-phase at the shell side is calculated by [35]

$$\alpha_{\mathrm{s,out}} = 0.36\cdot\frac{\lambda}{D_{\mathrm{es}}}\cdot\left(\frac{D_{\mathrm{es}}\cdot u\cdot\rho}{\mu}\right)^{0.55}\cdot\mathrm{Pr}^{1/3}\cdot\left(\frac{\mu}{\mu_w}\right)^{0.14} \tag{18}$$

where $D_{\mathrm{es}}$ is the equivalent diameter of the shell-side flow channel defined as

$$D_{es} = \frac{1.10P_{\mathrm{t}}^{2}}{D_{\mathrm{out}}} - D_{\mathrm{out}} \tag{19}$$

The heat transfer process of the two-phase flow consists of the evaporation and the condensation processes. It is assumed that the organic fluid flows inside the tube for the vapor generators, condensers and evaporator, then the evaporation heat transfer

coefficient is given by [36]

$$\alpha_{\mathrm{tp,evp}} = 0.023\left[\frac{G(1-x)d}{\mu_{\mathrm{l}}}\right]^{0.8} \mathrm{Pr}_{\mathrm{l}}^{0.4} \cdot \frac{\lambda_{\mathrm{l}}}{d}\left[1+3000Bo^{0.86}+1.12\left(\frac{x}{1-x}\right)^{0.75}\left(\frac{\rho_{\mathrm{l}}}{\rho_{\mathrm{v}}}\right)^{0.41}\right] \quad (20)$$

where *Bo* denotes the boiling number and expressed as

$$Bo = \frac{q_{\mathrm{m}}}{G \cdot r_{\mathrm{f}}} \quad (21)$$

The condensation heat transfer coefficient is defined as [37]

$$\alpha_{\mathrm{tp,cnd}} = 0.023\left[\frac{G_{\mathrm{f}}(1-x)d}{\mu_{\mathrm{l}}}\right]^{0.8} \mathrm{Pr}_{\mathrm{l}}^{0.4} \cdot \frac{\lambda_{\mathrm{l}}}{d}\left[(1-x)^{0.8}+\frac{3.8x^{0.76}(1-x)^{0.04}}{p_{\mathrm{r}}^{0.38}}\right] \quad (22)$$

In Eq. (22), $p_{\mathrm{r}}$ denotes the reduced pressure which is the ratio of state point pressure to critical pressure of the fluid.

Eventually, the area of each heat exchanger can be obtained by adding up the areas for all subsections from both single-phase and two-phase regions.

*2) Volume of the separator*

Vertical BOC (bottoming outlet cyclone separator) separator is selected in this study, due to its high separator efficiency and simple structure. The calculations of the vessel dimensions are all given based on the two-phase inlet pipe. The pipe size is calculated as follows [38]

$$A_{\mathrm{ip}} = \frac{Q_{\mathrm{vs}}}{\nu_{\mathrm{t}}} \quad (23)$$

$$D_{\mathrm{ip}} = \left[\frac{4A_{\mathrm{ip}}}{\pi}\right]^{\frac{1}{2}} \quad (24)$$

where $A_{\mathrm{ip}}$ and $D_{\mathrm{ip}}$ denote the cross sectional area and the diameter of the inlet pipe, respectively; $Q_{\mathrm{vs}}$ is the volumetric flow; and $\nu_{\mathrm{t}}$ is terminal velocity of the two phase flow, which is given by [38]

$$v_t = K\left[\frac{\rho_l - \rho_v}{\rho_v}\right] \tag{25}$$

In Eq. (25), $K$ is a constant with a value of 0.069 ($m \cdot s^{-1}$).

In order to simplify the calculation, the vertical BOC separator is considered as a cylindrical vessel with a height of ($L_A + L_B$) and a diameter of $D_{sep}$, the calculation of the volume for the separator is given by

$$V_{sep} = \frac{\pi \cdot D_{sep}{}^2 \cdot (L_A + L_B)}{4} \tag{26}$$

where $L_A$ is the length of the part which is above the inlet pipe, and $L_B$ is the length of the part which is below the inlet pipe. It is recommended by Ref [38]: $D_{sep}$=3$D_{ip}$, $L_A$=7$D_{ip}$ and $L_B$=4.5$D_{ip}$. After that, Eq. (26) could be written as

$$V_{sep} = \frac{\pi \cdot (3D_{ip})^2}{4} \cdot (7D_{ip} + 4.5D_{ip}) \tag{27}$$

*3.2.2 Costs of equipments*

For the sake of estimating the equipment costs, the method of equipment module costing [39] is used in this paper. This method of costing relates all costs of the equipment to the purchased cost of equipment evaluated for some base conditions. The deviations from base conditions are handled by using multiplying factors depending on the specific equipment type, system pressure and materials of construction. Considering the effect of inflation, the CEPCI (Chemical Engineering Plant Cost Index) is employed to update the equipment costs to the year of 2014 [40], which is expressed as

$$C_{2014} = C_b \cdot \left(\frac{I_{2014}}{I_b}\right) \tag{28}$$

where $C_b$ refers to the cost at the base time; $I_{2014}$ and $I_b$ are the cost indexes assigned 576.1 and 397, respectively.

The purchased cost of the equipment, at ambient pressures and using carbon steel construction, is calculated as [39]

$$\log C_{eq}^{0} = K_{1,eq} + K_{2,eq} \cdot \log(X) + K_{3,eq} \cdot [\log(X)]^2 \tag{29}$$

where $K_{1,eq}$, $K_{2,eq}$ and $K_{2,eq}$ are the constants for the equipment. And $X$ is the size or capacity parameter for the equipment, representing the total heat transfer area of the heat exchanger ($A_{he}$), the power generation by the turbine ($W_{turb}$), the volume of the separator ($V_{sep}$) and the power consumption by the pump ($W_{pump}$) or compressor ($W_{comp}$).

It is assumed that each heat exchanger of the system is made from the material of carbon steel, with a type of shell-and-tube. Then the cost is given by

$$C_{he} = \frac{576.1}{397} \cdot C_{he}^{0} \cdot (B_{1,he} + B_{2,he} \cdot F_{M,he} \cdot F_{P,he}) \tag{30}$$

where $B_{1,he}$ and $B_{2,he}$ are the constants according to the type of the heat exchanger; $F_{M,he}$ is the material factor; $F_{P,he}$ is the pressure factor, which is expressed as

$$\log F_{P,he} = C_{1,he} + C_{2,he} \cdot \log P_{he} + C_{3,he} \cdot (\log P_{he})^2 \tag{31}$$

where $C_{1,he}$, $C_{2,he}$ and $C_{3,he}$ are the constants according to the type and the pressure range of the heat exchanger.

The turbines in this study are made from the material of carbon steel, with axial types, and the costs are calculated as

$$C_{turb} = \frac{576.1}{397} \cdot C_{turb}^{0} \cdot F_{BM,turb} \tag{32}$$

where $F_{BM,turb}$ denotes the bare module factor based on the type and material of

construction for the turbine.

The compressor is axial type made from carbon material, and the cost is given by

$$C_{\text{comp}} = \frac{576.1}{397} \cdot C_{\text{comp}}^{0} \cdot F_{\text{BM,comp}} \tag{33}$$

where $F_{\text{BM,comp}}$ is the bare module factor for the compressor.

For the separator, the material of carbon steel and the vertical type are designed for the construction. The cost is expressed as

$$C_{\text{sep}} = \frac{576.1}{397} \cdot C_{\text{sep}}^{0} \cdot (B_{1,\text{sep}} + B_{2,\text{sep}} \cdot F_{\text{M,sep}} \cdot F_{\text{P,sep}}) \tag{34}$$

where $B_{1,\text{sep}}$ and $B_{2,\text{sep}}$ are the constants based on the type of the separator; $F_{\text{M,sep}}$ is the material factor; $F_{\text{P,sep}}$ is the pressure factor, which is calculated by

$$F_{\text{P,sep}} = \max\left\{ \frac{\dfrac{(P_{\text{sep}}+1)*D_{\text{sep}}}{2\cdot[850-0.6\cdot(P_{\text{sep}}+1)]}+0.00315}{0.0063}, 1 \right\} \tag{35}$$

The pumps are designed to centrifugal type and made from stainless steel, and the costs of them are given by

$$C_{\text{pump}} = \frac{576.1}{397} \cdot C_{\text{pump}}^{0} \cdot (B_{1,\text{pump}} + B_{2,\text{pump}} \cdot F_{\text{M,pump}} \cdot F_{\text{P,pump}}) \tag{36}$$

where $B_{1,\text{pump}}$ and $B_{2,\text{pump}}$ are the constants based on the type of the pump; $F_{\text{M,pump}}$ is the material factor; $F_{\text{P,pump}}$ is the pressure factor, which is given by

$$\log F_{\text{P,pump}} = C_{1,\text{pump}} + C_{2,\text{pump}} \cdot \log P_{\text{pump}} + C_{3,\text{pump}} \cdot (\log P_{\text{pump}})^{2} \tag{37}$$

where $C_{1,\text{pump}}$, $C_{2,\text{pump}}$ and $C_{3,\text{pump}}$ are the constants in terms of the type and the pressure range of the pump.

The costs of the ejector, the valve and the working fluid are neglected in this paper, since their costs are much lower than those of other equipments [41, 42]. The constants mentioned above are all listed in Table 3.

*3.2.3 Exergoeconomic analysis*

In order to relate the present value of the expenditure to the equivalent annually levelized costs， the capital recovery factor (CRF) is used, which is calculated as [43]

$$CRF = \frac{i_{\text{eff}} \cdot (1+i_{\text{eff}})^{\text{n}}}{(1+i_{\text{eff}})^{\text{n}} - 1} \tag{38}$$

where $i_{\text{eff}}$ is the interest rate with a value of 0.05, and $n$ is the lifetime of the CCP system with a value of 30 [44].

The equipment annually levelized costs is given by

$$Z_{\text{i}} = CRF \cdot C_{\text{i}} \tag{39}$$

It is assumed that the annual working time of the CCP system is 8000 hours [45]. The annual exergy transfer rates ($E_{\text{y}}$), annual power generation and consumption ($W_{\text{y}}$) are then obtained by this assumption.

From the exergoeconomic point of view, each exergy flow is related to a cost, and the cost balance for $k$th component of the CCP system is given by [43]

$$\sum_{\text{out}} (c_{\text{out}} \cdot E_{\text{out}})_{\text{k}} + c_{\text{w,k}} \cdot W_{\text{k}} = c_{\text{q,k}} \cdot E_{\text{q,k}} + \sum_{\text{in}} (c_{\text{in}} \cdot E_{\text{in}})_{\text{k}} + Z_{\text{k}} \tag{40}$$

where $c_{\text{out}}$, $c_{\text{in}}$, $c_{\text{w,k}}$, and $c_{\text{q,k}}$ denote the average costs per unit of exergy. Note that the term ($c_{\text{w,k}} \cdot W_{\text{k}}$) would move with its positive sign to the right side of this equation if a component consumes power (such as the pump or compressor). The term ($c_{\text{q,k}} \cdot \text{E}_{\text{q,k}}$) would come out with its positive sign on the left side when there is a heat transfer from the component. Detailed cost balances and auxiliary cost relations for the components in CCP system are summarized in Table 4.

The average costs per unit of exergy for the heat source of exhaust gases and jacket, the water entering to the condensers and evaporator are considered as zero [46]. Thus,

the average costs per unit of exergy for each flow can be solved by resolving the linear equation system.

In addition, taken the given conditions into account, the average costs per unit of exergy product for the turbines and evaporator could be written by

$$c_{\mathrm{bt}} = \frac{c_1 \cdot (E_{1,\mathrm{y}} - E_{2,\mathrm{y}})}{W_{\mathrm{bt,y}}} + \frac{Z_{\mathrm{bt}}}{W_{\mathrm{bt,y}}} \tag{41}$$

$$c_{\mathrm{ot}} = \frac{c_7 \cdot (E_{7,\mathrm{y}} - E_{8,\mathrm{y}})}{W_{\mathrm{ot,y}}} + \frac{Z_{\mathrm{ot}}}{W_{\mathrm{ot,y}}} \tag{42}$$

$$c_{\mathrm{cool}} = \frac{c_{18} \cdot (E_{18} - E_{19})}{E_{29}} + \frac{Z_{\mathrm{evap}}}{E_{29}} \tag{43}$$

where $c_{\mathrm{cool}}$ denotes the average costs per unit of cold exergy produced by evaporator and is equal to $c_{29}$. On the right side of the equations, the former part is defined as the fuel-exergy-related part, while the latter is considered as the equipment-cost-related part.

In this paper, the average cost per unit of exergy product is used as an indicator for the system performance from the viewpoint of exergoeconomics, which is defined as

$$c_{\mathrm{product}} = \frac{(c_{\mathrm{wbt}} \cdot W_{\mathrm{bt,y}} + c_{\mathrm{wot}} \cdot W_{\mathrm{ot,y}} + c_{\mathrm{cool}} \cdot E_{\mathrm{cool,y}} + C_{\mathrm{diff,pc}} + C_{\mathrm{diff,cond1}} + C_{\mathrm{diff,cond2}})}{(W_{\mathrm{bt,y}} + W_{\mathrm{ot,y}} + E_{\mathrm{cool,y}})} \tag{44}$$

where $C_{\mathrm{diff,pc}}$, $C_{\mathrm{diff,cond1}}$ and $C_{\mathrm{diff,cond2}}$ denote the fictitious cost rates related to the utilization of dissipative components introduced by Ref [47], which are expressed as

$$C_{\mathrm{diff,pc}} = c_{23} \cdot E_{23,\mathrm{y}} - c_{22} \cdot E_{22,\mathrm{y}} = c_3 \cdot (E_3 - E_4) + Z_{\mathrm{pc}} \tag{45}$$

$$C_{\mathrm{diff,cond1}} = c_{25} \cdot E_{25,\mathrm{y}} - c_{24} \cdot E_{24,\mathrm{y}} = c_8 \cdot (E_8 - E_9) + Z_{\mathrm{cond1}} \tag{46}$$

$$C_{\mathrm{diff,cond2}} = c_{27} \cdot E_{27,\mathrm{y}} - c_{26} \cdot E_{26,\mathrm{y}} = c_{15} \cdot (E_{15} - E_{16}) + Z_{\mathrm{cond2}} \tag{47}$$

The simulation is performed under MATLAB software environment and REFPROP

9.0 [48] is employed to calculate the thermodynamic properties for the exhaust gases and the working fluids in this paper.

*3.3 Validation*

To ensure the accuracy of the calculation, validation for each cycle is considered based on the data from published literatures. The detailed comparisons between the present results and previous studies are listed in Table 5-Table 8. Note that the validation of ORC is divided into two parts, namely the separation part and the simple ORC part, respectively. And the working fluid of ORC is the same as that of ORC in the references only in this validation section. It can be seen from the tables that the simulation results in present study are in good agreement with the data from the references [49, 50, 11, 51].

## 4. Results and discussion

In this study, a commercial cogeneration engine is selected as the case study. The main parameters of the engine are listed in Table 9. It is assumed that the composition of the exhaust gases are $CO_2$, $H_2O$, $N_2$ and $O_2$ with mass fraction of 9.1%, 7.4%, 74.2% and 9.3%, respectively [4]. This assumption can be used to evaluate the properties of the exhaust gases.

Firstly, the thermodynamic performance of the proposed system is compared with those of the ones designed by Kim et al. [8] and Shu et al. [21], which focus on the waste heat recovery of engine exhaust and coolant. Then five key parameters such as the compressor pressure ratio, the compressor inlet temperature, the BC turbine inlet

temperature, the ORC turbine inlet pressure and the ejector primary flow pressure, are selected to examine the thermodynamic and exergoeconomic performances of the CCP system. In the process of parametric analysis, when one parameter is varied, the others parameters are kept constant. The detailed conditions of the simulation are listed in Table 10.

*4.1. Comparison of the proposed system and current systems*

Table 11 lists the comparison between the proposed system and the ones presented in references [8, 21]. It can be observed that total the net energy output （$W_{net}$+$Q_{cool}$） of proposed system is much higher than the maximum net energy output of the systems exhibited in the references under the same heat source conditions. Thus, the proposed system is more efficient to make better use of engine waste heat.

*4.2 Thermodynamic and exergoeconomic analyses*

Fig. 2 shows the effect of compressor pressure ratio on net power outputs, refrigeration capacity and exergy efficiency of the system.

It can be observed that net power output of Brayton cycle increases firstly and then decreases with the increasing compressor pressure ratio. The reason for this is that an increase in compressor pressure ratio leads to increases in enthalpy drop through the turbine and power consumption by pump. The former case can account for the initial rise of power output through the BC turbine. But as the effect of increasing power consumption through compressor gradually outweighs that of the increasing power produced by BC turbine, a decrease in net power output of BC occurs.

The net power output of organic Rankine cycle decreases when the compressor pressure ratio increases. Since an increase in compressor pressure ratio results in a reduction in BC turbine outlet temperature, then the ORC turbine inlet temperature decreases. In addition, the mass flow rate of vapor generated by the vapor generator 1 also decreases due to the reducing BC turbine outlet temperature. Hence the net power output of ORC decreases.

In ejector refrigeration cycle, the refrigeration capacity increases with the increasing pressure ratio of compressor. As the compressor pressure ratio increases, the compressor outlet temperature rises under the condition of invariable compressor inlet temperature. Since the terminal temperature difference of gas heater outlet is given as a constant, the exhaust gas temperature at vapor generator 2 inlet rises, leading to a higher mass flow rate of primary flows. Then the refrigeration capacity increases.

Since the exergy output of refrigeration capacity is much smaller than that of net power production in terms of exergy analysis, the exergy efficiency of the system is more related to the net power output of the system. With the decreasing net power output of the system ($W_{net}$), the exergy efficiency decreases.

Fig. 3 illustrates the effect of compressor pressure ratio on average cost per unit of exergy product for the turbines, the evaporator and the overall system.

It can be seen that the average cost per unit of exergy product for BC turbine rises with the increasing compressor pressure ratio. This can be explained by dividing that cost into two parts, namely the fuel-exergy-related part and the equipment-cost-related

part from Eq. (41). For the fuel-exergy-related part, it can be seen from Fig .3 that the average cost per unit of exergy fuel ($c_1$) increases with rise of pressure ratio in the compressor, leading to an increase in the fuel-exergy-related part of $c_{wbt}$. Referring to the equipment-cost-related part, the effect of the rise in BC turbine cost outweighs that of the BC turbine power output, resulting in an increase in equipment-cost-related part of $c_{wbt}$. Combining the effects of these two parts, the average cost per unit of product for BC turbine increases.

As the pressure ratio of compressor increases, the average cost per unit of exergy product for ORC turbine rises. Considering the fuel-exergy-related part, it can be observed from Fig. 3 that as the compressor pressure ratio increases, the average cost per unit of exergy fuel for ORC turbine rises ($c_7$), thus an increase in the fuel-exergy-related part of $c_{wot}$ occurs. For the equipment-cost-related part, the impact of the increase in ORC turbine cost is greater than that of the ORC turbine power output, leading to a rise in equipment-cost-related part of $c_{wot}$. As a result, the average cost per unit of product for ORC turbine increases.

The average cost per unit of refrigeration capacity exergy output decreases with the increasing compressor pressure ratio. The reason for this is that an increase in compressor pressure ratio leads to a decrease in the average cost per unit of exergy fuel for the evaporator, as shown in Fig. 3, reducing the numerical value of fuel-exergy-related part of $c_{cool}$. For the equipment-cost-related part, the impact of the decrease in evaporator cost is greater than that of the refrigeration capacity exergy output, resulting in a decrease in equipment-cost-related part of $c_{cool}$. Therefore, a

drop in average cost per unit of refrigeration capacity exergy output occurs.

As for the fictitious cost rate of precooler ($C_{\mathrm{diff,pc}}$), both the exergy transfer rate and the equipment cost declines, due to the reduction of temperature at the BC turbine outlet caused by the increasing compressor pressure ratio. In addition, the average cost per unit of the exergy for the flow across the precooler ($c_3$, which is equal to $c_1$) increases, as is shown in Fig. 3. Integrating the variations of all the parameters related to $C_{\mathrm{diff,pc}}$ in Eq. (45) , the fictitious cost rate of precooler increases. Referring to the fictitious cost rate associated with condenser 1 ($C_{\mathrm{diff,cond1}}$), the reduced mass flow rate of working fluid in ORC leads to decreases in exergy transfer rate and equipment cost of condenser 1. Meanwhile, it can be observed that the average cost per unit of exergy for the flow across the condenser 1 ($c_8$, which is equal to $c_7$) rises with the increasing compressor pressure ratio. Thus the fictitious cost rate of condenser 1 increases. For the fictitious cost rate associated with condenser 2 ($C_{\mathrm{diff,cond2}}$), the higher mass flow rate of primary flows is generated by vapor generator 2 when compressor pressure ratio increases, causing the exergy transfer rate and equipment cost of condenser 2 to increase. Even though the average cost per unit of exergy for the flow across the condenser 2 ($c_{15}$, which is equal to $c_{18}$) decreases, the fictitious cost rate of condenser 2 still increases.

The average cost per unit of exergy product of the overall system ($c_{\mathrm{product}}$) increases with the increasing compressor pressure ratio, after analyzing the variations for all parameters related to $c_{\mathrm{product}}$ in Eq. (44).

Fig. 4 shows the effect of compressor inlet temperature on net power outputs,

refrigeration capacity and exergy efficiency of the system.

It can be observed that the net power output of BC decreases with the increasing compressor inlet temperature. The reason is that as the compressor inlet temperature increases, the enthalpy increment in compressor and the mass flow rate of BC both increase, resulting in the increasing consumption of power through compressor. In the BC turbine, the power generation increases due to the raised mass flow rate of $CO_2$. Combining these factors, the net power output of BC decreases.

The net power output of ORC increases when the compressor inlet temperature rises. It is because an increase in mass flow rate of $CO_2$ leads to a larger amount of vapor produced by vapor generator 1, causing the power output of ORC turbine to rise. Thus the net power output of ORC increases.

In the ejector refrigeration cycle, the refrigeration capacity exergy output increases with the rising compressor inlet temperature. Since the rise of compressor inlet temperature enables the compressor outlet temperature to increase, the exhaust gases temperature at the gas heater outlet rises due to the constant terminal temperature difference at gas heater outlet. Therefore, more vapor is generated by vapor generator 2, contributing to an increase in the refrigeration capacity exergy output.

Considering the variations of net power outputs and the refrigeration capacity exergy output of the system, the exergy efficiency decreases.

Fig. 5 illustrates the effect of compressor inlet temperature on average cost per unit of exergy product for the turbines, the evaporator and the overall system.

It can be seen that the average cost per unit of exergy product for BC turbine

increases with the rising compressor inlet temperature. As the compressor inlet temperature rises, the fuel-exergy-related part of $c_{wbt}$ increases due to the rised average cost per unit of exergy fuel ($c_1$) for BC turbine. While for the equipment-cost-related part, the effect of the rise in BC turbine power output is greater than that of the BC turbine cost, leading to a decrease in equipment-cost-related part of $c_{wbt}$. Integrating the effects of these two parts, the average cost per unit of exergy product for BC turbine increases.

As shown in Fig. 5, the average cost per unit of exergy fuel ($c_7$) for ORC turbine increases when the compressor inlet temperature increases, resulting in an increase in fuel-exergy-related part of $c_{wot}$. Referring to the equipment-cost-related part, the impact of the increase in ORC turbine power output outweighs that of the ORC turbine cost when the compressor inlet temperature rises, leading to a decrease in the equipment-cost-related part of $c_{wot}$. As a result, the average cost per unit of exergy product for ORC turbine increases with the rising temperature of compressor inlet.

With the rising compressor inlet temperature, the average cost per unit of product for the evaporator decreases. For the fuel-exergy-related part, a decrease in the average cost per unit of exergy fuel ($c_{18}$) leads to a decrease in the fuel-exergy-related part of $c_{cool}$ for the evaporator. Considering the equipment-cost-related part, since the impact of the rise in refrigeration capacity exergy output is greater than that of the increase in evaporator cost, the equipment-cost-related part of $c_{cool}$ decreases. Therefore, $c_{cool}$ decreases.

Referring to the fictitious cost rate of precooler ($C_{diff,pc}$), as the compressor inlet

temperature increases, both the exergy transfer rate and the equipment cost for the precooler decrease. It can also be seen from the figure that the average cost per unit of exergy for the flow across the precooler ($c_3$, which is equal to $c_1$) increases slightly. Hence the fictitious cost rate of precooler decreases. For the fictitious cost rate of condenser 1 ($C_{\mathrm{diff,cond1}}$), a rise in mass flow rate of ORC leads to increases in both exergy transfer rate and the equipment cost of the condenser 1. Moreover, the average cost per unit of exergy for the flow across the condenser 1 ($c_8$, which is equal to $c_7$) increases. Thus the fictitious cost rate of the condenser 1 rises. Concerning the fictitious cost rate of condenser 2 ($C_{\mathrm{diff,cond2}}$), a larger mass flow rate of primary flow enables the exergy transfer rate and the equipment cost of the condenser 2 to increase. Whereas, the average cost per unit of exergy for the flow across the condenser 2 ($c_{15}$, which is equal to $c_{18}$) decreases. As a result, the fictitious cost rate of condenser 2 increases.

After analyzing the variations of all parameters related to $c_{\mathrm{product}}$ in Eq. (44), the average cost per unit of exergy product for the overall system increases with the increasing compressor inlet temperature.

Fig. 6 shows the effect of BC turbine inlet temperature on net power outputs, refrigeration capacity and exergy efficiency of the system.

As BC turbine inlet temperature increases, the mass flow rate of $CO_2$ decreases, leading to declines in both power generation through BC turbine and energy consumption by compressor. Since the impact of the decrease in power consumption by compressor is greater than that of the decrease in power generation through BC

turbine, the net power output of BC increases.

The net power output of ORC decreases when the BC turbine inlet temperature rises. Since the decrease in mass flow rate of $CO_2$ leads to a decrease in mass flow rate of working fluid for ORC, the power output of ORC turbine decreases, causing the net power output of ORC to decrease.

It can also be observed that the refrigeration capacity exergy output keeps constant with the increasing BC turbine inlet temperature. As BC turbine inlet temperature increases, the operation conditions of the compressor are not changed. Due to the constant terminal temperature difference of the gas heater outlet, the exhaust gases temperature stays unchanged at the vapor generator 2 inlet, resulting in the unchanged parameters of refrigeration cycle. Hence the refrigeration capacity exergy output is constant.

Finally, the exergy efficiency of the overall system increases with the rise of BC turbine inlet temperature, due to the increased net power output of the system ($W_{net}$).

Fig. 7 illustrates the effect of BC turbine inlet temperature on average cost per unit of exergy product for the turbines, the evaporator and the overall system.

It can be seen that the average cost per unit of exergy product for BC turbine decreases with the increasing BC turbine inlet temperature. As the BC turbine inlet temperature rises, the fuel-exergy-related part of $c_{wbt}$ decreases due to the reduced average cost per unit of exergy fuel ($c_1$). Meanwhile, the rising BC turbine inlet temperature leads to a greater impact of the decrease in BC turbine cost than that of the BC turbine power output and hence decreases the equipment-cost-related part of

$c_{wbt}$. Combining the effects of these two parts, the average cost per unit of exergy product for BC turbine decreases.

The average cost per unit of product for ORC turbine decreases with the increase of BC turbine inlet temperature. For the fuel-exergy-related part, as the BC turbine inlet temperature rises, the average cost per unit of exergy fuel ($c_7$) decreases, resulting in a decrease of the fuel-exergy-related part for $c_{wot}$. Considering the equipment-cost-related part, the degree of reduction for the ORC turbine cost outweighs that for ORC turbine power output when the BC turbine inlet temperature rises, thus the equipment-cost-related part of $c_{wot}$ decreases. As a result, the average cost per unit of exergy product for ORC turbine decreases.

Meanwhile, the average cost per unit of refrigeration capacity exergy output keeps constant when the BC turbine inlet temperature increases, for the reason that the parameter conditions of ejector are not changed.

Referring to the fictitious cost rate of precooler ($C_{diff,pc}$), as the BC turbine inlet temperature increases, the mass flow rate of $CO_2$ decreases, leading to decreases in both exergy transfer rate and equipment cost of the precooler. In addition, the average cost per unit of exergy for the flow in the precooler ($c_3$, which is equal to $c_1$) drops, as is shown in Fig. 7. Thus $C_{diff,pc}$ decreases. For the fictitious cost rate of condenser 1 ($C_{diff,cond1}$), on one hand, the exergy transfer rate and the equipment cost decrease due to the drop in mass flow rate of working fluid. On the other hand, the average cost per unit of exergy for the flow in the condenser 1 ($c_8$, which is equal to $c_7$) decreases, as shown in Fig. 7. Hence the increase of $C_{diff,cond1}$ occurs. Considering the fictitious cost

rate of condenser 2 ($C_{diff,cond2}$), $C_{diff,cond2}$ is a constant because of the unchanged parameters in condenser 2.

Integrating the effects of all the variables related to $c_{product}$ in Eq. (44), the average cost per unit of exergy product for the overall system decreases when BC turbine inlet temperature increases.

Fig. 8 shows the effect of ORC turbine inlet pressure on net power outputs, refrigeration capacity and exergy efficiency of the system.

It can be obtained from the figure that both the net power output of BC and the refrigeration capacity of the ejector refrigeration cycle remain as constants. Since the parameters of the BC turbine, compressor and the evaporator are unrelated to the inlet pressure of ORC turbine.

An increase in ORC turbine inlet pressure leads to a decrease in the mass flow rate of working fluid and an increase in enthalpy through the turbine. Since the impact of the increase in enthalpy drop is greater than that of the decrease in the mass flow rate of working fluid across the ORC turbine, the power output of ORC turbine rises. Consequently, the net power output of ORC increases.

Integrating the effects of the net power output and the refrigeration capacity exergy, the exergy efficiency increases with the increasing ORC turbine inlet pressure.

Fig. 9 illustrates the effect of ORC turbine inlet pressure on the average cost per unit of exergy product for the turbines, the evaporator and the overall system.

It can be seen that the average cost per unit of exergy product for BC turbine increases slightly with the increasing ORC turbine inlet pressure. Since a rise in the

average cost per unit of exergy fuel for the BC turbine ($c_1$) leads to an increase in the fuel-exergy-related part of $c_{wbt}$, and the equipment-cost-related part of $c_{wbt}$ is not varied due to the constant parameters of BC turbine. The average cost per unit of exergy product for BC turbine increases.

The average cost per unit of exergy product ORC turbine decreases with the rising ORC turbine inlet pressure. For the fuel-exergy-related part, as the ORC turbine inlet pressure rises, the average cost per unit of exergy fuel for the ORC turbine ($c_7$) decreases, resulting in a decrease in the fuel-exergy-related part of $c_{wot}$. Referring to the equipment-cost-related part, since the impact of the rise in ORC turbine power output is greater than that of the increase in ORC turbine cost, the equipment-cost-related part of $c_{wot}$ also decreases. Hence the average cost per unit of exergy product for ORC turbine decreases.

With the increasing ORC turbine inlet pressure, the average cost per unit of exergy product for the evaporator remains unchanged, due to the constant average cost per unit of exergy fuel ($c_{18}$) and the unchanged parameters for the evaporator.

Referring to the fictitious cost rate of precooler ($C_{diff,pc}$), as the ORC turbine inlet pressure increases, the temperature of saturated liquid at state point 13 rises, leading to an increase in the temperature at the precooler inlet. Then the exergy transfer and the equipment cost both increase. In addition, the average cost per unit of exergy for the flow across the precooler ($c_3$, which is equal to $c_1$) increases slightly. Consequently, $C_{diff,pc}$ increases. For the fictitious cost rate of condenser 1 ($C_{diff,cond1}$), $C_{diff,cond1}$ decreases mainly because of the decrease in the average cost per unit of exergy for the

flow across the condenser 1 ($c_8$, which is equal to $c_7$). Since the parameter conditions of the condenser 2 is unchanged, the fictitious cost rate of condenser 2 ($C_{\mathrm{diff,cond2}}$) keeps constant.

Due to the combined effects of all the variables related to $c_{\mathrm{product}}$ in Eq. (44), the average cost per unit of exergy product for the overall system decreases with the increasing ORC turbine inlet pressure.

Fig. 10 shows the effect of ejector primary flow pressure on net power outputs, refrigeration capacity and exergy efficiency of the system.

It can be observed the net power outputs of BC and ORC keep as constants, for the reason that the parameters are irrelevant to the primary flow pressure of the ejector.

Since a higher ejector primary flow pressure leads to a lower mass flow rate of the primary flow across the ejector, casing a drop in the mass flow rate of the secondary flow in the evaporator. The refrigeration capacity decreases.

The exergy transfer rate in vapor generator 2 decreases with the increasing ejector primary flow pressure. Considering the variations of net power output, the refrigeration capacity exergy output and the exergy transfer rate of the system, the exergy efficiency slightly increases.

Fig. 11 illustrates the effect of ejector primary flow pressure on the average cost per unit of exergy product for the turbines, the evaporator and the overall system.

As is shown in the figure, the average costs per unit of exergy product for the BC turbine and the ORC turbine are both constants, due to the unchanged operation conditions of them.

Meanwhile, the average cost per unit of exergy product for the evaporator increases with the rising ejector primary flow pressure. As the ejector primary flow pressure increases, the average cost per unit of exergy fuel ($c_{18}$) for the evaporator rises, resulting in an increase in the fuel-exergy-related part of $c_{\mathrm{cool}}$. While for the equipment-cost-related part, the impact of the increase in evaporator cost outweighs that of the evaporator refrigeration capacity exergy output, leading to an increase in the equipment-cost-related part of $c_{\mathrm{cool}}$. Therefore, $c_{\mathrm{cool}}$ increases.

For the fictitious cost rates of the precooler and condenser 1, both $C_{\mathrm{diff,pc}}$ and $C_{\mathrm{diff,cond1}}$ keep as constants since the operation conditions of them are not changed. While $C_{\mathrm{diff,cond2}}$ decreases by the reason of the decreased mass flow rate of working fluid across the condenser 2.

Combining the effects of all parameters related to $c_{\mathrm{product}}$ in Eq. (44), the average cost per unit of exergy product for the overall system increases with the increasing ejector primary flow pressure.

In order to obtain the optimal performance of the CCP system utilized engine waste heat, a single-objective optimization is conducted by means of genetic algorithm, which is a stochastic global search method that simulates natural biological evolution. The detailed computing method of genetic algorithm can refer to Ref. [3]. The average cost per unit of exergy product for the overall system is selected the as the objective function, since it combines exergy analysis and economic principles to provide information which is critical to the design and operation of a cost-effective system. Key parameters such as compressor pressure ratio, compressor inlet pressure,

BC turbine inlet temperature, ORC turbine inlet pressure and ejector primary flow pressure are chosen as the decision variables.

The detailed ranges of key parameters and the control parameters of GA are listed in Table 12 and Table 13, respectively.

Table 14 lists the results of parameter optimization for the CCP system with the objective function of the average cost per unit of exergy product for the overall system. It can be observed that the minimum $c_{product}$ is 63.53\$/MWh$^{-1}$, and the exergy efficiency, the net power output and the Refrigeration capacity of the system are 27.63%, 282.49kW and 20.01kW, respectively. The results indicate that the exergy efficiency obtained from the exgoeconimic optimization is also desirable, and the refrigeration capacity is optimized to be lower due to the higher cost per unit of exergy product for ejector refrigeration cycle. In addition, for the compressor pressure ratio, the optimal one is located at the lower boundary. Referring to the compressor inlet temperature and the ejector primary flow pressure, the optimum ones are settled near the lower boundaries. Concerning the optimal BC turbine inlet temperature and the ORC turbine inlet pressure, both of them are located near the upper boundaries. These results imply that all the optimal values of the key parameters are in accordance with the parametric analysis.

## 5. Conclusion

In this study, a CCP system is designed for the waste heat recovery of an ICE. The effects of five key parameters (i.e. compressor pressure ratio, compressor inlet pressure, BC turbine inlet temperature, ORC turbine inlet pressure and ejector primary

flow pressure) on thermodynamic and exergoeconomic performances are examined. Then a single-objective optimization by means of GA is conducted with an objective function of the average cost per unit of exergy product. The main conclusions drawn from investigation are summarized as follows:

(1) On the basis of parametric analysis, the increases of the BC turbine inlet temperature, the ORC turbine inlet pressure and the ejector primary flow pressure have positive effects on the exergy efficiency, while the rises in compressor pressure ratio and the compressor inlet temperature are undesirable to the thermodynamic performance of the system.

(2) Referring to the exergoeconimic analysis, lower average cost per unit of exergy product for the overall system can be achieved by increasing the BC turbine inlet temperature, the ORC turbine inlet pressure and the ejector primary flow pressure. However, the rises in compressor pressure and compressor inlet temperature lead to increases in average cost per unit of exergy product for the overall system.

(3) By the single-objective optimization, the lowest average cost per unit of exergy product for the overall system is obtained, and the exergy efficiency is also desirable. In addition, all the optimal values of the key parameters are in accordance with the parametric analysis.

## Acknowledgments

The authors gratefully acknowledge the financial support by the National Natural Science Foundation of China (Grant No. 51476121) and the Fundamental Research

Funds for the Central Universities (Grant No. 2013jdgz14).

**References**

[1] A. Domingues, H. Santos, M. Costa. Analysis of vehicle exhaust waste heat recovery potential using a Rankine cycle. Energy. 49 (2013) 71-85.

[2] C. Sprouse, C. Depcik. Review of organic Rankine cycles for internal combustion engine exhaust waste heat recovery. Appl Therm Eng. 51 (2013) 711-22.

[3] Y.P. Dai, J.F. Wang, L. Gao. Parametric optimization and comparative study of organic Rankine cycle (ORC) for low grade waste heat recovery. Energy Conv Manag. 50 (2009) 576-82.

[4] I. Vaja, A. Gambarotta. Internal Combustion Engine (ICE) bottoming with Organic Rankine Cycles (ORCs). Energy. 35 (2010) 1084-93.

[5] M. Tahani, S. Javan, M. Biglari. A comprehensive study on waste heat recovery from internal combustion engines using organic rankine cycle. Therm Sci. 17 (2013) 611-24.

[6] M.G. He, X.X. Zhang, K. Zeng, K. Gao. A combined thermodynamic cycle used for waste heat recovery of internal combustion engine. Energy. 36 (2011) 6821-9.

[7] E.H. Wang, H.G. Zhang, Y. Zhao, B.Y. Fan, Y.T. Wu, Q.H. Mu. Performance analysis of a novel system combining a dual loop organic Rankine cycle (ORC) with a gasoline engine. Energy. 43 (2012) 385-95.

[8] Y.M. Kim, D.G. Shin, C.G. Kim, G.B. Cho. Single-loop organic Rankine cycles for engine waste heat recovery using both low- and high-temperature heat sources.

Energy. 96 (2016) 482-94.

[9] B.T. Liu, K.H. Chien, C.C. Wang. Effect of working fluids on organic Rankine cycle for waste heat recovery. Energy. 29 (2004) 1207-17.

[10] H. Tian, G.Q. Shu, H.Q. Wei, X.Y. Liang, L.N. Liu. Fluids and parameters optimization for the organic Rankine cycles (ORCs) used in exhaust heat recovery of Internal Combustion Engine (ICE). Energy. 47 (2012) 125-36.

[11] E.H. Wang, H.G. Zhang, B.Y. Fan, M.G. Ouyang, Y. Zhao, Q.H. Mu. Study of working fluid selection of organic Rankine cycle (ORC) for engine waste heat recovery. Energy. 36 (2011) 3406-18.

[12] Y.R. Li, M.T. Du, C.M. Wu, S.Y. Wu, C. Liu. Potential of organic Rankine cycle using zeotropic mixtures as working fluids for waste heat recovery. Energy. 77 (2014) 509-19.

[13] G.Q. Shu, Y.Y. Gao, H. Tian, H.Q. Wei, X.Y. Liang. Study of mixtures based on hydrocarbons used in ORC (Organic Rankine Cycle) for engine waste heat recovery. Energy. 74 (2014) 428-38.

[14] L. Pierobon, R. Kandepu, F. Haglind, Asme. Waste heat recovery for offshore applications. Amer Soc Mechanical Engineers, New York, 2013.

[15] G.P. Yu, G.Q. Shu, H. Tian, H.Q. Wei, L.N. Liu. Simulation and thermodynamic analysis of a bottoming Organic Rankine Cycle (ORC) of diesel engine (DE). Energy. 51 (2013) 281-90.

[16] E.W. Miller, T.J. Hendricks, H. Wang, R.B. Peterson. Integrated dual-cycle energy recovery using thermoelectric conversion and an organic Rankine bottoming

cycle. Proc Inst Mech Eng Part A-J Power Energy. 225 (2011) 33-43.

[17] C.Y. Zhang, G.Q. Shu, H. Tian, H.Q. Wei, X.Y. Liang. Comparative study of alternative ORC-based combined power systems to exploit high temperature waste heat. Energy Conv Manag. 89 (2015) 541-54.

[18] H.G. Zhang, E.H. Wang, B.Y. Fan. A performance analysis of a novel system of a dual loop bottoming organic Rankine cycle (ORC) with a light-duty diesel engine. Applied Energy. 102 (2013) 1504-13.

[19] F.B. Yang, X.R. Dong, H.G. Zhang, Z. Wang, K. Yang, J. Zhang, et al. Performance analysis of waste heat recovery with a dual loop organic Rankine cycle (ORC) system for diesel engine under various operating conditions. Energy Conv Manag. 80 (2014) 243-55.

[20] B.C. Choi, Y.M. Kim. Thermodynamic analysis of a dual loop heat recovery system with trilateral cycle applied to exhaust gases of internal combustion engine for propulsion of the 6800 TEU container ship. Energy. 58 (2013) 404-16.

[21] G.Q. Shu, L.N. Liu, H. Tian, H.Q. Wei, G.P. Yu. Parametric and working fluid analysis of a dual-loop organic Rankine cycle (DORC) used in engine waste heat recovery. Applied Energy. 113 (2014) 1188-98.

[22] J. Song, C.W. Gu. Performance analysis of a dual-loop organic Rankine cycle (ORC) system with wet steam expansion for engine waste heat recovery. Applied Energy. 156 (2015) 280-9.

[23] Y.D. Zhou, Y.D. Wu, F. Li, L.J. Yu. Performance analysis of zeotropic mixtures for the dual-loop system combined with internal combustion engine. Energy Conv

Manag. 118 (2016) 406-14.

[24] Y.C. Liang, G.Q. Shu, H. Tian, H.Q. Wei, X.Y. Liang, L.N. Liu, et al. Theoretical analysis of a novel electricity-cooling cogeneration system (ECCS) based on cascade use of waste heat of marine engine. Energy Conv Manag. 85 (2014) 888-94.

[25] S. Wang, K. Bai, Y. Xie, J. Di, S. Cheng. Analysis of Combined Power and Refrigeration Generation Using the Carbon Dioxide Thermodynamic Cycle to Recover the Waste Heat of an Internal Combustion Engine. Mathematical Problems in Engineering. 2014 (2014) 1-12.

[26] A. Moisseytsev, J.J. Sienicki. Investigation of alternative layouts for the supercritical carbon dioxide Brayton cycle for a sodium-cooled fast reactor. Nucl Eng Des. 239 (2009) 1362-71.

[27] B.Y. Song, W.L. Zhuge, R.C. Zhao, X.Q. Zheng, Y.J. Zhang, Y. Yin, et al. An investigation on the performance of a Brayton cycle waste heat recovery system for turbocharged diesel engines. J Mech Sci Technol. 27 (2013) 1721-9.

[28] A.D. Akbari, S.M.S. Mahmoudi. Thermoeconomic analysis & optimization of the combined supercritical CO2 (carbon dioxide) recompression Brayton/organic Rankine cycle. Energy. 78 (2014) 501-12.

[29] G. Besagni, R. Mereu, F. Inzoli. Ejector refrigeration: A comprehensive review. Renew Sust Energ Rev. 53 (2016) 373-407.

[30] G.Q. Shu, X.N. Li, H. Tian, X.Y. Liang, H.Q. Wei, X. Wang. Alkanes as working fluids for high-temperature exhaust heat recovery of diesel engine using

organic Rankine cycle. Applied Energy. 119 (2014) 204-17.

[31] N.A. Lai, M. Wendland, J. Fischer. Working fluids for high-temperature organic Rankine cycles. Energy. 36 (2011) 199-211.

[32] D. Butrymowicz, K. Smierciew, J. Karwacki, J. Gagan. Experimental investigations of low-temperature driven ejection refrigeration cycle operating with isobutane. Int J Refrig-Rev Int Froid. 39 (2014) 196-209.

[33] J. Zhang, H.G. Zhang, K. Yang, F.B. Yang, Z. Wang, G.Y. Zhao, et al. Performance analysis of regenerative organic Rankine cycle (RORC) using the pure working fluid and the zeotropic mixture over the whole operating range of a diesel engine. Energy Conv Manag. 84 (2014) 282-94.

[34] F.P. Incropera, D.P. DeWitt. Fundamentals of heat and mass transfer. Wiley, New York, 2002.

[35] D.Q. Kern. Process heat transfer. McGraw-Hill, New York, 1950.

[36] K.E. Gungor, R.H.S. Winterton. Simplified general correlation for saturated flow boiling and comparisons of correlations with data. Chem Eng Res Des. 65 (1987) 148-56.

[37] M.M. Shah. A general correlation for heat transfer during film condensation inside pipes. International Journal of Heat and Mass Transfer. 22 (1979) 547-56.

[38] S.J. Zarrouka, M.H. Purnanto. Geothermal steam-water separators: Design overview. Geothermics. 53 (2015) 236-54.

[39] R. Turton. Analysis, synthesis, and design of chemical processes. Prentice Hall, Upper Saddle River, N.J, 2009.

[40] D. Lozowski. Start online account with the exclusive online plant cost index and get full archive access to chemical engineering. http://www.chemengonline.com/pci-home, Chemecal Engineering.

[41] L.G. Farshi, S.M.S. Mahmoudi, M.A. Rosen. Exergoeconomic comparison of double effect and combined ejector-double effect absorption refrigeration systems. Applied Energy. 103 (2013) 700-11.

[42] M.H. Yang, R.H. Yeh. Economic performances optimization of the transcritical Rankine cycle systems in geothermal application. Energy Conv Manag. 95 (2015) 20-31.

[43] A. Bejan, G. Tsatsaronis, M.J. Moran. Thermal design and optimization. Wiley, New York, 1996.

[44] D. Tempesti, D. Fiaschi. Thermo-economic assessment of a micro CHP system fuelled by geothermal and solar energy. Energy. 58 (2013) 45-51.

[45] F. Velez, J.J. Segovia, M.C. Martin, G. Antonlin, F. Chejne, A. Quijano. A technical, economical and market review of organic Rankine cycles for the conversion of low-grade heat for power generation. Renew Sust Energ Rev. 16 (2012) 4175-89.

[46] M. Sadeghi, S.M.S. Mahmoudi, R.K. Saray. Exergoeconomic analysis and multi-objective optimization of an ejector refrigeration cycle powered by an internal combustion (HCCI) engine. Energy Conv Manag. 96 (2015) 403-17.

[47] A. Lazzaretto, G. Tsatsaronis. SPECO: A systematic and general methodology for calculating efficiencies and costs in thermal systems. Energy. 31 (2006) 1257-89.

[48] E.W. Lemmon, M.L. Huber, M.O. McLinden. NIST Standard Reference

Database 23, Reference Fluid Thermodynamic and Transport Properties (REFPROP). version 90, National Institute of Standards and Technology. (2010).

[49] Y.M. Kim, C.G. Kim, D. Favrat. Transcritical or supercritical CO2 cycles using both low- and high-temperature heat sources. Energy. 43 (2012) 402-15.

[50] M. Yari. Exergetic analysis of various types of geothermal power plants. Renew Energy. 35 (2010) 112-21.

[51] B. Zheng, Y.W. Weng. A combined power and ejector refrigeration cycle for low temperature heat sources. Sol Energy. 84 (2010) 784-91.

**Figure captions:**

**Fig. 1** Schematic diagram of the CCP system

**Fig. 2** Effect of compressor pressure ratio on thermodynamic performance of the system

**Fig. 3**. Effect of compressor pressure ratio on exergoeconomic performance of the system

**Fig. 4** Effect of compressor inlet temperature on thermodynamic performance of the system

**Fig. 5** Effect of compressor inlet temperature on exergoeconomic performance of the system

**Fig. 6** Effect of BC turbine inlet temperature on thermodynamic performance of the system

**Fig. 7** Effect of BC turbine inlet temperature on exergoeconomic performance of the system

**Fig. 8** Effect of ORC turbine inlet pressure on thermodynamic performance of the system

**Fig. 9** Effect of ORC turbine inlet pressure on exergoeconomic performance of the system

**Fig. 10** Effect of ejector primary flow pressure on thermodynamic performance of the system

**Fig. 11** Effect of ejector primary flow pressure on exergoeconomic performance of the system

**Table 1** Energy relations for each component

| Component | Energy relations |
|---|---|
| Gas heater | $M_a \cdot (h_a - h_b) = M_1 \cdot (h_1 - h_5)$ |
| BC turbine | $W_{bt} = M_1 \cdot (h_1 - h_2) = M_1 \cdot (h_1 - h_{2s}) \cdot \eta_{bt}$ |
| Vapor generator 1 | $M_2 \cdot (h_2 - h_3) = M_6 \cdot (h_6 - h_{13})$ |
| Precooler | $M_3 \cdot (h_3 - h_4) = M_{22} \cdot (h_{23} - h_{22})$ |
| Compressor | $W_{comp} = M_4 \cdot (h_5 - h_4) = M_4 \cdot (h_{5s} - h_4) / \eta_{comp}$ |
| ORC turbine | $W_{ot} = M_7 \cdot (h_7 - h_8) = M_7 \cdot (h_7 - h_{8s}) \cdot \eta_{ot}$ |
| Condenser 1 | $M_8 \cdot (h_8 - h_9) = M_{24} \cdot (h_{25} - h_{24})$ |
| Pump1 | $W_{pump1} = M_9 \cdot (h_{10} - h_9) = M_9 \cdot (h_{10s} - h_9) / \eta_{pump1}$ |
| Preheater | $M_d \cdot (h_d - h_e) = M_{10} \cdot (h_{11} - h_{10})$ |
| Separator | $M_{11} \cdot h_{11} = M_{12} \cdot h_{12} + M_{13} \cdot h_{13}$ |
| Vapor generator 2 | $M_b \cdot (h_b - h_c) = M_{14} \cdot (h_{14} - h_{21})$ |
| Ejector | $M_{15} \cdot h_{15} = M_{14} \cdot h_{14} + M_{19} \cdot h_{19}$ |
| Evaporator | $M_{19} \cdot (h_{19} - h_{18}) = M_{28} \cdot (h_{28} - h_{29})$ |
| Throttle valve | $h_{18} = h_{17}$ |

**Table 2** Exergy analysis for each component in the CCP system

| Component | $E_F$ | $E_P$ | $E_D$ | $E_L$ |
|---|---|---|---|---|
| Gas heater | $E_a - E_b$ | $E_1 - E_5$ | $E_a + E_5 - E_b - E_1$ | / |
| BC turbine | $E_1 - E_2$ | $W_{bt}$ | $E_1 - E_2 - W_{bt}$ | / |
| Vapor generator 1 | $E_2 - E_3$ | $E_6 - E_{13}$ | $E_2 + E_{13} - E_3 - E_6$ | / |
| Precooler | / | / | $E_3 + E_{22} - E_4 - E_{23}$ | $E_{23} - E_{22}$ |
| Compressor | $W_{comp}$ | $E_5 - E_4$ | $W_{comp} + E_4 - E_5$ | / |
| ORC turbine | $E_7 - E_8$ | $W_{ot}$ | $E_7 - E_8 - W_{ot}$ | / |
| Condenser 1 | / | / | $E_8 + E_{24} - E_9 - E_{25}$ | $E_{25} - E_{24}$ |
| Pump 1 | $W_{pump1}$ | $E_{10} - E_9$ | $W_{pump1} + E_9 - E_{10}$ | / |
| Preheater | $E_d - E_e$ | $E_{11} - E_{10}$ | $E_d + E_{10} - E_e - E_{11}$ | / |
| Separator | $E_{11}$ | $E_{12} + E_{13}$ | $E_{11} - E_{12} - E_{13}$ | / |
| Vapor generator 2 | $E_b - E_c$ | $E_{14} - E_{21}$ | $E_b + E_{21} - E_c - E_{14}$ | / |
| Ejector | $E_{14} + E_{19}$ | $E_{15}$ | $E_{14} + E_{19} - E_{15}$ | / |
| Condenser 2 | / | / | $E_{15} + E_{26} - E_{16} - E_{27}$ | $E_{27} - E_{26}$ |
| Valve | / | / | $E_{17} - E_{18}$ | / |
| Evaporator | $E_{18} - E_{19}$ | $E_{29} - E_{28}$ | $E_{18} + E_{28} - E_{19} - E_{29}$ | / |
| Pump 2 | $W_{pump2}$ | $E_{21} - E_{20}$ | $W_{pump2} + E_{20} - E_{21}$ | / |

**Table 3** Constants for equipment costs calculation [39]

| Constant | value | Constant | value | Constant | value |
|---|---|---|---|---|---|
| $K_{1,he}$ | 4.3247 | $K_{2,pump}$ | 0.0536 | $C_{3,he}$ ($P_{he}$<0.5) | 0 |
| $K_{2,he}$ | -0.3030 | $K_{3,pump}$ | 0.1538 | $C_{1,pump}$ (1<$P_{pump}$<10) | − 0.3935 |
| $K_{3,he}$ | 0.1634 | $B_{1,he}$ | 1.63 | $C_{2,pump}$ (1<$P_{pump}$<10) | 0.3957 |
| $K_{1,turb}$ | 2.7051 | $B_{2,he}$ | 1.66 | $C_{3,pump}$ (1<$P_{pump}$<10) | − 0.00226 |
| $K_{2,turb}$ | 1.4398 | $B_{1,sep}$ | 2.25 | $C_{1,pump}$ ($P_{pump}$<1) | 0 |
| $K_{3,turb}$ | -0.1776 | $B_{2,sep}$ | 1.82 | $C_{2,pump}$ ($P_{pump}$<1) | 0 |
| $K_{1,comp}$ | 2.2897 | $B_{1,pump}$ | 1.89 | $C_{3,pump}$ ($P_{pump}$<1) | 0 |
| $K_{2,comp}$ | 1.3604 | $B_{2,pump}$ | 1.35 | $F_{M,he}$ | 1.0 |
| $K_{3,comp}$ | -0.1027 | $C_{1,he}$ (0.5<$P_{he}$<14) | 0.03881 | $F_{BM,turb}$ | 3.5 |
| $K_{1,sep}$ | 3.4974 | $C_{2,he}$ (0.5<$P_{he}$<14) | 0.11272 | $F_{BM,comp}$ | 2.7 |
| $K_{2,sep}$ | 0.4485 | $C_{3,he}$ (0.5<$P_{he}$<14) | 0.08183 | $F_{M,sep}$ | 1.0 |
| $K_{3,sep}$ | 0.1074 | $C_{1,he}$ ($P_{he}$<0.5) | 0 | $F_{M,pump}$ | 2.2 |
| $K_{1,pump}$ | 3.3892 | $C_{2,he}$ ($P_{he}$<0.5) | 0 | | |

**Table 4** Cost balance and auxiliary cost relations for each component [43]

| Component | Cost balance | Auxiliary equation |
|---|---|---|
| Gas heater | $c_1 \cdot E_{1,y} + c_b \cdot E_{b,y} = c_5 \cdot E_{5,y} + c_a \cdot E_{a,y} + Z_{gh}$ | $c_a = c_b$ |
| BC turbine | $c_2 \cdot E_{2,y} + c_{bt} \cdot W_{bt,y} = c_1 \cdot E_{1,y} + Z_{bt}$ | $c_1 = c_2$ |
| Vapor generator 1 | $c_3 \cdot E_{3,y} + c_6 \cdot E_{6,y} = c_2 \cdot E_{2,y} + Z_{vp1}$ | $c_2 = c_3$ |
| Precooler | $c_{23} \cdot E_{23,y} + c_4 \cdot E_{4,y} = c_{22} \cdot E_{22,y} + c_3 \cdot E_{3,y} + Z_{pc}$ | $c_3 = c_4$ |
| Compressor | $c_5 \cdot E_{5,y} = c_4 \cdot E_{4,y} + c_{comp} \cdot W_{comp,y} + Z_{comp}$ | / |
| ORC turbine | $c_1 \cdot E_{8,y} + c_{ot} \cdot W_{ot,y} = c_7 \cdot E_{7,y} + Z_{ot}$ | $c_7 = c_8$ |
| Condenser 1 | $c_{25} \cdot E_{25,y} + c_9 \cdot E_{9,y} = c_{24} \cdot E_{24,y} + c_8 \cdot E_{8,y} + Z_{cond1}$ | $c_8 = c_9$ |
| Pump 1 | $c_{10} \cdot E_{10,y} = c_9 \cdot E_{9,y} + c_{pump1} \cdot W_{pump1,y} + Z_{pump1}$ | / |
| Preheater | $c_e \cdot E_{e,y} + c_{11} \cdot E_{11,y} = c_d \cdot E_{d,y} + c_{10} \cdot E_{10,y} + Z_{ph}$ | $c_d = c_e$ |
| Separator | $c_{12} \cdot E_{12,y} + c_{13} \cdot E_{13,y} = c_{11} \cdot E_{11,y} + Z_{sep}$ | $c_{12} = c_{13}$ |
| Vapor generator2 | $c_{14} \cdot E_{14,y} + c_c \cdot E_{c,y} = c_{21} \cdot E_{21,y} + c_b \cdot E_{b,y} + Z_{vp2}$ | $c_b = c_c$ |
| Ejector | $c_{15} \cdot E_{15,y} = c_{14} \cdot E_{14,y} + c_{19} \cdot W_{19,y}$ | / |
| Condenser 2 | $c_{27} \cdot E_{27,y} + c_{16} \cdot E_{16,y} = c_{26} \cdot E_{26,y} + c_{15} \cdot E_{15,y} + Z_{cond2}$ | $c_{15} = c_{16}$ |
| Valve | / | $c_{17} = c_{18}$ |
| Evaporator | $c_{29} \cdot E_{29,y} + c_{19} \cdot E_{19,y} = c_{28} \cdot E_{28,y} + c_{18} \cdot E_{18,y} + Z_{evap}$ | $c_{18} = c_{19}$ |
| Pump 2 | $c_{21} \cdot E_{21,y} = c_{20} \cdot E_{20,y} + c_{pump2} \cdot W_{pump2,y} + Z_{pump2}$ | / |

**Table 5** Data comparison with Ref. [49] for the validation of Brayton cycle

| $T$/℃ | Present | Ref. | $P$/MPa | Present | Ref. | $W$/kJ kg$^{-1}$ | Present | Ref. |
|---|---|---|---|---|---|---|---|---|
| $T_1$ | 600 | 600 | $P_1$ | 20 | 20 | $W_{turb1}$ | 169.85 | 169.9 |
| $T_2$ | 449.05 | 449.0 | $P_2$ | 5.73 | 5.73 | $W_{comp}$ | 50.45 | 50.4 |
| $T_4$ | 20.01 | 20 | $P_4$ | 5.73 | 5.73 | | | |
| $T_5$ | 114.55 | 114.6 | $P_5$ | 20 | 20 | | | |

**Table 6** Data comparison with Ref. [50] for the validation of separation part in ORC

| State | *T*/℃ | | *P*/MPa | | *H*/kJ kg$^{-1}$ | | *S*/ kJ kg$^{-1}$K$^{-1}$ | | *M*/kg s$^{-1}$ | |
|---|---|---|---|---|---|---|---|---|---|---|
| | Present | Ref. | Present | Ref. | Present | Ref. | Present | Ref. | Present | Ref. |
| 11 | 163 | 163 | 0.6665 | 0.6665 | 990.14 | 990 | 2.664 | 2.664 | 1 | 1 |
| 12 | 163 | 163 | 0.6665 | 0.6665 | 2760.7 | 2761 | 6.724 | 6.725 | 0.1456 | 0.1454 |
| 13 | 163 | 163 | 0.6665 | 0.6665 | 688.43 | 688.7 | 1.972 | 1.973 | 0.8544 | 0.8546 |

**Table 7** Data comparison with Ref. [11] for the validation of the conventional part ORC

| Fluid | | $P_7$ /MPa | $T_7$ /℃ | $P_9$ /MPa | $T_9$ /℃ | $M$ /kg $s^{-1}$ | $W_{turb2}$ /kW | $W_{pump2}$ /kW | $\eta_{th}$ /% |
|---|---|---|---|---|---|---|---|---|---|
| R245fa | Present | 1.4293 | 107.75 | 0.1874 | 31.29 | 0.5041 | 10.615 | 0.621 | 8.40 |
| | Ref. | 1.4293 | 107.75 | 0.1874 | 31.29 | 0.4988 | 10.615 | 0.615 | 8.38 |
| R123 | Present | 1.5835 | 132.85 | 192.6 | 46.85 | 0.5457 | 10.652 | 0.652 | 8.88 |
| | Ref. | 1.5835 | 132.85 | 192.6 | 46.85 | 0.5458 | 10.652 | 0.644 | 8.6 |

**Table 8** Data comparison with Ref. [51] for the validation of ejector refrigeration cycle

| State | $T$/℃ | | $P$/MPa | | $H$/kJ kg$^{-1}$ | | $S$/ kJ kg$^{-1}$K$^{-1}$ | | $M$/kg s$^{-1}$ | |
|---|---|---|---|---|---|---|---|---|---|---|
| | Present | Ref. | Present | Ref. | Present | Ref. | Present | Ref. | Present | Ref. |
| 14 | 67.85 | 67.85 | 401 | 401 | 458.13 | 459.1 | 1.806 | 1.809 | 1 | 1 |
| 15 | 163 | 163 | 147.42 | 149 | 443.55 | 446.9 | 1.819 | 1.830 | 1.3175 | 1.3331 |
| 18 | 6.85 | 6.85 | 71.75 | 73 | 232.26 | 232.7 | 1.116 | 1.117 | 0.3135 | 0.3331 |
| 19 | 6.85 | 6.85 | 71.54 | 73 | 409.48 | 410.1 | 1.749 | 1.751 | 0.3135 | 0.3331 |

**Table 9** Main parameters of engine [4]

| Term | Value | Unit |
|---|---|---|
| Electrical power output | 2928 | kW |
| Engine speed | 1000 | rpm |
| Exhaust gas temperature | 470 | ℃ |
| Exhaust mass flow | 15673 | kg/h |
| Engine jacket temperatures | 79/90 | ℃ |
| Engine jacket flow | 90 | $m^3/h$ |

**Table 10** Simulation conditions of the CCP system

| Term | Value | Unit |
|---|---|---|
| Environment temperature | 15 | ℃ |
| Environment pressure | 0.1013 | MPa |
| Compressor inlet pressure | 0.3 | MPa |
| Compressor inlet temperature | 40 | ℃ |
| Compressor pressure ratio | 4 | / |
| BC turbine inlet temperature | 420 | ℃ |
| ORC turbine inlet pressure | 1.2 | MPa |
| Ejector primary flow inlet pressure | 1.5 | MPa |
| Terminal temperature difference at gas heat outlet | 15 | ℃ |
| Terminal temperature difference at vapor generator 1 inlet | 50 | ℃ |
| Terminal temperature difference at vapor generator 2 inlet | 65 | ℃ |
| Pinch point temperature difference in vapor generator 1 | 10 | ℃ |
| Pinch point temperature difference in vapor generator 2 | 60 | ℃ |
| Condensation temperature of condenser 1 | 35 | ℃ |
| Condensation temperature of condenser 2 | 25 | ℃ |
| Evaporation temperature of evaporator | 5 | ℃ |
| Isentropic efficiency of BC turbine | 80 | % |
| Isentropic efficiency of ORC turbine | 80 | % |
| Isentropic efficiency of compressor | 80 | % |
| Isentropic efficiency of pump 1 | 70 | % |

| | | |
|---|---|---|
| Isentropic efficiency of pump 2 | 70 | % |
| Inlet temperature of cooling water | 15 | ℃ |
| Outlet temperature of cooling water in precooler | 25 | ℃ |
| Outlet temperature of cooling water in condenser 1 | 30 | ℃ |
| Outlet temperature of cooling water in condenser 2 | 25 | ℃ |

**Table 11** Comparison between the proposed system and current systems

| Term | Ref. [8] | Present | Ref. [21] | Present |
|---|---|---|---|---|
| Engine power output/kW | 26.7 | 26.7 | 235.8 | 235.8 |
| Exhaust temperature/℃ | 689 | 689 | 519 | 519 |
| Engine coolant temperature/℃ | 100 | 100 | 83.3 | 83.3 |
| Exhaust mass flow rate/$kgh^{-1}$ | 118 | 118 | 990.79 | 990.79 |
| Net power output/kW | 5.63 | 6.38 | 36.77 | 33.79 |
| Cooling capacity/kW | 0 | 0.96 | 0 | 7.52 |
| Total net energy output/kW | 5.63 | 7.34 | 36.77 | 41.31 |

**Table 12** Ranges of the decision variables

| Decision variables | Range |
|---|---|
| compressor pressure ratio | 3-4.6 |
| compressor inlet temperature/℃ | 35-45 |
| BC turbine inlet temperature/℃ | 380-440 |
| ORC turbine inlet pressure/MPa | 0.5-1.4 |
| ejector primary flow pressure | 1.5-2.5 |

**Table 13** Control parameters of GA

| Tuning parameters | Value |
|---|---|
| Population size | 20 |
| Crossover probability | 0.8 |
| Mutation probability | 0.01 |
| Stop generation | 200 |

**Table 14** Single-objective optimization results

| Term | Value | Unit |
|---|---|---|
| Compressor pressure ratio | 3 | / |
| Compressor inlet temperature | 36.242 | ℃ |
| BC turbine inlet temperature | 435.404 | ℃ |
| ORC turbine inlet pressure | 1.363 | MPa |
| Ejector primary flow pressure | 1.556 | MPa |
| Net power output | 282.49 | kW |
| Refrigeration capacity | 20.01 | kW |
| Exergy efficiency | 27.63 | % |
| Average cost rate per unit of exergy product | 63.53 | $ $(MWh)^{-1}$ |

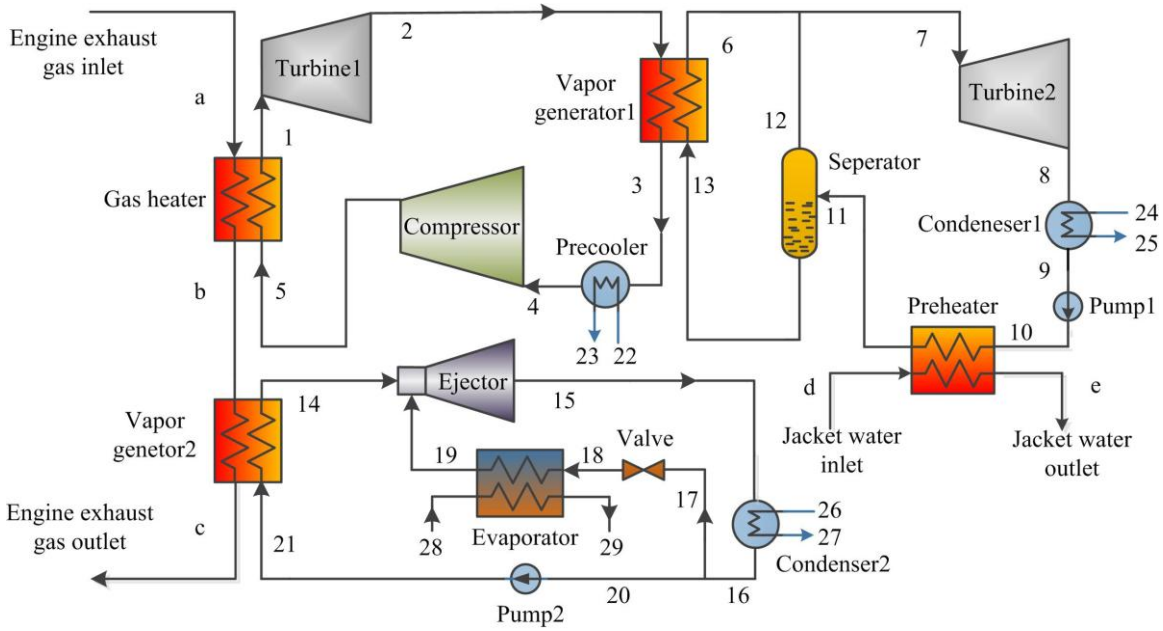


**Fig. 1** Schematic diagram of the CCP system

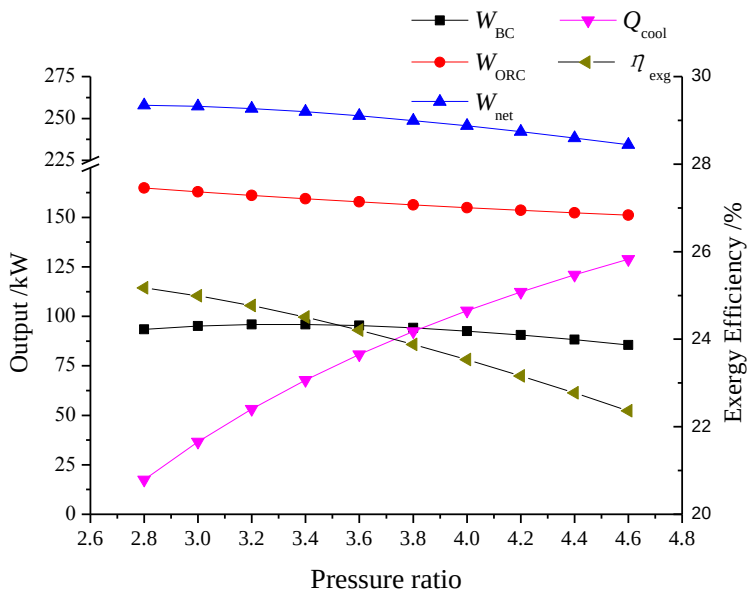


**Fig. 2** Effect of compressor pressure ratio on thermodynamic performance of the system

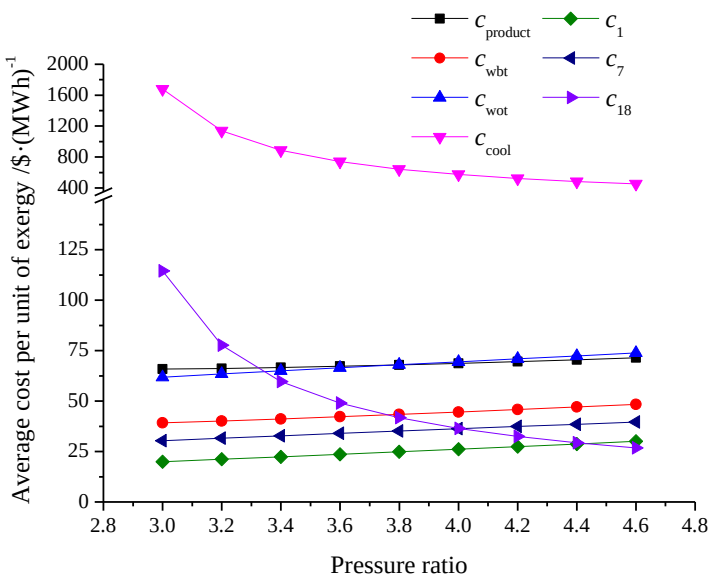


**Fig. 3** Effect of compressor pressure ratio on exergoeconomic performance of the system

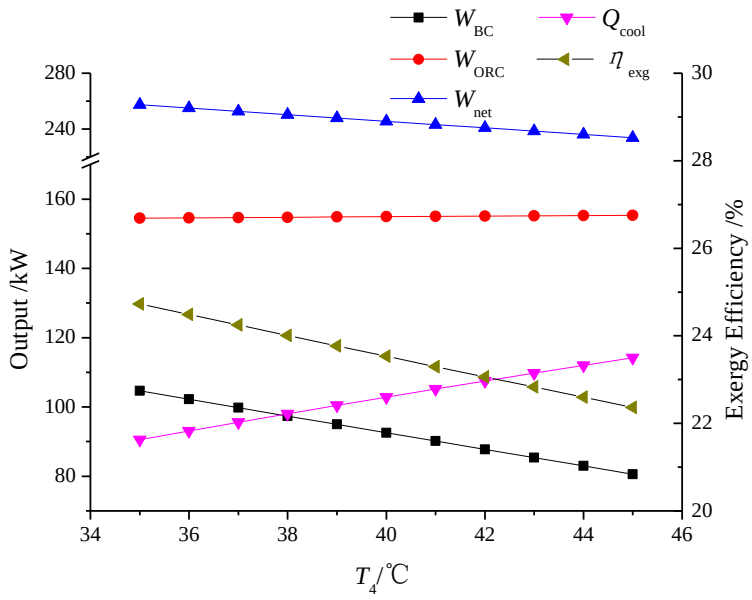


**Fig. 4** Effect of compressor inlet temperature on thermodynamic performance of the system

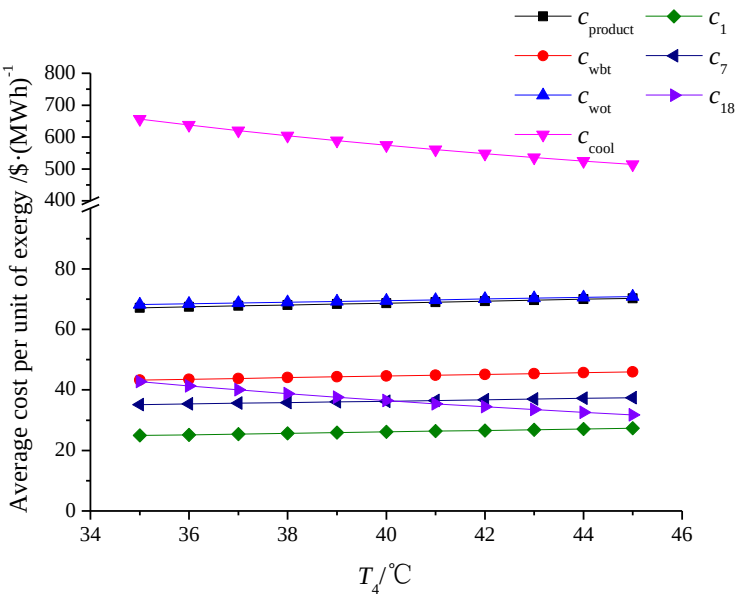


**Fig. 5** Effect of compressor inlet temperature on exergoeconomic performance of the system

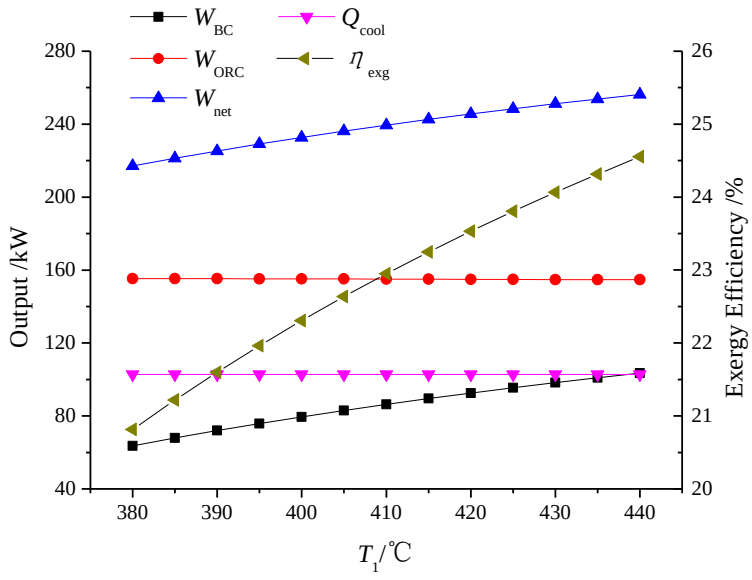


**Fig. 6** Effect of BC turbine inlet temperature on thermodynamic performance of the system

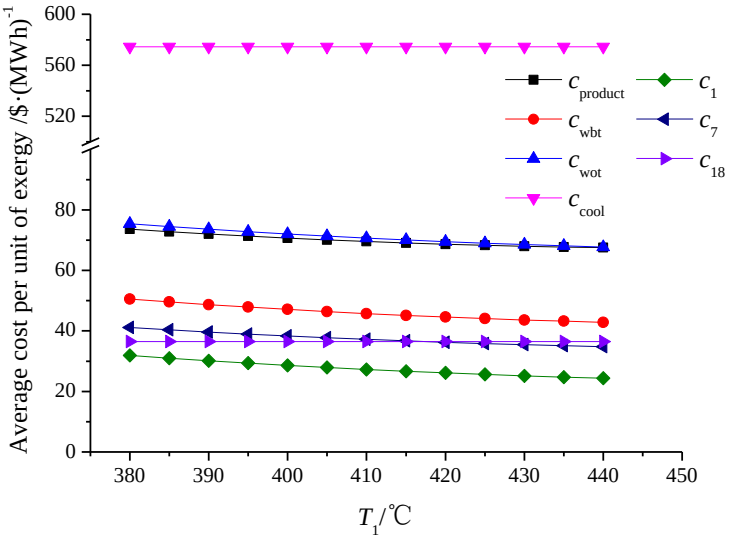


**Fig. 7** Effect of BC turbine inlet temperature on exergoeconomic performance of the system

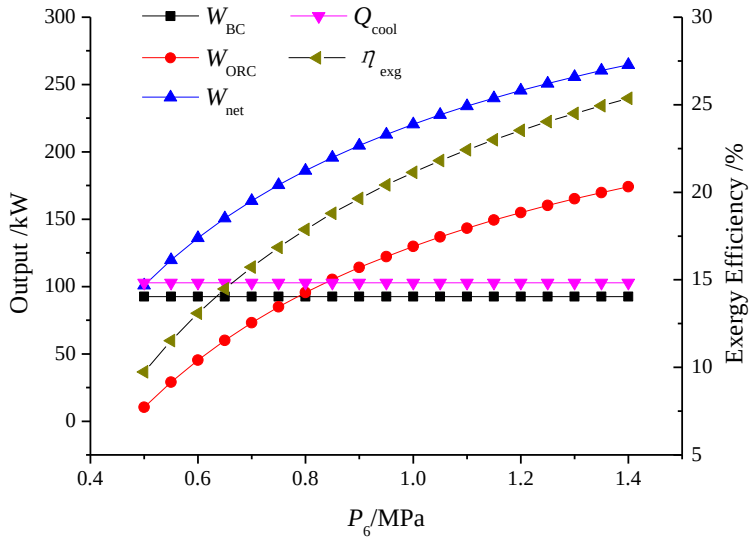


**Fig. 8** Effect of ORC turbine inlet pressure on thermodynamic performance of the system

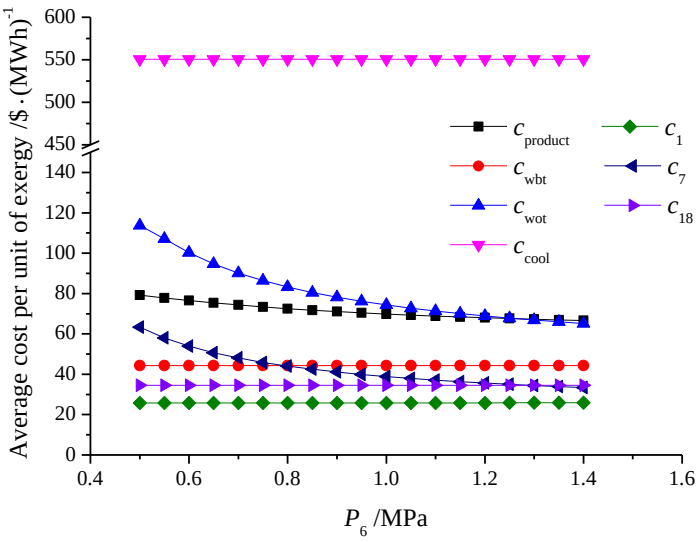


**Fig. 9** Effect of ORC turbine inlet pressure on exergoeconomic performance of the system

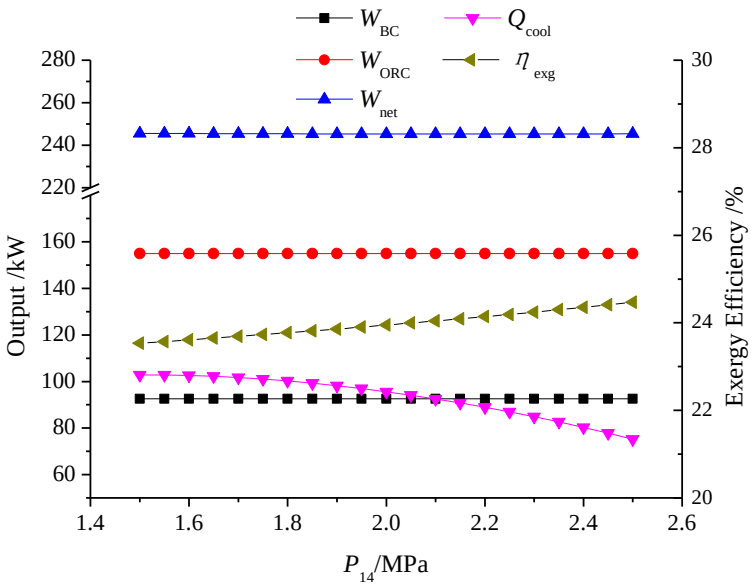


**Fig. 10** Effect of ejector primary flow pressure on thermodynamic performance of the system

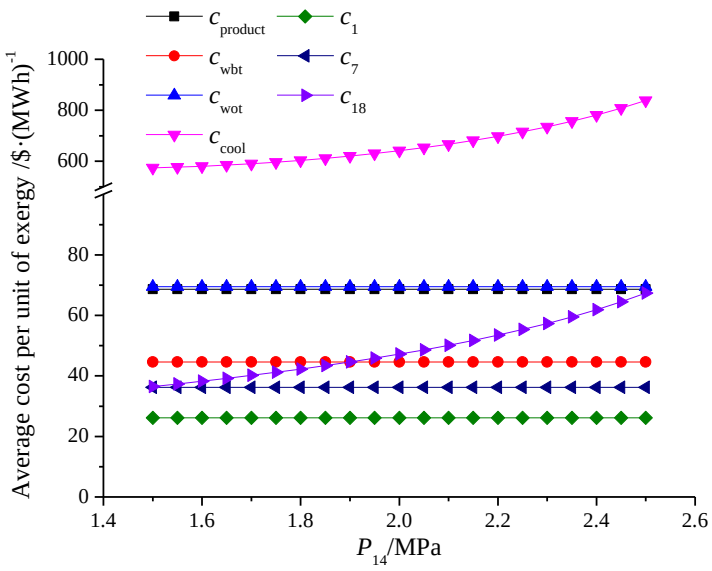


**Fig. 11** Effect of ejector primary flow pressure on exergoeconomic performance of the system

# Response to reviewers

Paper No. ECM-D-16-02929, Energy Conversion and Management

Title: Thermo-economic analysis and optimization of a combined cooling and power (CCP) system for engine waste heat recovery

Dear reviewers,

First of all, we would like to thank you very much for your review of our paper entitled "Thermo-economic analysis and optimization of a combined cooling and power (CCP) system for engine waste heat recovery", and for all your kind comments and recommendations. These comments and recommendations help us to make better modifications and improve the quality of the paper. We have modified the manuscript accordingly in the revised manuscript. Please find below our responses and explanations for your comments and questions.

**Reviewer #1**

This paper developed a combined cooling and power (CCP) system, which consisted of a CO2 Brayton cycle (BC), an organic Rankine cycle (ORC) and an ejector refrigeration cycle, to recover the waste heat from an internal combustion engine. And the exergoeconomic analysis and optimization are conducted to obtain the optimum system performance. This paper is very interesting and offers a new contribution to the field of CCP system integration. The writing is also good. I think this paper can be accepted if some comments are considered to further improve the quality of the paper.

1. The INTRODUCTION section should be shortened.

The INTRODUCTION section was reviewed again and modified to be shorter.

2. Compared to R123 and R245fa, why is Isobutane used as working fluid in ORC system?

Firstly, alkanes such as isobutane and isopentane are more suitable for high-temperature organic Rankine cycles, since higher working temperature can be reached by these compounds, as mentioned in Ref. [30,31]. Secondly, isobutane is a natural fluid which has zero ODP (Ozone Depletion Potential) and much lower value of GWP (Greenhouse Warming Potential) than those of R123 and R245fa.

**Reviewer #2**

The authors combined a CO2 Brayton cycle (BC), an organic Rankine cycle (ORC) and an ejector refrigeration cycle for the cascade utilization of waste heat from an internal combustion engine. Results show that the increases of the BC turbine inlet temperature, the ORC turbine inlet pressure and the ejector primary flow pressure are benefit to both thermodynamic and exergoeconimic performances of the CCP system. The contents of this paper are informative and valuable in the fields of heat recovery. Thermodynamic analysis and design process are very detail in this paper. However, there are still needs to make more in-depth consideration in practice. Furthermore, the authors should compare the difference between the results of present research and

experimental studies in order to demonstrate the availability of this study. I suggest that this paper must be modified to comply with the requirements of International Journal. Some recommendations need to clarify and revise as follows.

Firstly, since the proposed system is more complex, and the experimental test needs to undergo a long period of installation, test and operation, there is no experimental data for the proposed system right now. Therefore, it is unable to compare the difference between the results of present study and experimental studies. Secondly, it is important for the proposed system to conduct a theoretical analysis which can provide a support for building an experiment system. Of course, if the results of present study are compared with the experimental studies, the demonstration of the availability of the proposed system would be more convincing. So, we will build the experimental platform of the proposed system after conducting the theoretical investigations.

1. The contents of this paper is too long should be reasonably concise. I recommend Table 5-8 can be deleted.

The paper was reviewed again and modified to be more concise. Table 5-8 are used for verification and the detailed explanation is presented in the discussion of the next issue.

2. As shown in Table 5-8, you verified your data with references (Ref. [44, 45, 11, 46]) that results in these references are from simulation or calculation method. Therefore, the verification method is not meaningful. This verification does not establish the

practicality and feasibility for your research. Such verification method can only prove that your calculations are correct and can not verify the accuracy and reliability.

If the verification method is based on experimental studies, it will be better to verify the accuracy and reliability. However, as the proposed system is more complex, and the experimental test needs to undergo a long period of installation, test and operation, there is no experimental data for the proposed system right now. So, what we can only do now is to verify the simulation data with references.

3. The working fluid of ORC is R245fa and R123 in Table 7. However, your working fluid (in page 11) is isobutane (R600a). Why different working fluids get similar results? The verification results are very contradictory.

In the process of the verification, the working fluid of ORC in present study is the same as that of the comparison object in the reference. Thus, the working fluids of ORC in Table 7 are R245fa and R123, respectively. When the verification is completed, isobutane is used as the working fluid for further calculation of the proposed system.

4. Please confirm the unit of "Engine speed" in Table 9. Is rpm?

The unit of “Engine speed” is rpm, and it was modified in the revised manuscript.

5. The "Environment temperature" (second column of Table 10) should be revised to "Environment pressure.

It was corrected in the revised manuscript.

6. In Table 9, "Electrical power output" is correct? Or should the mechanical power output?

A commercial cogeneration engine which produces electrical power is selected as the case study in this paper. So "Electrical power output" is correct in Table 9.

7. The exhaust gas temperature is 470 ℃ in Table 9, however, the BC turbine inlet temperature is 420 ℃ in Table 10. 50 ℃ in recovery temperature difference seems unreasonable. Please explain the principles of the assumptions.

420℃ is the initial setting value of the BC turbine inlet temperature. In fact, that temperature could be higher. In the parametric analyses of Fig.6 and Fig.7, the BC turbine inlet temperatures both reach 440℃.

8. Table 10 is incomplete, misplaced data in page 55.

There is no unit for compressor pressure ratio, a symbol of "/" is added in Table 10

9. You should clearly illustrate the contribution or innovation of this paper. The heat recovery system is feasible or effective to compare with other heat recovery system? The simulation and calculation procedures that you proposed are more accuracy? The system design that you proposed is more efficient than the current heat recovery system (References)?

Comparisons between the proposed system and the current systems presented in references for the waste heat recovery of the exhaust and coolant from engines were added and highlighted in the paper, as shown in Table 11. It can be observed that the total net energy output of proposed system is much higher than the maximum net energy output of the systems exhibited in the references. Thus, the proposed system is more efficient to make better use of engine waste heat.

**Reviewer #3**

Literature review appears to be complete, but there can be find more article on this issues.

More references referring to the issues were added in the revised manuscript.

System description provides a detailed description of the combined cooling and power system (CCP).

For mathematical model there are no signs d and e in Figure 1 present in the formula no. 9.

Figure 1 was modified and the signs of d and e were presented.

Not been clarified for the validation of the model present in the Table 8 the difference between obtained data and the reference data. State 15 T / ° C Present value is 46.79

and Reference value is 163.

The error was corrected in Table 8.

There are errors in the text, e.g. Line 281 on page 18, line 536 on page 30.

The manuscript was reviewed again and errors were corrected and highlighted.

The results were discussed in detail.

# Thermo-economic analysis and optimization of a combined cooling and power (CCP) system for engine waste heat recovery

Jiaxi Xia, Jiangfeng Wang*, Juwei Lou, Pan Zhao, Yiping Dai

Institute of Turbomachinery, State Key Laboratory of Multiphase Flow in Power Engineering, School of Energy and Power Engineering,

Xi'an Jiaotong University, Xi'an, China, 710049, China

## Abstract

A combined cooling and power (CCP) system is developed, which comprises a $CO_2$ Brayton cycle (BC), an organic Rankine cycle (ORC) and an ejector refrigeration cycle for the cascade utilization of waste heat from an internal combustion engine. By establishing mathematical model to simulate the overall system, thermodynamic analysis and exergoeconomic analysis are conducted to examine the effects of five key parameters including the compressor pressure ratio, the compressor inlet temperature, the BC turbine inlet temperature, the ORC turbine inlet pressure and the ejector primary flow pressure on system performance. What's more, a single-objective optimization by means of genetic algorithm (GA) is carried out to search the optimal system performance from viewpoint of exergoeconomic. Results show that the increases of the BC turbine inlet temperature, the ORC turbine inlet pressure and the ejector primary flow pressure are benefit to both thermodynamic and exergoeconimic performances of the CCP system. However, the rises in compressor pressure ratio and compressor inlet temperature will lead to worse system performances. By the single-objective optimization, the lowest average cost per unit of exergy product for

the overall system is obtained.

**Key words**: Internal combustion engine; Waste heat recovery; Brayton cycle; Organic Rankine cycle; Ejector refrigeration cycle; Optimization.

**Nomenclature**

| | |
|---|---|
| $A$ | area, $m^2$ |
| $Bo$ | boiling number |
| $C$ | cost rate, \$ $year^{-1}$ |
| $CRF$ | capital recovery factor |
| $CEPCI$ | chemical engineering plant cost index |
| $c$ | average cost per unit of exergy, \$ $(MWh)^{-1}$ |
| $c_p$ | specific heat, kJ kg $K^{-1}$ |
| $D$ | diameter, m |
| $E$ | exergy flow rate, kJ $s^{-1}$ |
| $f$ | friction factor |
| $G$ | mass velocity, kg $m^{-2}$ $s^{-1}$ |
| $h$ | enthalpy, kJ $kg^{-1}$ |
| $i_{eff}$ | interest rate |
| $L$ | length, m |
| $M$ | mass flow rate, kg $s^{-1}$ |
| $n$ | lifetime, year |
| $Nu$ | Nusselt number |

| | |
|---|---|
| $P$ | pressure, MPa |
| $Pr$ | Prandtl number |
| $P_t$ | center distance between tubes, m |
| $p_r$ | reduced pressure |
| $Q$ | heat transfer rate, kW |
| $Q_{vs}$ | volumetric steam flow, $m^3\ s^{-1}$ |
| $q_m$ | average imposed wall heat flux, $W\ m^{-2}$ |
| $r$ | enthalpy of vaporization, $kJ\ kg^{-1}$ |
| $s$ | entropy, $kJ\ kg^{-1}\ K^{-1}$ |
| $T$ | temperature, K |
| $U$ | overall heat transfer coefficient, $W\ m^{-2}\ K^{-1}$ |
| $V$ | volume, $m^3$ |
| $v$ | velocity, $m\ s^{-1}$ |
| $W$ | power, kW |
| $X$ | size or capacity parameter |
| $x$ | vapor quality |
| $Z$ | annually levelized cost value, $\$\ year^{-1}$ |
| | |
| *Greek symbol* | |
| $\alpha$ | convection heat transfer coefficient, $W\ m^{-2}\ K^{-1}$ |
| $\eta$ | efficiency, % |
| $\lambda$ | thickness, m |

| | |
|---|---|
| $\rho$ | density, kg $m^{-3}$ |
| $\mu$ | dynamic viscosity, $m^2$ $s^{-1}$ |
| $\pi$ | compressor pressure ratio |
| | |
| *subscript* | |
| 1-29 | state points |
| a-e | state points |
| 0 | ambient state |
| BC | Brayton cycle |
| BM | bare module |
| bt | BC turbine |
| cf | cold fluid |
| cnd | condensation |
| comp | compressor |
| cool | refrigeration capacity output |
| cond1 | condenser 1 |
| cond2 | condenser 2 |
| D | destruction |
| eq | equipment |
| es | equivalent diameter |
| evp | evaporation |
| exg | exergy |

| | |
|---|---|
| evap | evaporator |
| F | fuel |
| gh | gas heater |
| he | heat exchanger |
| hf | hot fluid |
| in | inside |
| ip | inlet pipe |
| L | loss |
| l | liquid |
| M | material |
| m | mean |
| ORC | Organic Rankine cycle |
| ot | ORC turbine |
| out | outside |
| P | product; pressure |
| pc | precooler |
| pump | pump |
| pump1 | pump 1 |
| pump2 | pump 2 |
| sp | single-phase |
| sep | separator |
| turb | turbine |

| | |
|---|---|
| v | vapor |
| w | tube wall |
| wbt | power produced by BC turbine |
| wot | power produced by ORC turbine |

## 1. Introduction

With the development of world economy and industry, the energy shortage and environmental problems caused by fossil fuel consumption have attracted more and more attention. Internal combustion engines（ICES）which act as the major source of motive power, consume a large proportion of petroleum resources in the world. It is reported that only about one-third of the fuel energy in the internal combustion engines is converted into mechanical work, the remaining energy is mainly wasted by rejecting heat to the environment through the exhaust and the coolant [1]. Therefore, it would be of great significance to recover the waste heat effectively from Internal combustion engines.

The technique of organic Rankine cycle (ORC) has been proven to be a potential method to convert the engine waste heat into power, since it presents some advantages of operation flexibility and desirable efficiency [2, 3]. Much work has been carried out on the ORC configurations for the engine waste heat recovery. Vaja et al. [4] examined three different ORC setups, namely a simple cycle only recovering engine exhaust gases, a simple cycle recovering both exhaust gases and engine cooling water with a preheater and a cycle with regeneration. Tahani et al. [5] introduced two

different kinds of ORC including the preheat and two-stage configurations for the waste heat recovery of engine exhaust gases and coolant. He et al. [6] developed a combined thermodynamic system which contains two cycles: an ORC for the recovery of waste heat from high temperature exhaust gases and the lubricant, a Kalina cycle for the recovery of waste heat from cooling water. Wang et al. [7] studied the thermal performance of a dual-loop ORC coupled with a gasoline engine. Kim et al. [8] proposed a highly efficient single-loop ORC for the waste heat recovery of exhaust gases and coolant from a gasoline vehicle. Since the choice of working fluids had a great influence on thermodynamic performance of an ORC [9], other researchers had put their focuses on working fluid selection [10-13], considering both pure working fluids and zeotropic mixtures for ORCs used in waste heat recovery of ICEs.

Regarding all these studies mentioned above, the heat exchanges between exhaust gases and organic working fluids were conducted directly, that may cause decompositions of organic working fluids, due to the high temperature of exhaust gases (about 450-600℃) and the low decomposition temperatures of organic working fluids (about 200-300℃). In order to avoid this issue, an intermediate loop with thermal oil is placed between the exhaust gases and the ORC [14, 15]. Although the stability and safety of the system could be improved through this method, the great amount of high-temperature exhaust gases heat is not exploited at all. Several studies has been performed on exploring novel dual-loop systems combined ORCs with other thermodynamic cycles for engine waste heat recovery. Mliller et al. [16] developed a

system that combined ORC with thermoelectric conversion. Through a thermoelectric generator (TEG), the high temperature exhaust heat was converted into power, and the working fluid of ORC was preheated. But the application of this combined system is constrained due to the low energy conversion capacity of TEG [17]. Zhang et al. [18] analyzed the characteristics of a dual loop ORC system which was combined with a vehicular light-duty diesel engine. Yang et al. [19] explored system performance of the dual loop ORC system used for diesel engine waste heat recovery under various operating conditions. Choi et al. [20] presented a dual-loop power generation system including an upper trilateral cycle with water and a bottoming ORC. The former utilized the waste heat from the high-temperature exhaust gases discharged by a marine engine, and the latter reused the turbine exhaust heat of the upper cycle and the low-temperature exhaust gases waste heat. Shu et al. [21] designed a novel dual-loop ORC system which consists of a high-temperature (HT) loop and a low-temperature (LT). The HT loop was a steam Rankine cycle used for the waste heat recovery of the high-temperature part of exhaust gases, while the LT loop was an organic Ranking cycle recovering the coolant heat, the turbine exhaust heat from HT loop and the waste heat from low-temperature part of exhaust gases. With regard to the same dual-loop ORC system, Song et al. [22] considered the exploiting of wet steam expansion by applying a screw expander to the HT loop, and investigated the effect of the HT loop parameters on LT loop. Zhou et al. [23] studied the dual-loop ORC with zeotropic mixtures as the working fluid in the low temperature loop.

For the sake of satisfying the diverse consumers' demands, the combined cooling

and power (CCP) concept is also introduced for the engine waste heat recovery by a number of researchers. Liang et al. [24] developed a power and cooling cogeneration system which included an ORC and an absorption refrigeration cycle to utilize the exhaust gases heat of a marine engine. Wang [25] integrated the transcritical $CO_2$ refrigeration cycle with the supercritical $CO_2$ cycle to recover the waste heat of an ICE, producing both cooling and power energy.

However, for the dual-loop ORCs, most of the recent studies only considered the steam Rankine cycle as the HT loop for the heat recovery of high-temperature exhaust gases, neglecting the Brayton cycle, which has been proven to be suitable for recovering waste heat from high-temperature heat source, due to its highly efficiency, small structure and simply layout [26-28]. Even though Zhang et al. [17] have done some work about this, the waste heat recovery of the engine coolant was not taken into account, and the detailed parameter analysis including both HT-loop and LT-loop were not given. Meanwhile, in order to avoid the issue of the mismatching mass flow rate which is caused by the setting in series of the preheater utilized engine coolant heat and the evaporator utilized the residual heat of HT loop, only a part of engine coolant heat could be recovered [4, 5, 21]. What's more, few studies conducted the performance from the viewpoint of exergoeconomic for the system used for engine waste heat recovery. Referring to the CCP systems, little information has been published concerning their applications to recover both exhaust gases heat and coolant heat from engines.

In this study, an organic Rankine cycle coupled with a $CO_2$ Brayton cycle is

111 considered. In order to utilize the energy source more efficiently, an ejector
112 refrigeration cycle is added as well, since it can utilize low-grade heat sources and has
113 advantages of lower costs, higher reliability and simpler operation [29]. Therefore, a
114 combined cooling and power (CCP) system is designed to recover the waste heat of
115 an engine. The $CO_2$ Brayton cycle is used to recover the waste heat of the high
116 temperature exhaust gases, the organic Rankine cycle with a separator is utilized to
117 make full use of the coolant heat and the residual heat of Brayton cycle, while the
118 ejector refrigeration cycle is applied to reuse the waste heat of the low temperature
119 exhaust gases. The effects of five key parameters on thermodynamic and
120 exergoeconimic performances of the CCP system are examined. Furthermore, a
121 single-objective optimization by means of genetic algorithm is carried out to obtain a
122 better system performance.

123 ## 2. System description

124 The CCP system designed for this study is shown in Fig. 1. It consists of a $CO_2$
125 Brayton cycle (BC), an organic Rankine cycle (ORC), and an ejector refrigeration
126 cycle, which produces both power and refrigeration simultaneously. The high
127 temperature exhaust gases are firstly delivered to the gas heater to drive the BC.
128 Cooled $CO_2$ from the precooler is compressed to supercritical state by compressor,
129 and then passes through the gas heater to absorb heat, becoming high temperature and
130 high pressure vapor. The supercritical $CO_2$ enters to BC turbine where it expands to
131 produce power, and the $CO_2$ exhaust is cooled by the vapor generator 1 and precooler
132 in turn to complete the $CO_2$ Brayton cycle.

For the sake of recovering residual heat of $CO_2$ exhaust from the BC turbine, the bottoming loop (ORC) is coupled to the upper loop (BC) via vapor generator 1. Liquid organic working fluid from condenser 1 is pressured by pump 1 and delivered to the preheater, where it is heated by jacket water and becomes two-phase state. The two-phase working fluid is then delivered to separator and separated into saturated vapor and saturated liquid. After the separation process, saturated liquid goes through vapor generator 1 to absorb heat from $CO_2$ exhaust, producing superheated vapor. Then the superheated vapor is mixed with the saturated vapor from separator, and expands through the ORC turbine for power generation. At last, the exhaust from the ORC turbine is condensed to be liquid.

The ejector refrigeration cycle is used to recover the residual heat energy of exhaust gases after releasing heat through the gas heater. Liquid working fluid is divided into two parts after the condensation process in condenser 2. One part of working fluid enters pump 2 to be pumped to vapor generator 2, producing superheated vapor by absorbing heat from exhaust gas. The other part of working fluid passes through the throttle valve, being vaporized to vapor state in evaporator by absorbing heat from the cooling side, producing cooling capacity. After that, these two parts of working fluids are mixed in the ejector, and then enter condenser 2 to be condensed to liquid.

Isobutane is selected as the working fluid for Organic Rankine cycle and ejector refrigeration cycle, since it is suitable for high-temperature ORCs [30, 31] and has good performance in thermodynamic and environmental fields [32]. In addition, water at ambient temperature is chosen as the coolant in the precooler and condensers.

## 3. Mathematical models and performance criteria

In order to simplify the simulation of the system, several assumptions are employed as follows:

(1) The system reaches a steady state.

(2) The pressure losses in pipes are neglected and there is a 2% pressure drop in each heat exchanger.

(3) The heat losses in each component are not taken into account.

(4) The working fluid at the condenser outlet is saturated liquid. And the state of evaporator outlet is saturated vapor.

(5) The isentropic efficiencies of turbines and compressor are 80%, and those of pumps are set to be 70%.

(6) The exhaust temperature at the outlet of vapor generator 2 is confined to be over 110℃, in order to avoid the low-temperature corrosion [33].

### *3.1 Thermodynamic analysis*

#### *3.1.1 Energy analysis*

The mathematical model of energy analysis for each component is established based on the principles of mass and energy conservation, the equations are given by

$$\sum M_{\text{in}} = \sum M_{\text{out}} \tag{1}$$

$$\sum Q - \sum W = \sum M_{\text{out}} \cdot h_{\text{out}} - \sum M_{\text{in}} \cdot h_{\text{in}} \tag{2}$$

The detailed energy balance equations for the CCP system components are listed in Table 1.

176 The net power output of Brayton cycle is expressed as

177 $$W_{\mathrm{BC}} = W_{\mathrm{bt}} - W_{\mathrm{comp}} \tag{3}$$

178 The net power output of organic Rankine is calculated as

179 $$W_{\mathrm{ORC}} = W_{\mathrm{ot}} - W_{\mathrm{pump1}} \tag{4}$$

180 The net power output of system is given by

181 $$W_{\mathrm{net}} = W_{\mathrm{bt}} + W_{\mathrm{ot}} - W_{\mathrm{comp}} - W_{\mathrm{pump1}} - W_{\mathrm{pump2}} \tag{5}$$

182 The cooling capacity output is

183 $$Q_{\mathrm{cool}} = M_{28} \cdot (h_{28} - h_{29}) \tag{6}$$

184 *3.1.2 Exergy analysis*

185 Exergy is the maximum theoretical work obtainable from an overall system
186 consisting of a system and the environment as the system comes into equilibrium with
187 the environment (passes to the dead state). The exergy flow rate of a fluid at *k*th state
188 point is expressed as

189 $$E_{\mathrm{k}} = M_{\mathrm{k}} \cdot [(h_{\mathrm{k}} - h_0) - T_0 \cdot (s_{\mathrm{k}} - s_0)] \tag{7}$$

190 where the subscript 0 denotes the state of ambient conditions.

191 The exergy rate balance equation for each component is written as

192 $$E_{\mathrm{F}} = E_{\mathrm{P}} + E_{\mathrm{D}} + E_{\mathrm{L}} \tag{8}$$

193 The detailed calculations of $E_{\mathrm{F}}$, $E_{\mathrm{P}}$, $E_{\mathrm{D}}$ and $E_{\mathrm{L}}$ for each component in the CCP
194 system are listed in Table 2.

195 The exergy efficiency is used to evaluate the thermodynamic performance of the
196 system, which is given by

$$\eta_{\mathrm{exg}} = \frac{W_{\mathrm{net}} + E_{\mathrm{cool}}}{(E_{\mathrm{a}} - E_{\mathrm{c}}) + (E_{\mathrm{d}} - E_{\mathrm{e}})} \tag{9}$$

where $E_{\mathrm{cool}}$ denotes the exergy rate of refrigeration process in the evaporator, which is equal to $(E_{29} - E_{28})$.

### *3.2 Exergoeconomic analysis*

#### *3.2.1 Size of main equipments*

*1) Areas of heat exchangers*

In this study, all heat exchangers are set as shell-and-tube type. Single-phase heat transfer process occurs in the gas heater and the precooler, two-phase heat transfer process takes place in the evaporator, while both single-phase and two-phase heat transfer processes are conducted in the vapor generators and condensers. As the thermodynamic properties of the working fluid will undergo changes in heat convection heat transfer process, this process is discretized to many subsections for each heat exchanger. For one subsection, the properties of working fluid are assumed to be constant. The heat transfer equation for each subsection is given by

$$Q_{\mathrm{i}} = U_{\mathrm{i}} \cdot A_{\mathrm{i}} \cdot \Delta t_{\mathrm{i}} \tag{10}$$

where $\Delta t_{\mathrm{i}}$ is the log-mean temperature difference (LMTD)

$$\Delta t_{\mathrm{i}} = \frac{(T_{\mathrm{hf,i+1}} - T_{\mathrm{cf,i+1}}) - (T_{\mathrm{hf,i}} - T_{\mathrm{cf,i}})}{\ln \dfrac{T_{\mathrm{hf,i+1}} - T_{\mathrm{cf,i+1}}}{T_{\mathrm{hf,i}} - T_{\mathrm{cf,i}}}} \tag{11}$$

The total heat transfer coefficient for each subsection is calculated as

$$\frac{1}{U_{\mathrm{i}}} = \frac{1}{\alpha_{\mathrm{hf,i}}} + \frac{\delta}{\lambda} + \frac{1}{\alpha_{\mathrm{cf,i}}} \tag{12}$$

For single-phase flow, the convection heat transfer coefficient at the tube side is [34]

$$\alpha_{\mathrm{s,in}} = \frac{\lambda_{\mathrm{f}}}{D_{\mathrm{in}}}\left[\frac{\frac{f}{8}\cdot Re\cdot Pr}{12.7\cdot\left(\frac{f}{8}\right)^{0.5}\cdot\left(Pr^{\frac{2}{3}}-1\right)+1.07}\right] \tag{13}$$

In Eq. (13), *f*, *Re* and *Pr* denote the Darcy friction factor, the Reynolds number and the Prandtl number, respectively, which are defined as

$$f = (0.790\ln Re - 1.64)^{-2} \tag{14}$$

$$\mathrm{Re} = \frac{G_{\mathrm{in}} D_{\mathrm{in}}}{\mu} \tag{15}$$

$$\mathrm{Pr} = \frac{c_{\mathrm{p}}\mu}{\lambda} \tag{16}$$

where $G_{\mathrm{in}}$ is the mass velocity of the flow inside the tube, being given by

$$G_{\mathrm{in}} = \frac{4M}{N\cdot\pi\cdot {D_{\mathrm{in}}}^2} \tag{17}$$

The convection heat transfer coefficient for single-phase at the shell side is calculated by [35]

$$\alpha_{\mathrm{s,out}} = 0.36\cdot\frac{\lambda}{D_{\mathrm{es}}}\cdot\left(\frac{D_{\mathrm{es}}\cdot u\cdot\rho}{\mu}\right)^{0.55}\cdot \mathrm{Pr}^{1/3}\cdot\left(\frac{\mu}{\mu_w}\right)^{0.14} \tag{18}$$

where $D_{\mathrm{es}}$ is the equivalent diameter of the shell-side flow channel defined as

$$D_{es} = \frac{1.10P_{\mathrm{t}}^2}{D_{\mathrm{out}}} - D_{\mathrm{out}} \tag{19}$$

The heat transfer process of the two-phase flow consists of the evaporation and the condensation processes. It is assumed that the organic fluid flows inside the tube for the vapor generators, condensers and evaporator, then the evaporation heat transfer

coefficient is given by [36]

$$\alpha_{\mathrm{tp,evp}} = 0.023\left[\frac{G(1-x)d}{\mu_{\mathrm{l}}}\right]^{0.8} \mathrm{Pr}_{\mathrm{l}}^{0.4}\cdot\frac{\lambda_{\mathrm{l}}}{d}\left[1+3000Bo^{0.86}+1.12\left(\frac{x}{1-x}\right)^{0.75}\left(\frac{\rho_{\mathrm{l}}}{\rho_{\mathrm{v}}}\right)^{0.41}\right] \quad (20)$$

where *Bo* denotes the boiling number and expressed as

$$Bo = \frac{q_{\mathrm{m}}}{G\cdot r_{\mathrm{f}}} \quad (21)$$

The condensation heat transfer coefficient is defined as [37]

$$\alpha_{\mathrm{tp,cnd}} = 0.023\left[\frac{G_{\mathrm{f}}(1-x)d}{\mu_{\mathrm{l}}}\right]^{0.8} \mathrm{Pr}_{\mathrm{l}}^{0.4}\cdot\frac{\lambda_{\mathrm{l}}}{d}\left[(1-x)^{0.8}+\frac{3.8x^{0.76}(1-x)^{0.04}}{p_{\mathrm{r}}^{0.38}}\right] \quad (22)$$

In Eq. (22), $p_{\mathrm{r}}$ denotes the reduced pressure which is the ratio of state point pressure to critical pressure of the fluid.

Eventually, the area of each heat exchanger can be obtained by adding up the areas for all subsections from both single-phase and two-phase regions.

*2) Volume of the separator*

Vertical BOC (bottoming outlet cyclone separator) separator is selected in this study, due to its high separator efficiency and simple structure. The calculations of the vessel dimensions are all given based on the two-phase inlet pipe. The pipe size is calculated as follows [38]

$$A_{\mathrm{ip}} = \frac{Q_{\mathrm{vs}}}{\nu_{\mathrm{t}}} \quad (23)$$

$$D_{\mathrm{ip}} = \left[\frac{4A_{\mathrm{ip}}}{\pi}\right]^{\frac{1}{2}} \quad (24)$$

where $A_{\mathrm{ip}}$ and $D_{\mathrm{ip}}$ denote the cross sectional area and the diameter of the inlet pipe, respectively; $Q_{\mathrm{vs}}$ is the volumetric flow; and $\nu_{\mathrm{t}}$ is terminal velocity of the two phase flow, which is given by [38]

$$v_t = K\left[\frac{\rho_l - \rho_v}{\rho_v}\right] \tag{25}$$

In Eq. (25), $K$ is a constant with a value of 0.069 ($m \cdot s^{-1}$).

In order to simplify the calculation, the vertical BOC separator is considered as a cylindrical vessel with a height of ($L_A + L_B$) and a diameter of $D_{sep}$, the calculation of the volume for the separator is given by

$$V_{sep} = \frac{\pi \cdot D_{sep}{}^2 \cdot (L_A + L_B)}{4} \tag{26}$$

where $L_A$ is the length of the part which is above the inlet pipe, and $L_B$ is the length of the part which is below the inlet pipe. It is recommended by Ref [38]: $D_{sep}=3D_{ip}$, $L_A=7D_{ip}$ and $L_B=4.5D_{ip}$. After that, Eq. (26) could be written as

$$V_{sep} = \frac{\pi \cdot (3D_{ip})^2}{4} \cdot (7D_{ip} + 4.5D_{ip}) \tag{27}$$

*3.2.2 Costs of equipments*

For the sake of estimating the equipment costs, the method of equipment module costing [39] is used in this paper. This method of costing relates all costs of the equipment to the purchased cost of equipment evaluated for some base conditions. The deviations from base conditions are handled by using multiplying factors depending on the specific equipment type, system pressure and materials of construction. Considering the effect of inflation, the CEPCI (Chemical Engineering Plant Cost Index) is employed to update the equipment costs to the year of 2014 [40], which is expressed as

$$C_{2014} = C_b \cdot \left(\frac{I_{2014}}{I_b}\right) \tag{28}$$

where $C_b$ refers to the cost at the base time; $I_{2014}$ and $I_b$ are the cost indexes assigned 576.1 and 397, respectively.

The purchased cost of the equipment, at ambient pressures and using carbon steel construction, is calculated as [39]

$$\log C_{eq}^{0} = K_{1,eq} + K_{2,eq} \cdot \log(X) + K_{3,eq} \cdot [\log(X)]^2 \tag{29}$$

where $K_{1,eq}$, $K_{2,eq}$ and $K_{2,eq}$ are the constants for the equipment. And $X$ is the size or capacity parameter for the equipment, representing the total heat transfer area of the heat exchanger ($A_{he}$), the power generation by the turbine ($W_{turb}$), the volume of the separator ($V_{sep}$) and the power consumption by the pump ($W_{pump}$) or compressor ($W_{comp}$).

It is assumed that each heat exchanger of the system is made from the material of carbon steel, with a type of shell-and-tube. Then the cost is given by

$$C_{he} = \frac{576.1}{397} \cdot C_{he}^{0} \cdot (B_{1,he} + B_{2,he} \cdot F_{M,he} \cdot F_{P,he}) \tag{30}$$

where $B_{1,he}$ and $B_{2,he}$ are the constants according to the type of the heat exchanger; $F_{M,he}$ is the material factor; $F_{P,he}$ is the pressure factor, which is expressed as

$$\log F_{P,he} = C_{1,he} + C_{2,he} \cdot \log P_{he} + C_{3,he} \cdot (\log P_{he})^2 \tag{31}$$

where $C_{1,he}$, $C_{2,he}$ and $C_{3,he}$ are the constants according to the type and the pressure range of the heat exchanger.

The turbines in this study are made from the material of carbon steel, with axial types, and the costs are calculated as

$$C_{turb} = \frac{576.1}{397} \cdot C_{turb}^{0} \cdot F_{BM,turb} \tag{32}$$

where $F_{BM,turb}$ denotes the bare module factor based on the type and material of

296 construction for the turbine.

297 The compressor is axial type made from carbon material, and the cost is given by

298 $$C_{\text{comp}} = \frac{576.1}{397} \cdot C_{\text{comp}}^{0} \cdot F_{\text{BM,comp}} \tag{33}$$

299 where $F_{\text{BM,comp}}$ is the bare module factor for the compressor.

300 For the separator, the material of carbon steel and the vertical type are designed for

301 the construction. The cost is expressed as

302 $$C_{\text{sep}} = \frac{576.1}{397} \cdot C_{\text{sep}}^{0} \cdot (B_{1,\text{sep}} + B_{2,\text{sep}} \cdot F_{\text{M,sep}} \cdot F_{\text{P,sep}}) \tag{34}$$

303 where $B_{1,\text{sep}}$ and $B_{2,\text{sep}}$ are the constants based on the type of the separator; $F_{\text{M,sep}}$ is the

304 material factor; $F_{\text{P,sep}}$ is the pressure factor, which is calculated by

305 $$F_{\text{P,sep}} = \max\left\{ \frac{\dfrac{(P_{\text{sep}}+1)*D_{\text{sep}}}{2\cdot[850-0.6\cdot(P_{\text{sep}}+1)]}+0.00315}{0.0063}, 1 \right\} \tag{35}$$

306 The pumps are designed to centrifugal type and made from stainless steel, and the

307 costs of them are given by

308 $$C_{\text{pump}} = \frac{576.1}{397} \cdot C_{\text{pump}}^{0} \cdot (B_{1,\text{pump}} + B_{2,\text{pump}} \cdot F_{\text{M,pump}} \cdot F_{\text{P,pump}}) \tag{36}$$

309 where $B_{1,\text{pump}}$ and $B_{2,\text{pump}}$ are the constants based on the type of the pump; $F_{\text{M,pump}}$ is

310 the material factor; $F_{\text{P,pump}}$ is the pressure factor, which is given by

311 $$\log F_{\text{P,pump}} = C_{1,\text{pump}} + C_{2,\text{pump}} \cdot \log P_{\text{pump}} + C_{3,\text{pump}} \cdot (\log P_{\text{pump}})^2 \tag{37}$$

312 where $C_{1,\text{pump}}$, $C_{2,\text{pump}}$ and $C_{3,\text{pump}}$ are the constants in terms of the type and the

313 pressure range of the pump.

314 The costs of the ejector, the valve and the working fluid are neglected in this paper,

315 since their costs are much lower than those of other equipments [41, 42]. The

316 constants mentioned above are all listed in Table 3.

*3.2.3 Exergoeconomic analysis*

In order to relate the present value of the expenditure to the equivalent annually levelized costs， the capital recovery factor (CRF) is used, which is calculated as [43]

$$CRF = \frac{i_{\mathrm{eff}} \cdot (1+i_{\mathrm{eff}})^{\mathrm{n}}}{(1+i_{\mathrm{eff}})^{\mathrm{n}} - 1} \tag{38}$$

where $i_{\mathrm{eff}}$ is the interest rate with a value of 0.05, and $n$ is the lifetime of the CCP system with a value of 30 [44].

The equipment annually levelized costs is given by

$$Z_{\mathrm{i}} = CRF \cdot C_{\mathrm{i}} \tag{39}$$

It is assumed that the annual working time of the CCP system is 8000 hours [45]. The annual exergy transfer rates ($E_{\mathrm{y}}$), annual power generation and consumption ($W_{\mathrm{y}}$) are then obtained by this assumption.

From the exergoeconomic point of view, each exergy flow is related to a cost, and the cost balance for $k$th component of the CCP system is given by [43]

$$\sum_{\mathrm{out}} (c_{\mathrm{out}} \cdot E_{\mathrm{out}})_{\mathrm{k}} + c_{\mathrm{w,k}} \cdot W_{\mathrm{k}} = c_{\mathrm{q,k}} \cdot E_{\mathrm{q,k}} + \sum_{\mathrm{in}} (c_{\mathrm{in}} \cdot E_{\mathrm{in}})_{\mathrm{k}} + Z_{\mathrm{k}} \tag{40}$$

where $c_{\mathrm{out}}$, $c_{\mathrm{in}}$, $c_{\mathrm{w,k}}$, and $c_{\mathrm{q,k}}$ denote the average costs per unit of exergy. Note that the term ($c_{\mathrm{w,k}} \cdot W_{\mathrm{k}}$) would move with its positive sign to the right side of this equation if a component consumes power (such as the pump or compressor). The term ($c_{\mathrm{q,k}} \cdot \mathrm{E}_{\mathrm{q,k}}$) would come out with its positive sign on the left side when there is a heat transfer from the component. Detailed cost balances and auxiliary cost relations for the components in CCP system are summarized in Table 4.

The average costs per unit of exergy for the heat source of exhaust gases and jacket, the water entering to the condensers and evaporator are considered as zero [46]. Thus,

339 the average costs per unit of exergy for each flow can be solved by resolving the
340 linear equation system.

341 In addition, taken the given conditions into account, the average costs per unit of
342 exergy product for the turbines and evaporator could be written by

343 $$c_{\mathrm{bt}} = \frac{c_1 \cdot (E_{1,\mathrm{y}} - E_{2,\mathrm{y}})}{W_{\mathrm{bt,y}}} + \frac{Z_{\mathrm{bt}}}{W_{\mathrm{bt,y}}} \tag{41}$$

344 $$c_{\mathrm{ot}} = \frac{c_7 \cdot (E_{7,\mathrm{y}} - E_{8,\mathrm{y}})}{W_{\mathrm{ot,y}}} + \frac{Z_{\mathrm{ot}}}{W_{\mathrm{ot,y}}} \tag{42}$$

345 $$c_{\mathrm{cool}} = \frac{c_{18} \cdot (E_{18} - E_{19})}{E_{29}} + \frac{Z_{\mathrm{evap}}}{E_{29}} \tag{43}$$

346 where $c_{\mathrm{cool}}$ denotes the average costs per unit of cold exergy produced by evaporator
347 and is equal to $c_{29}$. On the right side of the equations, the former part is defined as the
348 fuel-exergy-related part, while the latter is considered as the equipment-cost-related
349 part.

350 In this paper, the average cost per unit of exergy product is used as an indicator for
351 the system performance from the viewpoint of exergoeconomics, which is defined as

352 $$c_{\mathrm{product}} = \frac{(c_{\mathrm{wbt}} \cdot W_{\mathrm{bt,y}} + c_{\mathrm{wot}} \cdot W_{\mathrm{ot,y}} + c_{\mathrm{cool}} \cdot E_{\mathrm{cool,y}} + C_{\mathrm{diff,pc}} + C_{\mathrm{diff,cond1}} + C_{\mathrm{diff,cond2}})}{(W_{\mathrm{bt,y}} + W_{\mathrm{ot,y}} + E_{\mathrm{cool,y}})} \tag{44}$$

353 where $C_{\mathrm{diff,pc}}$, $C_{\mathrm{diff,cond1}}$ and $C_{\mathrm{diff,cond2}}$ denote the fictitious cost rates related to the
354 utilization of dissipative components introduced by Ref [47], which are expressed as

355 $$C_{\mathrm{diff,pc}} = c_{23} \cdot E_{23,\mathrm{y}} - c_{22} \cdot E_{22,\mathrm{y}} = c_3 \cdot (E_3 - E_4) + Z_{\mathrm{pc}} \tag{45}$$

356 $$C_{\mathrm{diff,cond1}} = c_{25} \cdot E_{25,\mathrm{y}} - c_{24} \cdot E_{24,\mathrm{y}} = c_8 \cdot (E_8 - E_9) + Z_{\mathrm{cond1}} \tag{46}$$

357 $$C_{\mathrm{diff,cond2}} = c_{27} \cdot E_{27,\mathrm{y}} - c_{26} \cdot E_{26,\mathrm{y}} = c_{15} \cdot (E_{15} - E_{16}) + Z_{\mathrm{cond2}} \tag{47}$$

358 The simulation is performed under MATLAB software environment and REFPROP

359 9.0 [48] is employed to calculate the thermodynamic properties for the exhaust gases
360 and the working fluids in this paper.

361 *3.3 Validation*

362 To ensure the accuracy of the calculation, validation for each cycle is considered
363 based on the data from published literatures. The detailed comparisons between the
364 present results and previous studies are listed in Table 5-Table 8. Note that the
365 validation of ORC is divided into two parts, namely the separation part and the simple
366 ORC part, respectively. And the working fluid of ORC is the same as that of ORC in
367 the references only in this validation section. It can be seen from the tables that the
368 simulation results in present study are in good agreement with the data from the
369 references [49, 50, 11, 51].

370 ## 4. Results and discussion

371 In this study, a commercial cogeneration engine is selected as the case study. The
372 main parameters of the engine are listed in Table 9. It is assumed that the composition
373 of the exhaust gases are $CO_2$, $H_2O$, $N_2$ and $O_2$ with mass fraction of 9.1%, 7.4%,
374 74.2% and 9.3%, respectively [4]. This assumption can be used to evaluate the
375 properties of the exhaust gases.

376 Firstly, the thermodynamic performance of the proposed system is compared with
377 those of the ones designed by Kim et al. [8] and Shu et al. [21], which focus on the
378 waste heat recovery of engine exhaust and coolant. Then five key parameters such as
379 the compressor pressure ratio, the compressor inlet temperature, the BC turbine inlet

temperature, the ORC turbine inlet pressure and the ejector primary flow pressure, are selected to examine the thermodynamic and exergoeconomic performances of the CCP system. In the process of parametric analysis, when one parameter is varied, the others parameters are kept constant. The detailed conditions of the simulation are listed in Table 10.

### *4.1. Comparison of the proposed system and current systems*

Table 11 lists the comparison between the proposed system and the ones presented in references [8, 21]. It can be observed that total the net energy output （$W_{net}$+$Q_{cool}$） of proposed system is much higher than the maximum net energy output of the systems exhibited in the references under the same heat source conditions. Thus, the proposed system is more efficient to make better use of engine waste heat.

### *4.2 Thermodynamic and exergoeconomic analyses*

Fig. 2 shows the effect of compressor pressure ratio on net power outputs, refrigeration capacity and exergy efficiency of the system.

It can be observed that net power output of Brayton cycle increases firstly and then decreases with the increasing compressor pressure ratio. The reason for this is that an increase in compressor pressure ratio leads to increases in enthalpy drop through the turbine and power consumption by pump. The former case can account for the initial rise of power output through the BC turbine. But as the effect of increasing power consumption through compressor gradually outweighs that of the increasing power produced by BC turbine, a decrease in net power output of BC occurs.

The net power output of organic Rankine cycle decreases when the compressor pressure ratio increases. Since an increase in compressor pressure ratio results in a reduction in BC turbine outlet temperature, then the ORC turbine inlet temperature decreases. In addition, the mass flow rate of vapor generated by the vapor generator 1 also decreases due to the reducing BC turbine outlet temperature. Hence the net power output of ORC decreases.

In ejector refrigeration cycle, the refrigeration capacity increases with the increasing pressure ratio of compressor. As the compressor pressure ratio increases, the compressor outlet temperature rises under the condition of invariable compressor inlet temperature. Since the terminal temperature difference of gas heater outlet is given as a constant, the exhaust gas temperature at vapor generator 2 inlet rises, leading to a higher mass flow rate of primary flows. Then the refrigeration capacity increases.

Since the exergy output of refrigeration capacity is much smaller than that of net power production in terms of exergy analysis, the exergy efficiency of the system is more related to the net power output of the system. With the decreasing net power output of the system ($W_{net}$), the exergy efficiency decreases.

Fig. 3 illustrates the effect of compressor pressure ratio on average cost per unit of exergy product for the turbines, the evaporator and the overall system.

It can be seen that the average cost per unit of exergy product for BC turbine rises with the increasing compressor pressure ratio. This can be explained by dividing that cost into two parts, namely the fuel-exergy-related part and the equipment-cost-related

part from Eq. (41). For the fuel-exergy-related part, it can be seen from Fig .3 that the average cost per unit of exergy fuel ($c_1$) increases with rise of pressure ratio in the compressor, leading to an increase in the fuel-exergy-related part of $c_{wbt}$. Referring to the equipment-cost-related part, the effect of the rise in BC turbine cost outweighs that of the BC turbine power output, resulting in an increase in equipment-cost-related part of $c_{wbt}$. Combining the effects of these two parts, the average cost per unit of product for BC turbine increases.

As the pressure ratio of compressor increases, the average cost per unit of exergy product for ORC turbine rises. Considering the fuel-exergy-related part, it can be observed from Fig. 3 that as the compressor pressure ratio increases, the average cost per unit of exergy fuel for ORC turbine rises ($c_7$), thus an increase in the fuel-exergy-related part of $c_{wot}$ occurs. For the equipment-cost-related part, the impact of the increase in ORC turbine cost is greater than that of the ORC turbine power output, leading to a rise in equipment-cost-related part of $c_{wot}$. As a result, the average cost per unit of product for ORC turbine increases.

The average cost per unit of refrigeration capacity exergy output decreases with the increasing compressor pressure ratio. The reason for this is that an increase in compressor pressure ratio leads to a decrease in the average cost per unit of exergy fuel for the evaporator, as shown in Fig. 3, reducing the numerical value of fuel-exergy-related part of $c_{cool}$. For the equipment-cost-related part, the impact of the decrease in evaporator cost is greater than that of the refrigeration capacity exergy output, resulting in a decrease in equipment-cost-related part of $c_{cool}$. Therefore, a

drop in average cost per unit of refrigeration capacity exergy output occurs.

As for the fictitious cost rate of precooler ($C_{\mathrm{diff,pc}}$), both the exergy transfer rate and the equipment cost declines, due to the reduction of temperature at the BC turbine outlet caused by the increasing compressor pressure ratio. In addition, the average cost per unit of the exergy for the flow across the precooler ($c_3$, which is equal to $c_1$) increases, as is shown in Fig. 3. Integrating the variations of all the parameters related to $C_{\mathrm{diff,pc}}$ in Eq. (45) , the fictitious cost rate of precooler increases. Referring to the fictitious cost rate associated with condenser 1 ($C_{\mathrm{diff,cond1}}$), the reduced mass flow rate of working fluid in ORC leads to decreases in exergy transfer rate and equipment cost of condenser 1. Meanwhile, it can be observed that the average cost per unit of exergy for the flow across the condenser 1 ($c_8$, which is equal to $c_7$) rises with the increasing compressor pressure ratio. Thus the fictitious cost rate of condenser 1 increases. For the fictitious cost rate associated with condenser 2 ($C_{\mathrm{diff,cond2}}$), the higher mass flow rate of primary flows is generated by vapor generator 2 when compressor pressure ratio increases, causing the exergy transfer rate and equipment cost of condenser 2 to increase. Even though the average cost per unit of exergy for the flow across the condenser 2 ($c_{15}$, which is equal to $c_{18}$) decreases, the fictitious cost rate of condenser 2 still increases.

The average cost per unit of exergy product of the overall system ($c_{\mathrm{product}}$) increases with the increasing compressor pressure ratio, after analyzing the variations for all parameters related to $c_{\mathrm{product}}$ in Eq. (44).

Fig. 4 shows the effect of compressor inlet temperature on net power outputs,

refrigeration capacity and exergy efficiency of the system.

It can be observed that the net power output of BC decreases with the increasing compressor inlet temperature. The reason is that as the compressor inlet temperature increases, the enthalpy increment in compressor and the mass flow rate of BC both increase, resulting in the increasing consumption of power through compressor. In the BC turbine, the power generation increases due to the raised mass flow rate of $CO_2$. Combining these factors, the net power output of BC decreases.

The net power output of ORC increases when the compressor inlet temperature rises. It is because an increase in mass flow rate of $CO_2$ leads to a larger amount of vapor produced by vapor generator 1, causing the power output of ORC turbine to rise. Thus the net power output of ORC increases.

In the ejector refrigeration cycle, the refrigeration capacity exergy output increases with the rising compressor inlet temperature. Since the rise of compressor inlet temperature enables the compressor outlet temperature to increase, the exhaust gases temperature at the gas heater outlet rises due to the constant terminal temperature difference at gas heater outlet. Therefore, more vapor is generated by vapor generator 2, contributing to an increase in the refrigeration capacity exergy output.

Considering the variations of net power outputs and the refrigeration capacity exergy output of the system, the exergy efficiency decreases.

Fig. 5 illustrates the effect of compressor inlet temperature on average cost per unit of exergy product for the turbines, the evaporator and the overall system.

It can be seen that the average cost per unit of exergy product for BC turbine

489 increases with the rising compressor inlet temperature. As the compressor inlet
490 temperature rises, the fuel-exergy-related part of $c_{wbt}$ increases due to the rised
491 average cost per unit of exergy fuel ($c_1$) for BC turbine. While for the
492 equipment-cost-related part, the effect of the rise in BC turbine power output is
493 greater than that of the BC turbine cost, leading to a decrease in
494 equipment-cost-related part of $c_{wbt}$. Integrating the effects of these two parts, the
495 average cost per unit of exergy product for BC turbine increases.

496 As shown in Fig. 5, the average cost per unit of exergy fuel ($c_7$) for ORC turbine
497 increases when the compressor inlet temperature increases, resulting in an increase in
498 fuel-exergy-related part of $c_{wot}$. Referring to the equipment-cost-related part, the
499 impact of the increase in ORC turbine power output outweighs that of the ORC
500 turbine cost when the compressor inlet temperature rises, leading to a decrease in the
501 equipment-cost-related part of $c_{wot}$. As a result, the average cost per unit of exergy
502 product for ORC turbine increases with the rising temperature of compressor inlet.

503 With the rising compressor inlet temperature, the average cost per unit of product
504 for the evaporator decreases. For the fuel-exergy-related part, a decrease in the
505 average cost per unit of exergy fuel ($c_{18}$) leads to a decrease in the fuel-exergy-related
506 part of $c_{cool}$ for the evaporator. Considering the equipment-cost-related part, since the
507 impact of the rise in refrigeration capacity exergy output is greater than that of the
508 increase in evaporator cost, the equipment-cost-related part of $c_{cool}$ decreases.
509 Therefore, $c_{cool}$ decreases.

510 Referring to the fictitious cost rate of precooler ($C_{diff,pc}$), as the compressor inlet

temperature increases, both the exergy transfer rate and the equipment cost for the precooler decrease. It can also be seen from the figure that the average cost per unit of exergy for the flow across the precooler ($c_3$, which is equal to $c_1$) increases slightly. Hence the fictitious cost rate of precooler decreases. For the fictitious cost rate of condenser 1 ($C_{\mathrm{diff,cond1}}$), a rise in mass flow rate of ORC leads to increases in both exergy transfer rate and the equipment cost of the condenser 1. Moreover, the average cost per unit of exergy for the flow across the condenser 1 ($c_8$, which is equal to $c_7$) increases. Thus the fictitious cost rate of the condenser 1 rises. Concerning the fictitious cost rate of condenser 2 ($C_{\mathrm{diff,cond2}}$), a larger mass flow rate of primary flow enables the exergy transfer rate and the equipment cost of the condenser 2 to increase. Whereas, the average cost per unit of exergy for the flow across the condenser 2 ($c_{15}$, which is equal to $c_{18}$) decreases. As a result, the fictitious cost rate of condenser 2 increases.

After analyzing the variations of all parameters related to $c_{\mathrm{product}}$ in Eq. (44), the average cost per unit of exergy product for the overall system increases with the increasing compressor inlet temperature.

Fig. 6 shows the effect of BC turbine inlet temperature on net power outputs, refrigeration capacity and exergy efficiency of the system.

As BC turbine inlet temperature increases, the mass flow rate of $CO_2$ decreases, leading to declines in both power generation through BC turbine and energy consumption by compressor. Since the impact of the decrease in power consumption by compressor is greater than that of the decrease in power generation through BC

turbine, the net power output of BC increases.

The net power output of ORC decreases when the BC turbine inlet temperature rises. Since the decrease in mass flow rate of $CO_2$ leads to a decrease in mass flow rate of working fluid for ORC, the power output of ORC turbine decreases, causing the net power output of ORC to decrease.

It can also be observed that the refrigeration capacity exergy output keeps constant with the increasing BC turbine inlet temperature. As BC turbine inlet temperature increases, the operation conditions of the compressor are not changed. Due to the constant terminal temperature difference of the gas heater outlet, the exhaust gases temperature stays unchanged at the vapor generator 2 inlet, resulting in the unchanged parameters of refrigeration cycle. Hence the refrigeration capacity exergy output is constant.

Finally, the exergy efficiency of the overall system increases with the rise of BC turbine inlet temperature, due to the increased net power output of the system ($W_{net}$).

Fig. 7 illustrates the effect of BC turbine inlet temperature on average cost per unit of exergy product for the turbines, the evaporator and the overall system.

It can be seen that the average cost per unit of exergy product for BC turbine decreases with the increasing BC turbine inlet temperature. As the BC turbine inlet temperature rises, the fuel-exergy-related part of $c_{wbt}$ decreases due to the reduced average cost per unit of exergy fuel ($c_1$). Meanwhile, the rising BC turbine inlet temperature leads to a greater impact of the decrease in BC turbine cost than that of the BC turbine power output and hence decreases the equipment-cost-related part of

555 $c_{wbt}$. Combining the effects of these two parts, the average cost per unit of exergy
556 product for BC turbine decreases.

557 The average cost per unit of product for ORC turbine decreases with the increase of
558 BC turbine inlet temperature. For the fuel-exergy-related part, as the BC turbine inlet
559 temperature rises, the average cost per unit of exergy fuel ($c_7$) decreases, resulting in a
560 decrease of the fuel-exergy-related part for $c_{wot}$. Considering the
561 equipment-cost-related part, the degree of reduction for the ORC turbine cost
562 outweighs that for ORC turbine power output when the BC turbine inlet temperature
563 rises, thus the equipment-cost-related part of $c_{wot}$ decreases. As a result, the average
564 cost per unit of exergy product for ORC turbine decreases.

565 Meanwhile, the average cost per unit of refrigeration capacity exergy output keeps
566 constant when the BC turbine inlet temperature increases, for the reason that the
567 parameter conditions of ejector are not changed.

568 Referring to the fictitious cost rate of precooler ($C_{diff,pc}$), as the BC turbine inlet
569 temperature increases, the mass flow rate of $CO_2$ decreases, leading to decreases in
570 both exergy transfer rate and equipment cost of the precooler. In addition, the average
571 cost per unit of exergy for the flow in the precooler ($c_3$, which is equal to $c_1$) drops, as
572 is shown in Fig. 7. Thus $C_{diff,pc}$ decreases. For the fictitious cost rate of condenser 1
573 ($C_{diff,cond1}$), on one hand, the exergy transfer rate and the equipment cost decrease due
574 to the drop in mass flow rate of working fluid. On the other hand, the average cost per
575 unit of exergy for the flow in the condenser 1 ($c_8$, which is equal to $c_7$) decreases, as
576 shown in Fig. 7. Hence the increase of $C_{diff,cond1}$ occurs. Considering the fictitious cost

577 rate of condenser 2 ($C_{diff,cond2}$), $C_{diff,cond2}$ is a constant because of the unchanged
578 parameters in condenser 2.

579 Integrating the effects of all the variables related to $c_{product}$ in Eq. (44), the average
580 cost per unit of exergy product for the overall system decreases when BC turbine inlet
581 temperature increases.

582 Fig. 8 shows the effect of ORC turbine inlet pressure on net power outputs,
583 refrigeration capacity and exergy efficiency of the system.

584 It can be obtained from the figure that both the net power output of BC and the
585 refrigeration capacity of the ejector refrigeration cycle remain as constants. Since the
586 parameters of the BC turbine, compressor and the evaporator are unrelated to the inlet
587 pressure of ORC turbine.

588 An increase in ORC turbine inlet pressure leads to a decrease in the mass flow rate
589 of working fluid and an increase in enthalpy through the turbine. Since the impact of
590 the increase in enthalpy drop is greater than that of the decrease in the mass flow rate
591 of working fluid across the ORC turbine, the power output of ORC turbine rises.
592 Consequently, the net power output of ORC increases.

593 Integrating the effects of the net power output and the refrigeration capacity exergy,
594 the exergy efficiency increases with the increasing ORC turbine inlet pressure.

595 Fig. 9 illustrates the effect of ORC turbine inlet pressure on the average cost per
596 unit of exergy product for the turbines, the evaporator and the overall system.

597 It can be seen that the average cost per unit of exergy product for BC turbine
598 increases slightly with the increasing ORC turbine inlet pressure. Since a rise in the

599 average cost per unit of exergy fuel for the BC turbine ($c_1$) leads to an increase in the
600 fuel-exergy-related part of $c_{wbt}$, and the equipment-cost-related part of $c_{wbt}$ is not
601 varied due to the constant parameters of BC turbine. The average cost per unit of
602 exergy product for BC turbine increases.

603 The average cost per unit of exergy product ORC turbine decreases with the rising
604 ORC turbine inlet pressure. For the fuel-exergy-related part, as the ORC turbine inlet
605 pressure rises, the average cost per unit of exergy fuel for the ORC turbine ($c_7$)
606 decreases, resulting in a decrease in the fuel-exergy-related part of $c_{wot}$. Referring to
607 the equipment-cost-related part, since the impact of the rise in ORC turbine power
608 output is greater than that of the increase in ORC turbine cost, the
609 equipment-cost-related part of $c_{wot}$ also decreases. Hence the average cost per unit of
610 exergy product for ORC turbine decreases.

611 With the increasing ORC turbine inlet pressure, the average cost per unit of exergy
612 product for the evaporator remains unchanged, due to the constant average cost per
613 unit of exergy fuel ($c_{18}$) and the unchanged parameters for the evaporator.

614 Referring to the fictitious cost rate of precooler ($C_{diff,pc}$), as the ORC turbine inlet
615 pressure increases, the temperature of saturated liquid at state point 13 rises, leading
616 to an increase in the temperature at the precooler inlet. Then the exergy transfer and
617 the equipment cost both increase. In addition, the average cost per unit of exergy for
618 the flow across the precooler ($c_3$, which is equal to $c_1$) increases slightly. Consequently,
619 $C_{diff,pc}$ increases. For the fictitious cost rate of condenser 1 ($C_{diff,cond1}$), $C_{diff,cond1}$
620 decreases mainly because of the decrease in the average cost per unit of exergy for the

621 flow across the condenser 1 ($c_8$, which is equal to $c_7$). Since the parameter conditions
622 of the condenser 2 is unchanged, the fictitious cost rate of condenser 2 ($C_{\mathrm{diff,cond2}}$)
623 keeps constant.

624 Due to the combined effects of all the variables related to $c_{\mathrm{product}}$ in Eq. (44), the
625 average cost per unit of exergy product for the overall system decreases with the
626 increasing ORC turbine inlet pressure.

627 Fig. 10 shows the effect of ejector primary flow pressure on net power outputs,
628 refrigeration capacity and exergy efficiency of the system.

629 It can be observed the net power outputs of BC and ORC keep as constants, for the
630 reason that the parameters are irrelevant to the primary flow pressure of the ejector.

631 Since a higher ejector primary flow pressure leads to a lower mass flow rate of the
632 primary flow across the ejector, casing a drop in the mass flow rate of the secondary
633 flow in the evaporator. The refrigeration capacity decreases.

634 The exergy transfer rate in vapor generator 2 decreases with the increasing ejector
635 primary flow pressure. Considering the variations of net power output, the
636 refrigeration capacity exergy output and the exergy transfer rate of the system, the
637 exergy efficiency slightly increases.

638 Fig. 11 illustrates the effect of ejector primary flow pressure on the average cost per
639 unit of exergy product for the turbines, the evaporator and the overall system.

640 As is shown in the figure, the average costs per unit of exergy product for the BC
641 turbine and the ORC turbine are both constants, due to the unchanged operation
642 conditions of them.

643 Meanwhile, the average cost per unit of exergy product for the evaporator increases
644 with the rising ejector primary flow pressure. As the ejector primary flow pressure
645 increases, the average cost per unit of exergy fuel ($c_{18}$) for the evaporator rises,
646 resulting in an increase in the fuel-exergy-related part of $c_{cool}$. While for the
647 equipment-cost-related part, the impact of the increase in evaporator cost outweighs
648 that of the evaporator refrigeration capacity exergy output, leading to an increase in
649 the equipment-cost-related part of $c_{cool}$. Therefore, $c_{cool}$ increases.

650 For the fictitious cost rates of the precooler and condenser 1, both $C_{diff,pc}$ and
651 $C_{diff,cond1}$ keep as constants since the operation conditions of them are not changed.
652 While $C_{diff,cond2}$ decreases by the reason of the decreased mass flow rate of working
653 fluid across the condenser 2.

654 Combining the effects of all parameters related to $c_{product}$ in Eq. (44), the average
655 cost per unit of exergy product for the overall system increases with the increasing
656 ejector primary flow pressure.

657 In order to obtain the optimal performance of the CCP system utilized engine waste
658 heat, a single-objective optimization is conducted by means of genetic algorithm,
659 which is a stochastic global search method that simulates natural biological evolution.
660 The detailed computing method of genetic algorithm can refer to Ref. [3]. The
661 average cost per unit of exergy product for the overall system is selected the as the
662 objective function, since it combines exergy analysis and economic principles to
663 provide information which is critical to the design and operation of a cost-effective
664 system. Key parameters such as compressor pressure ratio, compressor inlet pressure,

BC turbine inlet temperature, ORC turbine inlet pressure and ejector primary flow pressure are chosen as the decision variables.

The detailed ranges of key parameters and the control parameters of GA are listed in Table 12 and Table 13, respectively.

Table 14 lists the results of parameter optimization for the CCP system with the objective function of the average cost per unit of exergy product for the overall system. It can be observed that the minimum $c_{product}$ is 63.53\$/MWh$^{-1}$, and the exergy efficiency, the net power output and the Refrigeration capacity of the system are 27.63%, 282.49kW and 20.01kW, respectively. The results indicate that the exergy efficiency obtained from the exgoeconimic optimization is also desirable, and the refrigeration capacity is optimized to be lower due to the higher cost per unit of exergy product for ejector refrigeration cycle. In addition, for the compressor pressure ratio, the optimal one is located at the lower boundary. Referring to the compressor inlet temperature and the ejector primary flow pressure, the optimum ones are settled near the lower boundaries. Concerning the optimal BC turbine inlet temperature and the ORC turbine inlet pressure, both of them are located near the upper boundaries. These results imply that all the optimal values of the key parameters are in accordance with the parametric analysis.

.

## 5. Conclusion

In this study, a CCP system is designed for the waste heat recovery of an ICE. The effects of five key parameters (i.e. compressor pressure ratio, compressor inlet

pressure, BC turbine inlet temperature, ORC turbine inlet pressure and ejector primary flow pressure) on thermodynamic and exergoeconomic performances are examined. Then a single-objective optimization by means of GA is conducted with an objective function of the average cost per unit of exergy product. The main conclusions drawn from investigation are summarized as follows:

(1) On the basis of parametric analysis, the increases of the BC turbine inlet temperature, the ORC turbine inlet pressure and the ejector primary flow pressure have positive effects on the exergy efficiency, while the rises in compressor pressure ratio and the compressor inlet temperature are undesirable to the thermodynamic performance of the system.

(2) Referring to the exergoeconimic analysis, lower average cost per unit of exergy product for the overall system can be achieved by increasing the BC turbine inlet temperature, the ORC turbine inlet pressure and the ejector primary flow pressure. However, the rises in compressor pressure and compressor inlet temperature lead to increases in average cost per unit of exergy product for the overall system.

(3) By the single-objective optimization, the lowest average cost per unit of exergy product for the overall system is obtained, and the exergy efficiency is also desirable. In addition, all the optimal values of the key parameters are in accordance with the parametric analysis.

## Acknowledgments

The authors gratefully acknowledge the financial support by the National Natural

709 Science Foundation of China (Grant No. 51476121) and the Fundamental Research
710 Funds for the Central Universities (Grant No. 2013jdgz14).

711

712 **References**

713 [1] A. Domingues, H. Santos, M. Costa. Analysis of vehicle exhaust waste heat
714 recovery potential using a Rankine cycle. Energy. 49 (2013) 71-85.
715 [2] C. Sprouse, C. Depcik. Review of organic Rankine cycles for internal combustion
716 engine exhaust waste heat recovery. Appl Therm Eng. 51 (2013) 711-22.
717 [3] Y.P. Dai, J.F. Wang, L. Gao. Parametric optimization and comparative study of
718 organic Rankine cycle (ORC) for low grade waste heat recovery. Energy Conv
719 Manag. 50 (2009) 576-82.
720 [4] I. Vaja, A. Gambarotta. Internal Combustion Engine (ICE) bottoming with
721 Organic Rankine Cycles (ORCs). Energy. 35 (2010) 1084-93.
722 [5] M. Tahani, S. Javan, M. Biglari. A comprehensive study on waste heat recovery
723 from internal combustion engines using organic rankine cycle. Therm Sci. 17 (2013)
724 611-24.
725 [6] M.G. He, X.X. Zhang, K. Zeng, K. Gao. A combined thermodynamic cycle used
726 for waste heat recovery of internal combustion engine. Energy. 36 (2011) 6821-9.
727 [7] E.H. Wang, H.G. Zhang, Y. Zhao, B.Y. Fan, Y.T. Wu, Q.H. Mu. Performance
728 analysis of a novel system combining a dual loop organic Rankine cycle (ORC) with a
729 gasoline engine. Energy. 43 (2012) 385-95.
730 [8] Y.M. Kim, D.G. Shin, C.G. Kim, G.B. Cho. Single-loop organic Rankine cycles

731 for engine waste heat recovery using both low- and high-temperature heat sources.
732 Energy. 96 (2016) 482-94.
733 [9] B.T. Liu, K.H. Chien, C.C. Wang. Effect of working fluids on organic Rankine
734 cycle for waste heat recovery. Energy. 29 (2004) 1207-17.
735 [10] H. Tian, G.Q. Shu, H.Q. Wei, X.Y. Liang, L.N. Liu. Fluids and parameters
736 optimization for the organic Rankine cycles (ORCs) used in exhaust heat recovery of
737 Internal Combustion Engine (ICE). Energy. 47 (2012) 125-36.
738 [11] E.H. Wang, H.G. Zhang, B.Y. Fan, M.G. Ouyang, Y. Zhao, Q.H. Mu. Study of
739 working fluid selection of organic Rankine cycle (ORC) for engine waste heat
740 recovery. Energy. 36 (2011) 3406-18.
741 [12] Y.R. Li, M.T. Du, C.M. Wu, S.Y. Wu, C. Liu. Potential of organic Rankine cycle
742 using zeotropic mixtures as working fluids for waste heat recovery. Energy. 77 (2014)
743 509-19.
744 [13] G.Q. Shu, Y.Y. Gao, H. Tian, H.Q. Wei, X.Y. Liang. Study of mixtures based on
745 hydrocarbons used in ORC (Organic Rankine Cycle) for engine waste heat recovery.
746 Energy. 74 (2014) 428-38.
747 [14] L. Pierobon, R. Kandepu, F. Haglind, Asme. Waste heat recovery for offshore
748 applications. Amer Soc Mechanical Engineers, New York, 2013.
749 [15] G.P. Yu, G.Q. Shu, H. Tian, H.Q. Wei, L.N. Liu. Simulation and thermodynamic
750 analysis of a bottoming Organic Rankine Cycle (ORC) of diesel engine (DE). Energy.
751 51 (2013) 281-90.
752 [16] E.W. Miller, T.J. Hendricks, H. Wang, R.B. Peterson. Integrated dual-cycle

753 energy recovery using thermoelectric conversion and an organic Rankine bottoming
754 cycle. Proc Inst Mech Eng Part A-J Power Energy. 225 (2011) 33-43.
755 [17] C.Y. Zhang, G.Q. Shu, H. Tian, H.Q. Wei, X.Y. Liang. Comparative study of
756 alternative ORC-based combined power systems to exploit high temperature waste
757 heat. Energy Conv Manag. 89 (2015) 541-54.
758 [18] H.G. Zhang, E.H. Wang, B.Y. Fan. A performance analysis of a novel system of
759 a dual loop bottoming organic Rankine cycle (ORC) with a light-duty diesel engine.
760 Applied Energy. 102 (2013) 1504-13.
761 [19] F.B. Yang, X.R. Dong, H.G. Zhang, Z. Wang, K. Yang, J. Zhang, et al.
762 Performance analysis of waste heat recovery with a dual loop organic Rankine cycle
763 (ORC) system for diesel engine under various operating conditions. Energy Conv
764 Manag. 80 (2014) 243-55.
765 [20] B.C. Choi, Y.M. Kim. Thermodynamic analysis of a dual loop heat recovery
766 system with trilateral cycle applied to exhaust gases of internal combustion engine for
767 propulsion of the 6800 TEU container ship. Energy. 58 (2013) 404-16.
768 [21] G.Q. Shu, L.N. Liu, H. Tian, H.Q. Wei, G.P. Yu. Parametric and working fluid
769 analysis of a dual-loop organic Rankine cycle (DORC) used in engine waste heat
770 recovery. Applied Energy. 113 (2014) 1188-98.
771 [22] J. Song, C.W. Gu. Performance analysis of a dual-loop organic Rankine cycle
772 (ORC) system with wet steam expansion for engine waste heat recovery. Applied
773 Energy. 156 (2015) 280-9.
774 [23] Y.D. Zhou, Y.D. Wu, F. Li, L.J. Yu. Performance analysis of zeotropic mixtures

775 for the dual-loop system combined with internal combustion engine. Energy Conv
776 Manag. 118 (2016) 406-14.
777 [24] Y.C. Liang, G.Q. Shu, H. Tian, H.Q. Wei, X.Y. Liang, L.N. Liu, et al.
778 Theoretical analysis of a novel electricity-cooling cogeneration system (ECCS) based
779 on cascade use of waste heat of marine engine. Energy Conv Manag. 85 (2014)
780 888-94.
781 [25] S. Wang, K. Bai, Y. Xie, J. Di, S. Cheng. Analysis of Combined Power and
782 Refrigeration Generation Using the Carbon Dioxide Thermodynamic Cycle to
783 Recover the Waste Heat of an Internal Combustion Engine. Mathematical Problems in
784 Engineering. 2014 (2014) 1-12.
785 [26] A. Moisseytsev, J.J. Sienicki. Investigation of alternative layouts for the
786 supercritical carbon dioxide Brayton cycle for a sodium-cooled fast reactor. Nucl Eng
787 Des. 239 (2009) 1362-71.
788 [27] B.Y. Song, W.L. Zhuge, R.C. Zhao, X.Q. Zheng, Y.J. Zhang, Y. Yin, et al. An
789 investigation on the performance of a Brayton cycle waste heat recovery system for
790 turbocharged diesel engines. J Mech Sci Technol. 27 (2013) 1721-9.
791 [28] A.D. Akbari, S.M.S. Mahmoudi. Thermoeconomic analysis & optimization of
792 the combined supercritical CO2 (carbon dioxide) recompression Brayton/organic
793 Rankine cycle. Energy. 78 (2014) 501-12.
794 [29] G. Besagni, R. Mereu, F. Inzoli. Ejector refrigeration: A comprehensive review.
795 Renew Sust Energ Rev. 53 (2016) 373-407.
796 [30] G.Q. Shu, X.N. Li, H. Tian, X.Y. Liang, H.Q. Wei, X. Wang. Alkanes as

797 working fluids for high-temperature exhaust heat recovery of diesel engine using
798 organic Rankine cycle. Applied Energy. 119 (2014) 204-17.
799 [31] N.A. Lai, M. Wendland, J. Fischer. Working fluids for high-temperature organic
800 Rankine cycles. Energy. 36 (2011) 199-211.
801 [32] D. Butrymowicz, K. Smierciew, J. Karwacki, J. Gagan. Experimental
802 investigations of low-temperature driven ejection refrigeration cycle operating with
803 isobutane. Int J Refrig-Rev Int Froid. 39 (2014) 196-209.
804 [33] J. Zhang, H.G. Zhang, K. Yang, F.B. Yang, Z. Wang, G.Y. Zhao, et al.
805 Performance analysis of regenerative organic Rankine cycle (RORC) using the pure
806 working fluid and the zeotropic mixture over the whole operating range of a diesel
807 engine. Energy Conv Manag. 84 (2014) 282-94.
808 [34] F.P. Incropera, D.P. DeWitt. Fundamentals of heat and mass transfer. Wiley,
809 New York, 2002.
810 [35] D.Q. Kern. Process heat transfer. McGraw-Hill, New York, 1950.
811 [36] K.E. Gungor, R.H.S. Winterton. Simplified general correlation for saturated flow
812 boiling and comparisons of correlations with data. Chem Eng Res Des. 65 (1987)
813 148-56.
814 [37] M.M. Shah. A general correlation for heat transfer during film condensation
815 inside pipes. International Journal of Heat and Mass Transfer. 22 (1979) 547-56.
816 [38] S.J. Zarrouka, M.H. Purnanto. Geothermal steam-water separators: Design
817 overview. Geothermics. 53 (2015) 236-54.
818 [39] R. Turton. Analysis, synthesis, and design of chemical processes. Prentice Hall,

819 Upper Saddle River, N.J, 2009.
820 [40] D. Lozowski. Start online account with the exclusive online plant cost index and
821 get full archive access to chemical engineering.
822 http://www.chemengonline.com/pci-home, Chemecal Engineering.
823 [41] L.G. Farshi, S.M.S. Mahmoudi, M.A. Rosen. Exergoeconomic comparison of
824 double effect and combined ejector-double effect absorption refrigeration systems.
825 Applied Energy. 103 (2013) 700-11.
826 [42] M.H. Yang, R.H. Yeh. Economic performances optimization of the transcritical
827 Rankine cycle systems in geothermal application. Energy Conv Manag. 95 (2015)
828 20-31.
829 [43] A. Bejan, G. Tsatsaronis, M.J. Moran. Thermal design and optimization. Wiley,
830 New York, 1996.
831 [44] D. Tempesti, D. Fiaschi. Thermo-economic assessment of a micro CHP system
832 fuelled by geothermal and solar energy. Energy. 58 (2013) 45-51.
833 [45] F. Velez, J.J. Segovia, M.C. Martin, G. Antonlin, F. Chejne, A. Quijano. A
834 technical, economical and market review of organic Rankine cycles for the conversion
835 of low-grade heat for power generation. Renew Sust Energ Rev. 16 (2012) 4175-89.
836 [46] M. Sadeghi, S.M.S. Mahmoudi, R.K. Saray. Exergoeconomic analysis and
837 multi-objective optimization of an ejector refrigeration cycle powered by an internal
838 combustion (HCCI) engine. Energy Conv Manag. 96 (2015) 403-17.
839 [47] A. Lazzaretto, G. Tsatsaronis. SPECO: A systematic and general methodology
840 for calculating efficiencies and costs in thermal systems. Energy. 31 (2006) 1257-89.

[48] E.W. Lemmon, M.L. Huber, M.O. McLinden. NIST Standard Reference Database 23, Reference Fluid Thermodynamic and Transport Properties (REFPROP). version 90, National Institute of Standards and Technology. (2010).

[49] Y.M. Kim, C.G. Kim, D. Favrat. Transcritical or supercritical CO2 cycles using both low- and high-temperature heat sources. Energy. 43 (2012) 402-15.

[50] M. Yari. Exergetic analysis of various types of geothermal power plants. Renew Energy. 35 (2010) 112-21.

[51] B. Zheng, Y.W. Weng. A combined power and ejector refrigeration cycle for low temperature heat sources. Sol Energy. 84 (2010) 784-91.

**Figure captions:**

**Fig. 1** Schematic diagram of the CCP system

**Fig. 2** Effect of compressor pressure ratio on thermodynamic performance of the system

**Fig. 3**. Effect of compressor pressure ratio on exergoeconomic performance of the system

**Fig. 4** Effect of compressor inlet temperature on thermodynamic performance of the system

**Fig. 5** Effect of compressor inlet temperature on exergoeconomic performance of the system

**Fig. 6** Effect of BC turbine inlet temperature on thermodynamic performance of the system

**Fig. 7** Effect of BC turbine inlet temperature on exergoeconomic performance of the system

**Fig. 8** Effect of ORC turbine inlet pressure on thermodynamic performance of the system

**Fig. 9** Effect of ORC turbine inlet pressure on exergoeconomic performance of the system

**Fig. 10** Effect of ejector primary flow pressure on thermodynamic performance of the system

**Fig. 11** Effect of ejector primary flow pressure on exergoeconomic performance of the system

885 **Table 1** Energy relations for each component

| Component | Energy relations |
|---|---|
| Gas heater | $M_a \cdot (h_a - h_b) = M_1 \cdot (h_1 - h_5)$ |
| BC turbine | $W_{bt} = M_1 \cdot (h_1 - h_2) = M_1 \cdot (h_1 - h_{2s}) \cdot \eta_{bt}$ |
| Vapor generator 1 | $M_2 \cdot (h_2 - h_3) = M_6 \cdot (h_6 - h_{13})$ |
| Precooler | $M_3 \cdot (h_3 - h_4) = M_{22} \cdot (h_{23} - h_{22})$ |
| Compressor | $W_{comp} = M_4 \cdot (h_5 - h_4) = M_4 \cdot (h_{5s} - h_4) / \eta_{comp}$ |
| ORC turbine | $W_{ot} = M_7 \cdot (h_7 - h_8) = M_7 \cdot (h_7 - h_{8s}) \cdot \eta_{ot}$ |
| Condenser 1 | $M_8 \cdot (h_8 - h_9) = M_{24} \cdot (h_{25} - h_{24})$ |
| Pump1 | $W_{pump1} = M_9 \cdot (h_{10} - h_9) = M_9 \cdot (h_{10s} - h_9) / \eta_{pump1}$ |
| Preheater | $M_d \cdot (h_d - h_e) = M_{10} \cdot (h_{11} - h_{10})$ |
| Separator | $M_{11} \cdot h_{11} = M_{12} \cdot h_{12} + M_{13} \cdot h_{13}$ |
| Vapor generator 2 | $M_b \cdot (h_b - h_c) = M_{14} \cdot (h_{14} - h_{21})$ |
| Ejector | $M_{15} \cdot h_{15} = M_{14} \cdot h_{14} + M_{19} \cdot h_{19}$ |
| Evaporator | $M_{19} \cdot (h_{19} - h_{18}) = M_{28} \cdot (h_{28} - h_{29})$ |
| Throttle valve | $h_{18} = h_{17}$ |

886

887

888

889

890

891

892 **Table 2** Exergy analysis for each component in the CCP system

| Component | $E_F$ | $E_P$ | $E_D$ | $E_L$ |
|---|---|---|---|---|
| Gas heater | $E_a - E_b$ | $E_1 - E_5$ | $E_a + E_5 - E_b - E_1$ | / |
| BC turbine | $E_1 - E_2$ | $W_{bt}$ | $E_1 - E_2 - W_{bt}$ | / |
| Vapor generator 1 | $E_2 - E_3$ | $E_6 - E_{13}$ | $E_2 + E_{13} - E_3 - E_6$ | / |
| Precooler | / | / | $E_3 + E_{22} - E_4 - E_{23}$ | $E_{23} - E_{22}$ |
| Compressor | $W_{comp}$ | $E_5 - E_4$ | $W_{comp} + E_4 - E_5$ | / |
| ORC turbine | $E_7 - E_8$ | $W_{ot}$ | $E_7 - E_8 - W_{ot}$ | / |
| Condenser 1 | / | / | $E_8 + E_{24} - E_9 - E_{25}$ | $E_{25} - E_{24}$ |
| Pump 1 | $W_{pump1}$ | $E_{10} - E_9$ | $W_{pump1} + E_9 - E_{10}$ | / |
| Preheater | $E_d - E_e$ | $E_{11} - E_{10}$ | $E_d + E_{10} - E_e - E_{11}$ | / |
| Separator | $E_{11}$ | $E_{12} + E_{13}$ | $E_{11} - E_{12} - E_{13}$ | / |
| Vapor generator 2 | $E_b - E_c$ | $E_{14} - E_{21}$ | $E_b + E_{21} - E_c - E_{14}$ | / |
| Ejector | $E_{14} + E_{19}$ | $E_{15}$ | $E_{14} + E_{19} - E_{15}$ | / |
| Condenser 2 | / | / | $E_{15} + E_{26} - E_{16} - E_{27}$ | $E_{27} - E_{26}$ |
| Valve | / | / | $E_{17} - E_{18}$ | / |
| Evaporator | $E_{18} - E_{19}$ | $E_{29} - E_{28}$ | $E_{18} + E_{28} - E_{19} - E_{29}$ | / |
| Pump 2 | $W_{pump2}$ | $E_{21} - E_{20}$ | $W_{pump2} + E_{20} - E_{21}$ | / |

893

894

895

896

**Table 3** Constants for equipment costs calculation [39]

| Constant | value | Constant | value | Constant | value |
|---|---|---|---|---|---|
| $K_{1,he}$ | 4.3247 | $K_{2,pump}$ | 0.0536 | $C_{3,he}$ ($P_{he}$<0.5) | 0 |
| $K_{2,he}$ | -0.3030 | $K_{3,pump}$ | 0.1538 | $C_{1,pump}$ (1<$P_{pump}$<10) | − 0.3935 |
| $K_{3,he}$ | 0.1634 | $B_{1,he}$ | 1.63 | $C_{2,pump}$ (1<$P_{pump}$<10) | 0.3957 |
| $K_{1,turb}$ | 2.7051 | $B_{2,he}$ | 1.66 | $C_{3,pump}$ (1<$P_{pump}$<10) | − 0.00226 |
| $K_{2,turb}$ | 1.4398 | $B_{1,sep}$ | 2.25 | $C_{1,pump}$ ($P_{pump}$<1) | 0 |
| $K_{3,turb}$ | -0.1776 | $B_{2,sep}$ | 1.82 | $C_{2,pump}$ ($P_{pump}$<1) | 0 |
| $K_{1,comp}$ | 2.2897 | $B_{1,pump}$ | 1.89 | $C_{3,pump}$ ($P_{pump}$<1) | 0 |
| $K_{2,comp}$ | 1.3604 | $B_{2,pump}$ | 1.35 | $F_{M,he}$ | 1.0 |
| $K_{3,comp}$ | -0.1027 | $C_{1,he}$ (0.5<$P_{he}$<14) | 0.03881 | $F_{BM,turb}$ | 3.5 |
| $K_{1,sep}$ | 3.4974 | $C_{2,he}$ (0.5<$P_{he}$<14) | 0.11272 | $F_{BM,comp}$ | 2.7 |
| $K_{2,sep}$ | 0.4485 | $C_{3,he}$ (0.5<$P_{he}$<14) | 0.08183 | $F_{M,sep}$ | 1.0 |
| $K_{3,sep}$ | 0.1074 | $C_{1,he}$ ($P_{he}$<0.5) | 0 | $F_{M,pump}$ | 2.2 |
| $K_{1,pump}$ | 3.3892 | $C_{2,he}$ ($P_{he}$<0.5) | 0 | | |

905 **Table 4** Cost balance and auxiliary cost relations for each component [43]

| Component | Cost balance | Auxiliary equation |
|---|---|---|
| Gas heater | $c_1 \cdot E_{1,y} + c_b \cdot E_{b,y} = c_5 \cdot E_{5,y} + c_a \cdot E_{a,y} + Z_{gh}$ | $c_a = c_b$ |
| BC turbine | $c_2 \cdot E_{2,y} + c_{bt} \cdot W_{bt,y} = c_1 \cdot E_{1,y} + Z_{bt}$ | $c_1 = c_2$ |
| Vapor generator 1 | $c_3 \cdot E_{3,y} + c_6 \cdot E_{6,y} = c_2 \cdot E_{2,y} + Z_{vp1}$ | $c_2 = c_3$ |
| Precooler | $c_{23} \cdot E_{23,y} + c_4 \cdot E_{4,y} = c_{22} \cdot E_{22,y} + c_3 \cdot E_{3,y} + Z_{pc}$ | $c_3 = c_4$ |
| Compressor | $c_5 \cdot E_{5,y} = c_4 \cdot E_{4,y} + c_{comp} \cdot W_{comp,y} + Z_{comp}$ | / |
| ORC turbine | $c_1 \cdot E_{8,y} + c_{ot} \cdot W_{ot,y} = c_7 \cdot E_{7,y} + Z_{ot}$ | $c_7 = c_8$ |
| Condenser 1 | $c_{25} \cdot E_{25,y} + c_9 \cdot E_{9,y} = c_{24} \cdot E_{24,y} + c_8 \cdot E_{8,y} + Z_{cond1}$ | $c_8 = c_9$ |
| Pump 1 | $c_{10} \cdot E_{10,y} = c_9 \cdot E_{9,y} + c_{pump1} \cdot W_{pump1,y} + Z_{pump1}$ | / |
| Preheater | $c_e \cdot E_{e,y} + c_{11} \cdot E_{11,y} = c_d \cdot E_{d,y} + c_{10} \cdot E_{10,y} + Z_{ph}$ | $c_d = c_e$ |
| Separator | $c_{12} \cdot E_{12,y} + c_{13} \cdot E_{13,y} = c_{11} \cdot E_{11,y} + Z_{sep}$ | $c_{12} = c_{13}$ |
| Vapor generator2 | $c_{14} \cdot E_{14,y} + c_c \cdot E_{c,y} = c_{21} \cdot E_{21,y} + c_b \cdot E_{b,y} + Z_{vp2}$ | $c_b = c_c$ |
| Ejector | $c_{15} \cdot E_{15,y} = c_{14} \cdot E_{14,y} + c_{19} \cdot W_{19,y}$ | / |
| Condenser 2 | $c_{27} \cdot E_{27,y} + c_{16} \cdot E_{16,y} = c_{26} \cdot E_{26,y} + c_{15} \cdot E_{15,y} + Z_{cond2}$ | $c_{15} = c_{16}$ |
| Valve | / | $c_{17} = c_{18}$ |
| Evaporator | $c_{29} \cdot E_{29,y} + c_{19} \cdot E_{19,y} = c_{28} \cdot E_{28,y} + c_{18} \cdot E_{18,y} + Z_{evap}$ | $c_{18} = c_{19}$ |
| Pump 2 | $c_{21} \cdot E_{21,y} = c_{20} \cdot E_{20,y} + c_{pump2} \cdot W_{pump2,y} + Z_{pump2}$ | / |

906

907

908

909

**Table 5** Data comparison with Ref. [49] for the validation of Brayton cycle

| $T$/℃ | Present | Ref. | $P$/MPa | Present | Ref. | $W$/kJ kg$^{-1}$ | Present | Ref. |
|---|---|---|---|---|---|---|---|---|
| $T_1$ | 600 | 600 | $P_1$ | 20 | 20 | $W_{turb1}$ | 169.85 | 169.9 |
| $T_2$ | 449.05 | 449.0 | $P_2$ | 5.73 | 5.73 | $W_{comp}$ | 50.45 | 50.4 |
| $T_4$ | 20.01 | 20 | $P_4$ | 5.73 | 5.73 | | | |
| $T_5$ | 114.55 | 114.6 | $P_5$ | 20 | 20 | | | |

**Table 6** Data comparison with Ref. [50] for the validation of separation part in ORC

| State | $T$/℃ | | $P$/MPa | | $H$/kJ kg$^{-1}$ | | $S$/ kJ kg$^{-1}$K$^{-1}$ | | $M$/kg s$^{-1}$ | |
|---|---|---|---|---|---|---|---|---|---|---|
| | Present | Ref. | Present | Ref. | Present | Ref. | Present | Ref. | Present | Ref. |
| 11 | 163 | 163 | 0.6665 | 0.6665 | 990.14 | 990 | 2.664 | 2.664 | 1 | 1 |
| 12 | 163 | 163 | 0.6665 | 0.6665 | 2760.7 | 2761 | 6.724 | 6.725 | 0.1456 | 0.1454 |
| 13 | 163 | 163 | 0.6665 | 0.6665 | 688.43 | 688.7 | 1.972 | 1.973 | 0.8544 | 0.8546 |

944 **Table 7** Data comparison with Ref. [11] for the validation of the conventional part ORC

| Fluid | | $P_7$ /MPa | $T_7$ /℃ | $P_9$ /MPa | $T_9$ /℃ | $M$ /kg $s^{-1}$ | $W_{turb2}$ /kW | $W_{pump2}$ /kW | $\eta_{th}$ /% |
|---|---|---|---|---|---|---|---|---|---|
| R245fa | Present | 1.4293 | 107.75 | 0.1874 | 31.29 | 0.5041 | 10.615 | 0.621 | 8.40 |
| | Ref. | 1.4293 | 107.75 | 0.1874 | 31.29 | 0.4988 | 10.615 | 0.615 | 8.38 |
| R123 | Present | 1.5835 | 132.85 | 192.6 | 46.85 | 0.5457 | 10.652 | 0.652 | 8.88 |
| | Ref. | 1.5835 | 132.85 | 192.6 | 46.85 | 0.5458 | 10.652 | 0.644 | 8.6 |

945

946

947

948

949

950

951

952

953

954

955

956

957

958

959

960 **Table 8** Data comparison with Ref. [51] for the validation of ejector refrigeration cycle

| State | *T*/℃ | | *P*/MPa | | *H*/kJ kg$^{-1}$ | | *S*/ kJ kg$^{-1}$K$^{-1}$ | | *M*/kg s$^{-1}$ | |
|---|---|---|---|---|---|---|---|---|---|---|
| | Present | Ref. | Present | Ref. | Present | Ref. | Present | Ref. | Present | Ref. |
| 14 | 67.85 | 67.85 | 401 | 401 | 458.13 | 459.1 | 1.806 | 1.809 | 1 | 1 |
| 15 | 163 | 163 | 147.42 | 149 | 443.55 | 446.9 | 1.819 | 1.830 | 1.3175 | 1.3331 |
| 18 | 6.85 | 6.85 | 71.75 | 73 | 232.26 | 232.7 | 1.116 | 1.117 | 0.3135 | 0.3331 |
| 19 | 6.85 | 6.85 | 71.54 | 73 | 409.48 | 410.1 | 1.749 | 1.751 | 0.3135 | 0.3331 |

961

962

963

964

965

966

967

968

969

970

971

972

973

974

975

**Table 9** Main parameters of engine [4]

| Term | Value | Unit |
|---|---|---|
| Electrical power output | 2928 | kW |
| Engine speed | 1000 | rpm |
| Exhaust gas temperature | 470 | ℃ |
| Exhaust mass flow | 15673 | kg/h |
| Engine jacket temperatures | 79/90 | ℃ |
| Engine jacket flow | 90 | $m^3/h$ |

991 **Table 10** Simulation conditions of the CCP system

| Term | Value | Unit |
|---|---|---|
| Environment temperature | 15 | ℃ |
| Environment pressure | 0.1013 | MPa |
| Compressor inlet pressure | 0.3 | MPa |
| Compressor inlet temperature | 40 | ℃ |
| Compressor pressure ratio | 4 | / |
| BC turbine inlet temperature | 420 | ℃ |
| ORC turbine inlet pressure | 1.2 | MPa |
| Ejector primary flow inlet pressure | 1.5 | MPa |
| Terminal temperature difference at gas heat outlet | 15 | ℃ |
| Terminal temperature difference at vapor generator 1 inlet | 50 | ℃ |
| Terminal temperature difference at vapor generator 2 inlet | 65 | ℃ |
| Pinch point temperature difference in vapor generator 1 | 10 | ℃ |
| Pinch point temperature difference in vapor generator 2 | 60 | ℃ |
| Condensation temperature of condenser 1 | 35 | ℃ |
| Condensation temperature of condenser 2 | 25 | ℃ |
| Evaporation temperature of evaporator | 5 | ℃ |
| Isentropic efficiency of BC turbine | 80 | % |
| Isentropic efficiency of ORC turbine | 80 | % |
| Isentropic efficiency of compressor | 80 | % |
| Isentropic efficiency of pump 1 | 70 | % |

| | | |
|---|---|---|
| Isentropic efficiency of pump 2 | 70 | % |
| Inlet temperature of cooling water | 15 | ℃ |
| Outlet temperature of cooling water in precooler | 25 | ℃ |
| Outlet temperature of cooling water in condenser 1 | 30 | ℃ |
| Outlet temperature of cooling water in condenser 2 | 25 | ℃ |

**Table 11** Comparison between the proposed system and current systems

| Term | Ref. [8] | Present | Ref. [21] | Present |
|---|---|---|---|---|
| Engine power output/kW | 26.7 | 26.7 | 235.8 | 235.8 |
| Exhaust temperature/℃ | 689 | 689 | 519 | 519 |
| Engine coolant temperature/℃ | 100 | 100 | 83.3 | 83.3 |
| Exhaust mass flow rate/kgh$^{-1}$ | 118 | 118 | 990.79 | 990.79 |
| Net power output/kW | 5.63 | 6.38 | 36.77 | 33.79 |
| Cooling capacity/kW | 0 | 0.96 | 0 | 7.52 |
| Total net energy output/kW | 5.63 | 7.34 | 36.77 | 41.31 |

**Table 12** Ranges of the decision variables

| Decision variables | Range |
|---|---|
| compressor pressure ratio | 3-4.6 |
| compressor inlet temperature/℃ | 35-45 |
| BC turbine inlet temperature/℃ | 380-440 |
| ORC turbine inlet pressure/MPa | 0.5-1.4 |
| ejector primary flow pressure | 1.5-2.5 |

**Table 13** Control parameters of GA

| Tuning parameters | Value |
|---|---|
| Population size | 20 |
| Crossover probability | 0.8 |
| Mutation probability | 0.01 |
| Stop generation | 200 |

**Table 14** Single-objective optimization results

| Term | Value | Unit |
|---|---|---|
| Compressor pressure ratio | 3 | / |
| Compressor inlet temperature | 36.242 | ℃ |
| BC turbine inlet temperature | 435.404 | ℃ |
| ORC turbine inlet pressure | 1.363 | MPa |
| Ejector primary flow pressure | 1.556 | MPa |
| Net power output | 282.49 | kW |
| Refrigeration capacity | 20.01 | kW |
| Exergy efficiency | 27.63 | % |
| Average cost rate per unit of exergy product | 63.53 | $ $(MWh)^{-1}$ |

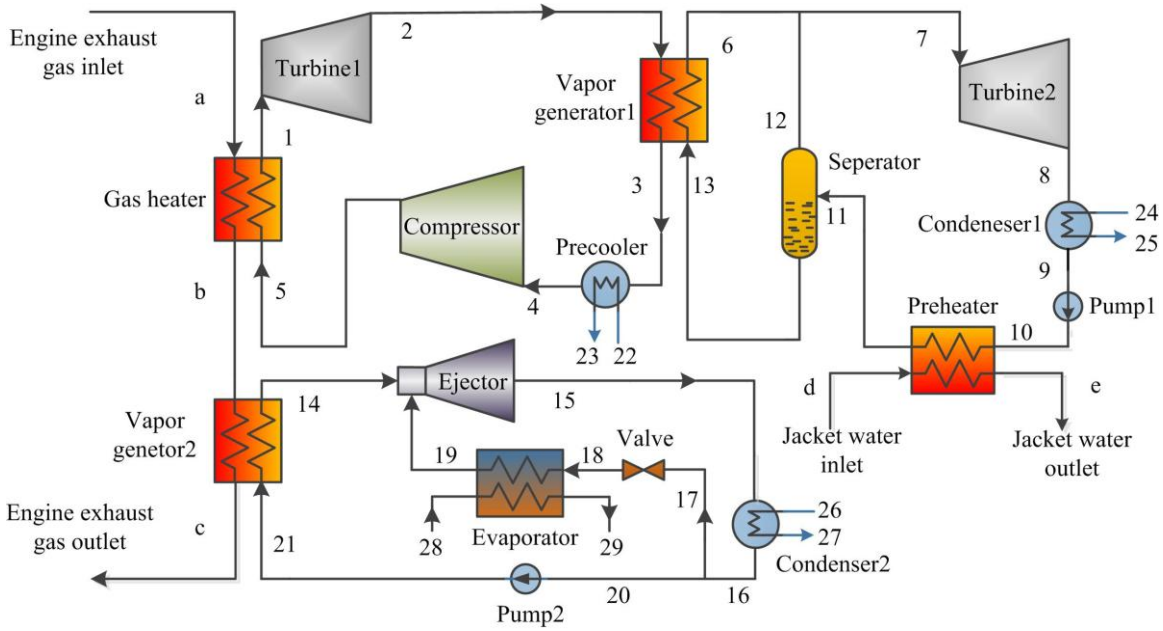


1063

1064 **Fig. 1** Schematic diagram of the CCP system

1065

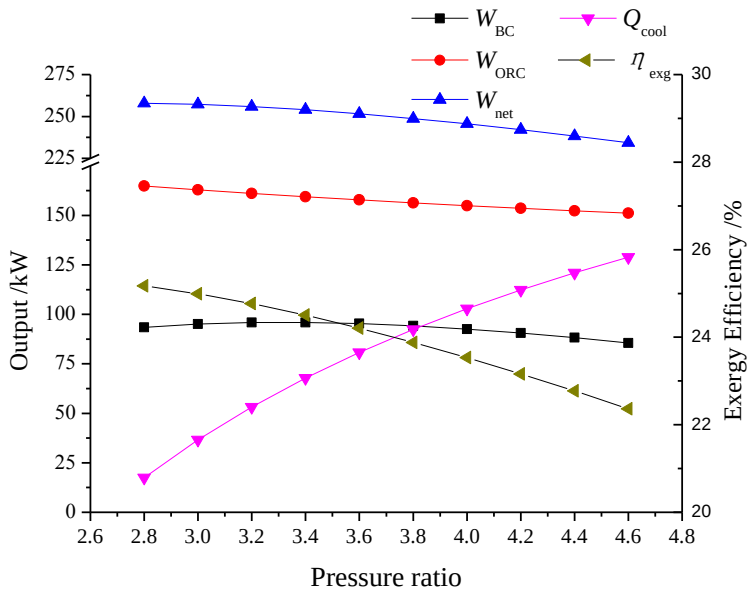


1066

1067 **Fig. 2** Effect of compressor pressure ratio on thermodynamic performance of the

1068 system

1069

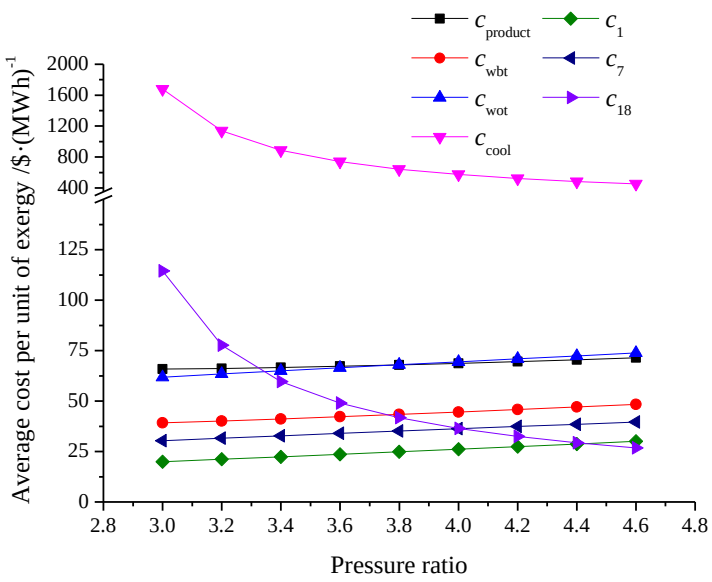


1070

1071 **Fig. 3** Effect of compressor pressure ratio on exergoeconomic performance of the

1072 system

1073

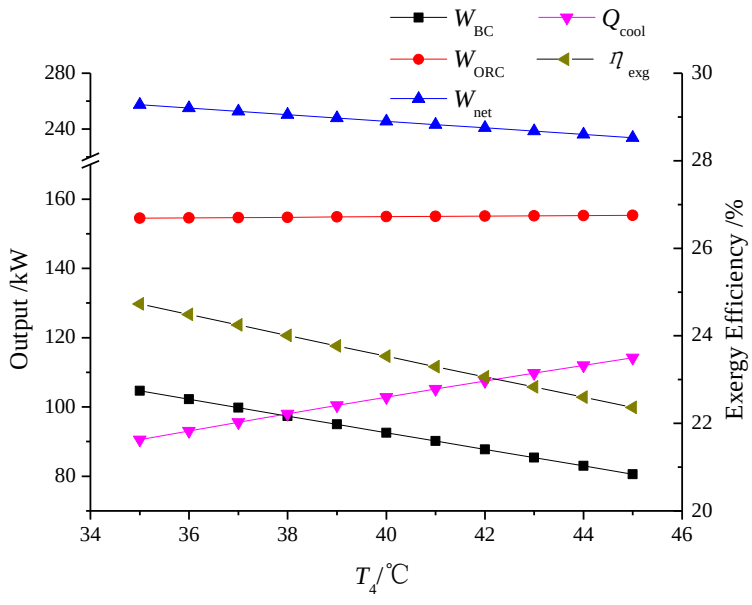


1074

1075 **Fig. 4** Effect of compressor inlet temperature on thermodynamic performance of the

1076 system

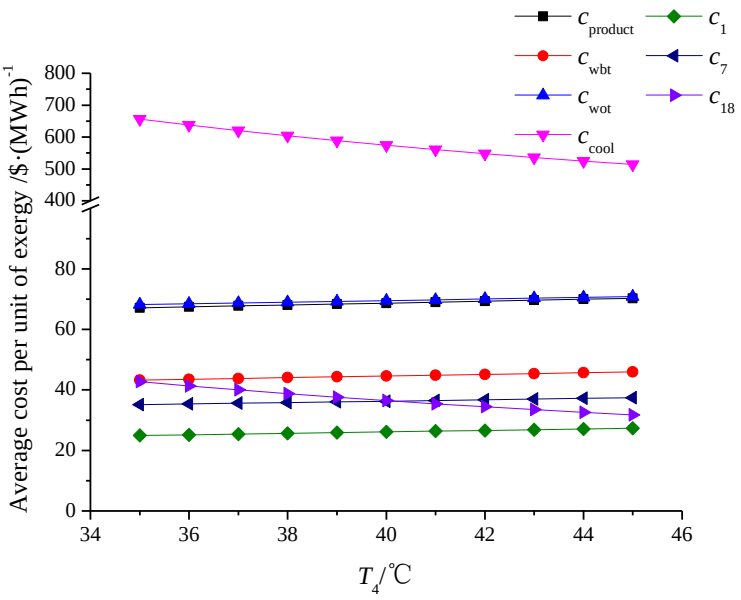


1077

1078 **Fig. 5** Effect of compressor inlet temperature on exergoeconomic performance of the

1079 system

1080

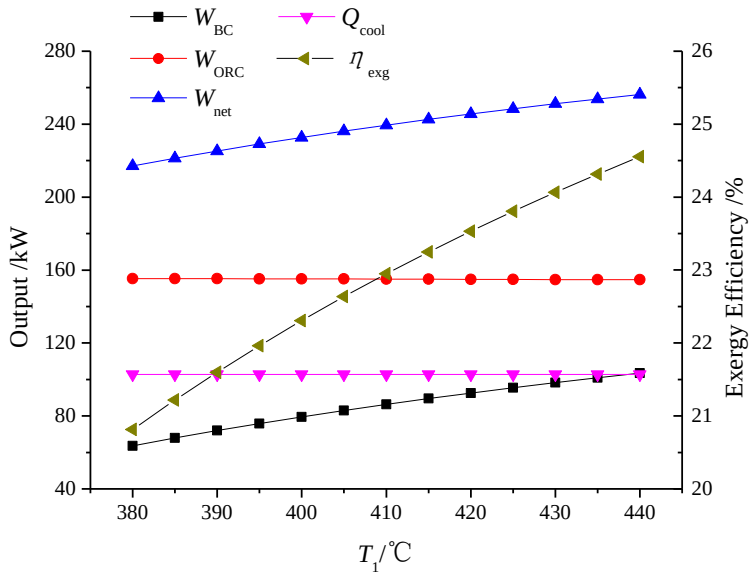


1081

1082 **Fig. 6** Effect of BC turbine inlet temperature on thermodynamic performance of the

1083 system

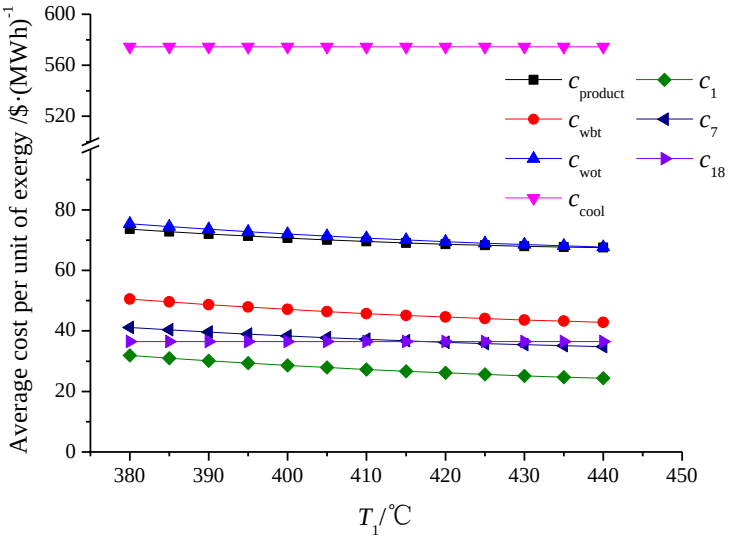


**Fig. 7** Effect of BC turbine inlet temperature on exergoeconomic performance of the system

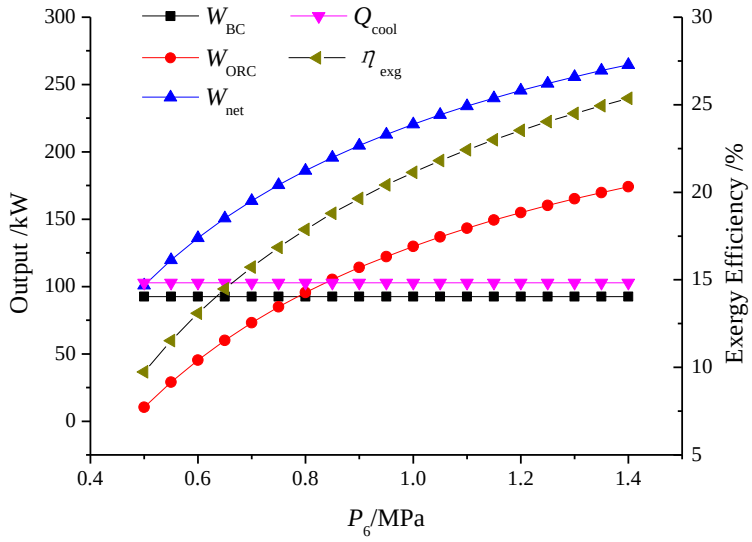


**Fig. 8** Effect of ORC turbine inlet pressure on thermodynamic performance of the system

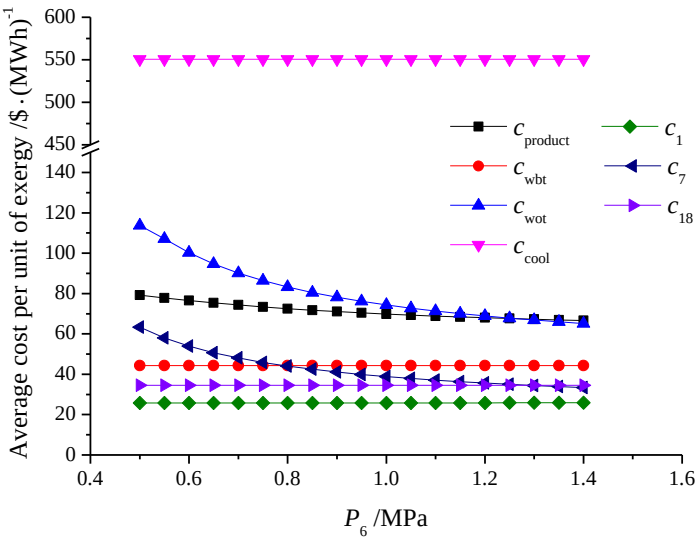


**Fig. 9** Effect of ORC turbine inlet pressure on exergoeconomic performance of the system

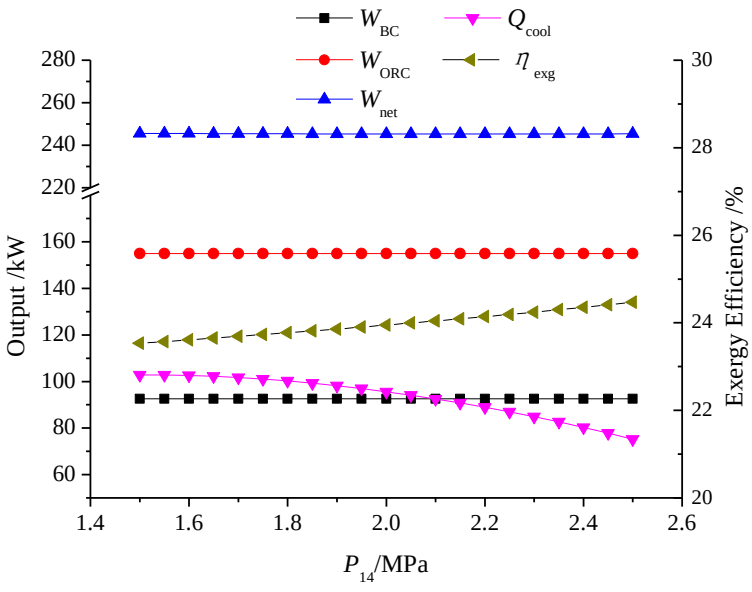


**Fig. 10** Effect of ejector primary flow pressure on thermodynamic performance of the system

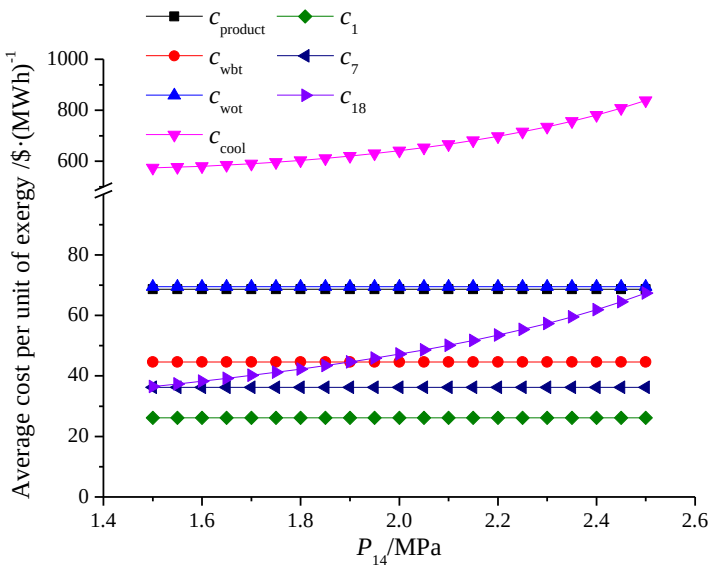


**Fig. 11** Effect of ejector primary flow pressure on exergoeconomic performance of the system